University of Minnesota
ST. ANTHONY FALLS HYDRAULIC LABORATORY

Project Report No. 132

Hydraulic Model Studies for the GURI HYDROELECTRIC PROJECT REPORT ON SPILLWAY CAVITATION DAMAGE

by
John F. Ripken
and
Warren Q. Dahlin

Prepared for
HARZA ENGINEERING COMPANY
and the
CORPORACION VENEZOLANA DE GUAYANA
Republic of Venezuela

February 1972
Minneapolis, Minnesota

CONTENTS

A STUDY OF CAVITATION DAMAGE ON THE DAM SPILLWAY OF THE GURI PROJECT

I. INTRODUCTION

The Guri Hydroelectric Project of the Corporation Venezolana de Guayana (CVG) is located on the Caroni River in northeastern Venezuela. The project includes a water impoundment created by a concrete gravity type dam. The dam contains a three-chute concrete spillway, each chute consisting of an overflow gated crest, a steep chute, and a terminal flip bucket. The spillway flow is projected from the bucket in a high arching jet which plunges into the tailwater pool for final dissipation of its energy.

Spillway flows were first released from the new structure early in 1969. Inspection of the spillway late in 1969 disclosed significant scouring or erosion of portions of the lips of the buckets and the ends of the side training walls. The Harza Engineering Company, which designed the structure and provided engineering assistance during the construction and initial operations, recommended to CVG that the damaged areas be restored with epoxy concrete and epoxy protective coatings. These repairs were made early in 1970 before the new seasonal water release. Subsequent inspections late in 1970 established that scouring had been renewed and even greater damage had been sustained than in the previous year. Field inspection suggested that the damage was due to the action of cavitation and that the damage might not be self-arresting and was thus potentially hazardous.

Early in 1971 staff members of the Harza Engineering Company reviewed the available evidence with staff members of the St. Anthony Falls Hydraulic Laboratory of the University of Minnesota. As a consequence of these discussions the Laboratory was authorized in February 1971 to proceed with an experimental study. The objective of this study was to establish the mechanism of the damage and the modifications of the existing design or operations which would prevent and alleviate future damage.

This report describes and summarizes the findings of the study.

II. THE PROBLEM AT GURI

A. The Existing Structure

In each of the three chutes of the spillway the flow entering from the headwater pool is controlled by three underflow crest tainter gates. The flow then proceeds down the rectangular concrete chute and through the curved flip bucket for final jetting into the tailwater pool. Figure 1 shows the general arrangement of the spillway, and Figs. 2 and 3 show the nature and significant dimensions of the spillway in plan and profile. The design adaptation of the spillway to the natural contours of the rock of the left or west bank results in three substantially different configurations in the upper reaches of the chutes. However, in the flip bucket terminal structure all chutes have a common form and dimensions as shown in sections BB and CC of Fig. 3.

Each spillway chute is fitted with vertical side training walls which are essentially non-overtopping in their upper portions. However, in the lower region above the flip bucket they flatten to a horizontal crest as shown in section CC of Fig. 3. It is noteworthy that the horizontal portion of these control walls may be lower than the tailwater pool for part of the potential range of the tailwater as shown in section AA of Fig. 3.

In the future it is proposed to raise the headwater pool in two stages of about 24 m each by increasing the height of the dam and its overflow crests. These dimensional changes, which will affect only the upper portion of the spillway, are typified by the ultimate profile shown in section AA of Fig. 3.

B. The Flow Variables

1. Discharge

The maximum design capacity of the spillway, which probably will never be reached, is 40,000 cms (1,413,000 cfs) under an initial head drop of 88 m (290 ft) between headwater and tailwater pools. The energy contained in this flow at the point of exit from the flip bucket is approximately 46,000,000 hp. Consequently, the damage potential is enormous. The spillway chute flows actually experienced during the three years in which damage occurred in the chutes ranged from zero to about 11,500 cms.

2. Lateral Tailwater Flow

High discharges of wastewater from the spillway along the west or left bank of the tailwater pool generate a large clockwise vortex in the pool as shown in Fig. 1. This vortex causes a substantial lateral pool velocity proceeding from east to west across the end of the flip bucket. No field measurements have been made for this velocity, but measurements in an earlier model study at St. Anthony Falls indicate that a velocity of about 4 mps (13 fps) can be expected for a variety of flow conditions. This lateral flow was considered to be a significant factor in the spillway damage and is referred to in subsequent observation and test data.

3. Chute Velocities

The velocity of the chute stream in the vicinity of the bucket lip where damage has been observed is another important factor in the damage mechanism. Field evaluations of this factor are difficult to make and were not attempted at Guri. Guidelines for establishing this value have been assembled by others and their findings have been applied to the conditions at Guri for the purpose of estimating the velocity which should be employed in the current model study. The ideal spillway velocity, which is taken as a base for estimates, is given by $\sqrt{2gH}$ where H is the vertical head existing between the normal elevation of the headwater pool, 215 m, and the elevation of the lip, 121.2 m. The resulting ideal velocity, V_I = 43 mps (140 fps), was then adjusted downward to 29.0 mps (95 fps). This assigns an arbitrary loss of about 30 per cent, which is assumed reasonable in light of the long spillway length and the moderate depths which existed during the damage period. The same procedure was used to estimate the new lip velocity which would result when the headwater stage was raised as a consequence of the planned ultimate increase in the height of the dam. For model design purposes this new prototype lip velocity was estimated to be 37 mps (120 fps).

4. Vortex Cavity Sources

In a discussion of the mechanism of cavitation damage, which is treated in a separate appendix, it was pointed out that the most common source of cavitation damage is the relatively small traveling vapor cavity. It was further shown that these traveling cavities generally result from the combination of low pressure at the center of an intense small vortex and the

concentrated on determining the relative influence of the overtopping disturbance and the tailwater back-up, including the contributions of the lateral flow.

5. Tailwater Stages

The potential range of tailwater stages at Guri is unusually large. This results from natural fluctuations of stage with spillway wastes, controlled fluctuations relating to powerhouse operations, and both natural and artificial controls from downstream channel conditions. Initial studies in the model employed tailwater stages taken from earlier model studies at St. Anthony Falls [1]* as shown in Figs. 8 and 9. Field data subsequently received from Guri have been added to Figs. 8 and 9 as shown. The substantial increase in field versus model stage values is due to the existence in the field of a bar in the exit channel of the tailwater pool. This bar is subject to future removal, but existed during the damaging flow conditions. In light of this potential range of stage and because of the unusually low setting of the bucket lip and training wall crest, the model study has included consideration of tailwater stages ranging from 120 to 130.5 m.

Subsequent studies establish that the stage level of the tailwater pool has a substantial influence on the pressure values which contribute to cavitation damage. It should be appreciated, however, that wave action or dynamic surging of the pool level is probably a significant part of this damage process. The extremely complex nature of the dynamic surging process involved (see Figs. 1 and 7) precludes obtaining clear knowledge of field conditions or any attempt to simulate these conditions precisely in the model.

C. The Observed Damage

1. Sill Damage

The most important damage was done to the concrete of the bucket lip and consisted of erosive removal of substantial volumes of concrete. The erosion prior to the time of this report had never become critical in extent, but had been progressive in nature with no indication that it might achieve a self-arresting condition. In view of the fact that the bucket lip was the principal controller of the location of the final dissipation of the flow energy, and in view of the enormous energy potential involved in this

*Numbers in brackets refer to list of references on page 40.

dissipation, there existed the threat that the disintegration of the lip could ultimately endanger the entire structure.

The material eroded from the bucket lip during the 1969 or first flood season is shown in location and extent in Fig. 10. The deepest erosion, about 0.5 m, occurred in a limited strip of the lip near the east end of the east chute, and its character is shown in the photo of Fig. 11. A somewhat shallower, but similar erosion occurred near the east end of the sill of the center chute. The sharp, pitted nature of the damage is characteristic of that found in other structures which have been damaged by cavitation.

In addition to slight damage at the lip in the west chute, the easterly half of the top of the sill and the downstream face of the sill also evidenced surface damage after the 1969 flood season. The nature of this particular damage was different from the sharp, pitted appearance common to cavitation damage and was instead of a smoother character common to abrasive erosion by solids. This evaluation was partially confirmed by 1970 bottom soundings taken across the pool at the foot of the spillway. At the center of the east chute these soundings indicated that original fill rock placed to a level of 117 m had been scoured to a depth of 111 m. Soundings near the east edge of the center chute indicated that fill rock placed to elev. 117 m had been scoured down to bedrock at elev. 114 m. At the west side of this chute, rock deposit was found at elev. 119 m. At the west chute rock deposit was found at elev. 115 m.

It is speculated that the strong lateral east-to-west flow in the tailwater pool moved loose rock in a bed transport action from east to west. It is further speculated that most of this rock found its way into the back flow and was entrained and sucked into the spillway jet discharging from the west chute. The high back flow velocity containing rock served to abrade the downstream face and top of the sill.

The holes eroded in the bucket lip during the 1970 flood season are also shown in Fig. 10; this damage was rather moderate with the exception of the loss at the east end of the center chute. The hole in this case went to a depth of 2 to 3 m. The seriousness of this particular loss precipitated the investigation covered by this report.

No repairs of the 1970 damage were made pending the determination of a more permanent cure from the laboratory investigation. It was also

felt that the damage might be self-arresting at some point. Diver observations of the damage were made in March 1970 and yielded the findings shown in Fig. 10. Observations which were made in July 1971 disclosed that conditions were much the same as in March 1971, but with a slight additional erosion.

Observations in December 1971 showed that the erosion at the east end of the center chute had increased markedly and lowered the sill to a position 4.1 m below the original sill configuration and that erosion in the west chute was down 2.8 m as shown in Fig. 10.

The schedule of discharges, tailwater stages, and gate openings which existed during the observed history of damages shown in Fig. 10 has not been reported from Guri.

2. Wall Damage

Concurrently with the previously described sill damage, damage was taking place on the vertical faces of the training walls adjacent to the chute sills. Of the four training walls abutting the three chutes, only the most easterly wall showed negligible erosive damage. The nature of this damage is shown in Fig. 12. Of the five training wall surfaces which showed damage, the appearance of four was essentially the same. The volume removed was in general shaped roughly like a half-cone. The tip of the cone began at the bucket lip and the axis of the cone ran up the wall at approximately 45° with the bucket sill as seen in Fig. 12. The depth of erosion was virtually zero adjacent to the bucket lip and was greatest near the top of the training wall. In 1969 some of these cones had already reached a depth of 0.3 m near the top of the wall. In subsequent years virtually the entire end of the wall has disappeared in some instances.

In addition to the conical pattern of damage, the east wall of the west chute showed damage in the area between the cone and the sill (Fig. 12). This shallow surface damage was somewhat similar to that found on the immediately adjacent sill which showed damage on the top and downstream side of its east end. This erosion was described previously under "Sill Damage" and was attributed to abrasion by rocks entrained from the pool. The shallow damage on the lower portion of this training wall is also believed due to this same rock abrasion.

Although the wall damage has been disfiguring to the appearance of the structure, it is not believed to endanger the structure itself. An ultimate solution to the more vital sill damage problem will in all probability also arrest the wall damage problem.

The fact that the high wall on the east side of the east chute did not evidence significant erosive damage, as is shown in Fig. 12, led to the comparative model tests with high and low training walls adjacent to the bucket.

III. THE TEST FACILITY AND SPILLWAY MODEL AT ST. ANTHONY FALLS

A. The Test Facility

The nature of the spillway flow and the location and character of the erosive damage at Guri strongly suggested that the damage mechanism was cavitation. Consequently it was decided to conduct the model investigation in a variable pressure test facility which would permit modeled cavitation processes. The largest facility available for such a study was the recirculating variable pressure water tunnel shown in Fig. 13. This tunnel, which has a 108 cm (42 in.) diameter test section, is intended to completely house a test model within its pressure shell to permit reduction of the model pressure environment and thus artificially promote cavitation in a model flow. For the purposes of this study, the 150 hp low head pump shown in Fig. 13 was bypassed by a higher head 25 hp pump (not shown). The maximum discharge and head of this pump, $Q = 0.0623$ cms (2.2 cfs), $H = 10$ m (32 ft), dictated the maximum flow conditions that could be modeled.

The model size was dictated by the largest windowed, rectangular test section housing that could be adapted to the existing 108 cm diameter tunnel piping. The new windowed, rectangular test section accommodated a model having a length up to 153 cm (60 in.), a width up to 61 cm (24 in.), and a height up to 76+ cm (30 in.).

Controls shown at the left of Fig. 14 permit detailed control of the flow velocity, environmental pressure (down to 0.13 atmosphere), gas content of the water down to 8.5 ppm, and tailwater depth.

The tunnel was also equipped with a small separate pump for the maintenance of a small lateral tailwater flow across the end of the spillway.

B. The Spillway Model

The spillway model, which was made as large as the test section would permit, was built at a scale of one meter in the prototype to one-half inch in the model, or a ratio of 78.7. This permitted modeling the downstream end of the spillway to a prototype length of about 90 m including a straight reach of approach chute 56 m long having a slope of 30° with the horizontal. This chute was followed by the full flip bucket and sill. The upper end of the chute was provided with a gated orifice which permitted independent selection of the water depth and velocity in the chute. Pressure measurements

across this orifice were used to evaluate the model discharges. The flip bucket model installed in the tunnel test section is shown in Figs. 14 and 15.

The pump discharge limitations required that less than the full width of a spillway chute be modeled, but this limitation was not considered serious, as the principal erosion problem was thought to occur adjacent to the side training wall and could be studied with a limited spillway width. A spillway width of 12 m (39 ft) prototype, or 15.2 cm (6 in.) model, was selected. Although the prototype training walls converged toward each other in the downstream direction with an included angle of $5^{\circ}17'$, the side walls of the model were made parallel for simplicity.

To permit visual and photographic observation, the model was constructed of transparent plexiglas. The model was built with a removable top on the back or west training wall above the bucket and sill. This permitted tests with a wall crest height of elev. 123 m prototype or an alternate high, non-overtopping crest height which was arbitrarily fixed at elev. 132.45 m. The model was also provided with removable sills which permitted the use of a soft aluminum alternate sill for cavitation erosion studies. This also permitted removable sill pieces of various heights simulating normal and eroded sills having prototype equivalent elevations of 121.23 m, 118.93 m, and 116.93 m. These are equivalent to various sill heights observed in the field erosion evaluations. The configurations are shown in Fig. 17.

As is discussed in Appendix B, which deals with the mechanism of cavitation, cavitation depends on the presence of regions of pressure well below atmospheric. The location of cavitation in a flow can be qualitatively evaluated from visual or photographic evidence of its actual presence, and the model was made transparent for such evaluation. However, a more powerful tool for locating and quantitatively evaluating a cavitation potential is to be found in the use of boundary pressure evaluations. Such potentials can be evaluated even without the actual occurrence of cavitation and have been relied upon heavily in this investigation. To permit this evaluation, two basic lines of boundary pressure taps were provided in the model. One of these lines was placed along the modeled spillway centerline at a distance from the training wall equivalent to 6 m in the prototype. (Note that the designated centerline relates to the narrow model and not to a full-width prototype chute.) A similar line of pressure taps was located at the base

of the west training wall. These taps, which were all of 1.6 mm (1/16 in.) diameter, were dimensionally located as shown in Fig. 17.

All the taps shown in Fig. 17 were provided with tubing connections to an external manometer for readout of mean static pressure values. These connections are shown in Fig. 14 and 15. The manometer tubes contained dyed water for readout, and all manometric evaluations were made with atmospheric pressure in the test section.

Of the many taps shown in Fig. 17, a selected few, located in critical areas, were fitted to accommodate a transient pressure measuring transducer. Their locations are designated in Fig. 17, which includes a typical detail of the pressure transducer mounting for these selected taps. Previous studies have shown that this type of transducer arrangement gives a readout response time in close agreement with pressure conditions at the input tap. The transducers used in these studies were of the strain gage diaphragm type with diaphragms of 1.26 cm (1/2 in.) diameter and a range from zero to 2.5 psi. The transducers used were Statham Scientific Instruments model PM 131TC $\pm$ 2.5 - 350 with a range of $\pm$ 2.5 psid and Consolidated Electrodynamics Corporation type 4-312-0127 with a range of $\pm$ 2.5 psid. The transducer signal was processed in several ways with the set-up shown in Fig. 16. Most commonly it was processed to provide a time-pressure paper chart record on a Sanborn Company recorder, model number 296.

The transducer signal was also analyzed for per cent of time below various datum levels using a probability density analyzer designed and constructed at the St. Anthony Falls Hydraulic Laboratory, a Disa Elecktronik random signal indicator and correlator model number 55A06, and a Hewlett Packard electronic counter model number 521c.

As mentioned earlier, the model was provided with a separate pump which drew water from the tunnel tailwater pool and discharged it laterally across the end of the chute in a fairly uniform stream. In the prototype this stream flows from east to west, but in the model, because of the corner tap positions, the flow was reversed.

C. Model Test Variables

A number of test variables were examined in the investigations. The range or value of these variables is as follows:

1. Discharge -- This varied from a minimum of about 2000 cms to 28,000 cms prototype. The lowest value significant to damage differed somewhat with tailwater stage and was established by the inability of the jet to flip free, resulting in full flooding of the bucket. Below these low flow conditions, high velocity, cavity-generating conditions cannot occur at the bucket lip. The highest discharge value of 28,000 cms prototype equivalent was established by the limits of the tunnel pump. Early tests established that higher values were not needed, because high bucket pressures accompany large discharges and cavitation disappears. Model discharges equivalent to the foregoing prototype values were established using the Froude gravity relation,

$$Q_m = (L_m/L_p)^{5/2} Q_p = (1/78.7)^{5/2} Q_p = Q_p/55,000$$

Unless otherwise stated, discharges relate to simultaneous flow in all three spillway chutes.

2. Velocity -- As previously stated, the estimated prototype velocity of flow at the bucket lip was 29.0 mps (95 fps) for the first stage dam height and 37 mps (120 fps) for the ultimate dam height. Model velocities equivalent to these values were established by the Froude relation

$$V_m = (L_m/L_p)^{1/2} V_p = (1/78.7)^{1/2} V_p = V_p/8.9$$

The model velocities are thus 3.27 mps (10.7 fps) and 4.15 mps (13.5 fps) respectively. In limited studies attempting to generate actual cavitation in the model, the velocity was raised to the maximum obtainable with the tunnel pump. This produced a test velocity in the model of 13+ mps (43 fps) maximum.

3. Flow Depth -- Suitable simulation of the flow discharge and velocity in accord with the Froude gravity relation as discussed in items 1 and 2 above will result in flow depths dimensionally scaled at the same ratio as the model itself.

4. Pressure -- The environmental pressure for the model during tests had either a low subatmospheric value or a normal atmospheric value. The low pressures were used only during the limited tests which attempted to produce actual cavitation in the model. In all other tests the model was operated at atmospheric pressure conditions. For the subatmospheric tests an external vacuum supercharge was imposed on the tunnel. This value was adjusted to produce the desired degree of cavitation as described separately under the cavitation tests.

   Since the bulk of the boundary pressure tap data were processed to yield equivalent prototype values, it was not necessary to actually measure the data at absolute pressure levels equivalent to prototype, but only in equivalent model pressure heads. The variations in pressure head are in the same model-to-prototype ratio as other dimensional properties of the model; i.e., 1:78.7.

5. Temperature -- The range of temperature of the water in the tunnel during the tests varied from 20°C (68°F) to 26°C (79°F).

6. Tailwater Stages -- For reasons described earlier, model tailwater stages were varied from 120 to 130.5 m elevation.

7. Training Wall Height -- As described earlier, one wall of the model was made removable to permit tests corresponding to the existing wall height of 123 m elevation. This height permitted wall overtopping flows when tests were conducted with tailwater stages above 123 m. As an alternative, tests were run with a wall height of 132.45 m. Since this height exceeds all the tailwater stages tested, no overtopping flow was involved with its use. The length of wall which was lowered to elevation 123 m was made 24.2 m as shown in Fig. 17. Since the significant overflow length varies for each of the four low training walls, the value of 24.2 m is an arbitrary compromise.

8. Sill Configurations -- In the initial stages of the tests the original design configuration of the sill was employed.

Subsequent tests employed an extension of the sill. This was designed to generate positive face pressures (see Appendix A). Following these tests, additional tests were made in which the sill height was lowered to 2 m below the original sill. These tests simulated the continuing potential for erosion that existed for field conditions known to exist in the early part of 1971. Later tests employed a sill height lowered to 4 m below the original sill. These later tests simulated the continuing potential for erosion that existed for field conditions that were found to exist late in 1971. All four of these sill configurations are dimensionally described in Fig. 17.

9. Lateral Flow -- In initial tests it was found that lateral flows always tended to provide somewhat lower transient pressure values than tests without lateral flow. Since it is difficult to conceive of field conditions without lateral flow, most of the transient pressure test data offered have been shown with lateral flow. This appeared to be a conservative approach.

IV. THE MODEL TESTS

A. Spillway Static Pressure Tests

1. The Original Sill Configuration

The theory relating to the pressures existing on the chute and flip bucket of the spillway are discussed separately in Appendix A. Model tests relating to the chute and entire bucket are shown in Figs. 18 and 19. These tests were conducted for the simple case of no lateral flow and no side wall overtopping, but with the relatively high tailwater conditions and velocity that prevailed at Guri during the damage period. The plottings are expressed in equivalent prototype values and are noteworthy for the following features:

a. Pressures on the upstream chute are essentially those to be expected from the hydrostatics of the chute depth, d.

b. Pressures at the center of the bucket (tap 9) are approximately in accord with centrifugal or vortex theory as discussed in Appendix A.

c. The transition from chute pressure to bucket vortex pressure is quite gradual and centers roughly about the tangent point of the bucket curvature (tap 6).

d. With the exception of the discharge of 2000 cms, the bucket flow depths are in orderly agreement with their respective discharges. The abnormal position of the curve for a discharge of 2000 cms is due to drowning of the jet in the bucket.

e. The pressures at the tap nearest to the bucket lip (tap 18a) appear to be heading toward zero or atmospheric at the bucket lip, but are positive for all depths. The lowest values relate to the shallowest depths of flow.

f. Pressures on the bucket sill are roughly in accord with the hydrostatics of the tailwater over the sill.

g. There are no evidences of negative static pressures to contribute to cavitation, but the lowest pressure potentials appear to center on the bucket lip where damage has occurred. Subsequent plottings will, therefore, focus only on this area.

h. Pressure data taken at the line of pressure taps at the base of the wall as shown in Fig. 19 are essentially the same as shown in the "centerline" data of Fig. 18.

Figures 20 and 21 extend the data of Figs. 18 and 19 to include the conditions of lateral flow, wall overtopping flow, and lateral flow combined with overtopping. The following differences are notable and apply to data from either the "centerline" or the sidewall taps:

a. Lateral flow alone produces no significant change in static pressures.

b. Overtopping causes flows of 2000 to 6000 cms to flood back and drown the jet in the bucket.

c. Overtopping causes flows from 8000 to 28,000 cms to flow with a significantly greater bucket pressure.

d. There are no evidences of negative static pressures anywhere on the bucket exit.

e. Items b and c might have been somewhat different for a full width model chute.

Figures 22 and 23 are similar to Figs. 20 and 21, but employ lower tailwater stages. The stage of 120 m is not a probable operating stage, but demonstrates the effect of discharge with the lip located above the tailwater. The low tailwater conditions are more comparable to those which were tested in the early model studies of Ref. [1]. These conditions may exist with possible future changes in the bed levels of the tailrace. The following differences are notable in comparison with the conditions of Figs. 18, 19, 20, and 21:

a. The smaller discharge, which is actually non-overtopping, is essentially the same as for the non-overtopping cases in Figs. 18 and 19 for the first 14 taps. Above tap 14 the pressure now falls earlier, indicating that there is less flow back-up with the lower tailwater stage.

b. The two larger discharges, which do overtop but to a lesser extent than in the earlier figures, show a significant reduction in pressures.

c. The freely discharging smaller discharge actually shows a negative static pressure of about 2 m. Surprisingly, this indicates potential cavitation damage even if the bucket lip is raised clear of all tailwater. A rationale for this is given in Appendix A. Expressed as a percentage of the dynamic head of the flow, the -2 m pressure is about 1.4 per cent.

2. The Sill Extension

The sill extension discussed in Appendix A and shown in Fig. 17 was subjected to pressure investigations quite similar to those shown in Figs. 18 through 21 for the original sill. The test data are shown in Figs. 24 through 27.

Comparison of Figs. 24 and 25 with Figs. 18 and 19 shows the following:

a. Pressure taps up to and including tap 15 show essentially the same pressure conditions, indicating no influence from the ramp extension.

b. Pressure taps downstream of tap 15, covering a distance of a few meters, show a significant increase in pressure head varying from about 2 to 4 m depending on discharge.

c. The additional resistance at the lip caused the discharge of 4000 cms to flood back and drown the jet in the bucket.

d. Pressures at the beginning of the ramp were substantially increased, thus removing the necessity for providing a sophisticated transition between the bucket curve and the extension ramp.

e. Conditions at the wall pressure taps are much the same as those for the "centerline" taps except for a slight reduction in pressures at tap 18b and some slight shift in the drowning of the jet for discharges of 4000 and 8000 cms.

Figures 26 and 27, which extend the data of Figs. 24 and 25 to include the contributions of lateral flow and overtopping, produce much the same kind of additional influences noted for Figs. 20 and 21.

3. The Sill Eroded Two Meters

Tests of the sill eroded to a depth of two meters below the original configuration represented a condition which prevailed during much of 1971. The tests were run to determine whether the potential for cavitation damage was diminishing to become self-arresting.

Figures 28 and 29 can be compared with the analogous data of Figs. 18 and 19 with the following noteworthy features:

a. Pressure taps up to and including tap 11 show essentially the same pressure conditions with no influence from the erosion.

b. Pressure taps downstream of tap 11 show an increasingly rapid falloff in pressure until the low pressure conditions at tap 13a become comparable to those which previously existed at tap 18a on the original lip. This suggests that as far as static pressures are concerned there is no tendency for the cavitation potential to become self-arresting.

c. Conditions at the wall taps are quite similar to those at the "centerline" taps except that the pressure falloff begins somewhat earlier.

Figures 30 and 31, which extend the data of Figs. 28 and 29 to include the contributions of lateral flow and overtopping, produce much the same kind of additional influences noted for Figs. 20 and 21. These data also suggest that there is no tendency for the cavitation damage to become self-arresting as the erosion proceeds.

4. The Sill Eroded Four Meters

Tests of the sill eroded to a depth of four meters below the original configuration represented the alarming condition which was found on inspections at Guri late in 1971. The tests were run to determine whether the potential for further cavitation damage was diminishing. The tests were run with the same typical 1971 tailwater stages employed in testing the original sill configuration and the sill eroded two meters. Two notable changes are apparent in this geometric arrangement when it is compared to the other, higher sill configurations seen in Fig. 17:

a. Lowering the sill 4 m allows freer access by the tailwater.

b. The original sill at the lip position had an angle of 45° between the bucket tangent and a horizontal line. With the sill lowered 4 m this angle is more nearly 30°.

Figures 32 and 33 show the operation of this sill with lateral flow and with lateral flow and overtopping. For the case of lateral flow alone the following can be noted:

a. Flows of 2000 and 4000 cms appear to have their jets drowned out in the bucket with a resulting increase in bucket pressures.

b. Flows of 6000 and 8000 cms appear to have most of the bucket swept out, but with a small rollback in the vicinity of taps 11 and 12.

c. Flows of 17,000 and 28,000 cms appear to have clean sweepout, but a fairly high dynamic pressure remains in the lip region.

d. Pressures on the sill are generally high and roughly in accord with the hydrostatic contribution of the tailwater head.

e. On the basis of static pressures the conditions do not appear conducive to cavitation.

For the condition of lateral flow with overtopping the following can be noted:

a. Flows of 2000 and 4000 cms appear to have their jets drowned out in the bucket with much the same pressure effects in the bucket as were found for the case with no overtopping.

b. Flow equal to or greater than 6000 cms appears to approximate a condition of jet sweepout in the bucket.

c. At the "centerline" (see Fig. 32), flows equal to or greater than 8000 cms are evidently deflected downward over the sill by the powerful overtopping stream from above. This causes the spillway jet to pass close to the sill with a very powerful aspirating action generated at the lip. The resulting very low lip pressures create vapor cavitites or possibly a steady supercavity which collapses only slightly farther downstream because of the rapidly rising sill pressure gradient.

d. Near the side wall (see Fig. 33), where the falling overtopping stream does not jet downward as strongly, the aspirated pressures near the lip are not nearly as low as they are farther out from the wall. They are, however, relatively very low and will strongly support cavitation damage. Farther out from the wall beyond the influence of the falling jet the pressures should rise to the higher values of lateral flow alone.

e. The cavitation erosion pattern of December 1971 as shown in Fig. 10 appears to be in good agreement with the concepts of items c and d above.

f. Under certain combinations of discharge and tailwater the low pressures under the jet actually pulled the entire jet down toward the sill, and the jet was drowned in the tailwater pool. This condition was unstable, and the jet would then slowly rise and spring free of the pool. This action of slowly falling and then rising took place in a cyclic manner. The conditions were created by the overtopping stream, and since the overtopping stream affected most of the channel width in the model, the entire jet rose and fell. It is doubtful that the same thing would have occurred in a full width model or in the prototype.

g. With the exception of the very low pressures generated by the overtopping action near the walls, static pressures near this bucket lip were greater than for the other lip configurations. There is some reason to believe that except for overtopping effects, cavitation damage might have occurred at a much reduced rate as the sill was lowered.

5. The Influence of Increased Dam Height

Static pressure tests with the original sill configuration (Type A) were carried out for the full chute and bucket exposed to a velocity of V = 37+ mps (120 fps). These studies represent the velocity which would occur under the ultimate stage development and are quite comparable in coverage to those of Figs. 22 and 23 which relate to the velocity V = 29 mps (95 fps) representing the first stage or existing dam condition. As in Figs. 22 and 23, the high head tests were in this case conducted with the

lower tailwater stages which are likely to occur in the future. The discharges and related tailwaters were 8000 cms and 120 m elev., 8000 cms and 123 m elev., 8000 cms and 124.6 m elev., 17,000 cms and 124.6 m elev., and 28,000 cms and 127 m elev.

The static pressure tests, which are not shown, exhibited the following trends:

a. The general shape of the pressure in the chute and flip bucket is much the same as for the lower velocity, but the pressure is appreciably greater in the bucket because of the greater centrifugal effect.

b. The fall in pressure from the high value at the bottom of the bucket toward the atmospheric low value near the bucket exit yielded gradients which became steeper near the bucket exit as the chute velocity increased.

c. With lateral flow and no overtopping the taps near the bucket lip at both the "centerline" and the wall exhibited about the same general pressure pattern. For taps up to 18, pressures remained above atmospheric. At tap 18a the flows of 8000 cms without submerging tailwaters gave negative pressures up to -4 m. All larger flows gave positive pressures. It is assumed that flows of less than 8000 cms would also have shown negative values.

d. Lowering the sidewall to permit overtopping produced relatively little change in the static pressure from the condition without overtopping.

e. It is noteworthy that low flows with the completely free tailwater condition (120 m elev.) produced negative static pressures of about -4 m. This compares with about -2 m of pressure at the same tap for $V = 29$ mps. When treated as percentages of their respective dynamic pressure heads, $V^2/2g$, these two negative pressures are similar; i.e., 4.7 per cent and 5.8 per cent.

f. It appears that static pressures on the lip are slightly lower (about 1 to 2 m) with the higher velocity, and only the last 25 cm of lip shows any tendency to produce negative pressures.

g. Pressures at sill taps 19 and 20 registered essentially hydrostatic pressures.

B. Bucket Lip Transient Pressure Fluctuation Tests

1. The Original Sill Configuration

Transient pressure fluctuation data were recorded for selected taps near the bucket lip where static pressure tests and field damage observations had indicated that negative pressures might be expected. One tap, C 18a, was used at the "centerline" at a point upstream from the lip a prototype distance of 12.5 cm. Taps C 18c and C 19 were also located on the sill centerline at 12.5 cm and 50 cm prototype distances downstream of the lip. Near the wall additional taps were used. These were L 17 and L 18, located upstream from the lip at prototype distances of 50 cm and 25 cm, and L 19, located downstream from the lip at a prototype distance of 50 cm. The tap positions are shown in Fig. 17. The bulk of the data relate to the velocity of flow associated with the first stage dam conditions. Figure 58 relates to the velocity of flow for the ultimate dam height. The latter data will be discussed as a separate item.

Typical paper chart records taken at these taps for the flow conditions of interest are shown in Figs. 34 through 43. These charts are shown in terms of equivalent prototype values and include an indication of the location of the calibrated zero datum.

Along with the chart recording of fluctuations, the recorder provided electronic readout of the average value of pressure. This average value and a manual readout of the minimum dips and maximum fluctuations of the paper chart record are tabulated for the various test conditions in the tables of Figs. 52 through 58. From the standpoint of cavitation damage the significant values from these tables are the negative pressure peak values. Notable features from the tabulated values are

a. The dynamic pressure depressions created by the passage of large turbulent eddies over the boundary are not fully represented by the minimum pressure values listed in the tables. These dynamic values are more properly the true or absolute difference between the listed minimum pressure values and the listed average pressure values. This difference is labeled ΔP in a separate column in the tables. For each column the maximum ΔP is selected and noted. This value is also calculated as a dimensionless pressure coefficient relative to the dynamic head of

the chute velocity and is so shown in the tables. The value of this coefficient, expressed as a percentage, is referred to in the discussions which follow.

b. At the bucket exit the transient fluctuations give rapidly increasing negative values as the flow in the bucket approaches the lip. At tap L 17, which would be 50 cm from the lip in the prototype, there are no negative pressures with only lateral flow (see Fig. 56). The addition of overtopping flow diminishes the pressures slightly, but with only weak negative values (see Fig. 56).

c. At tap L 18, which would be 25 cm from the lip in the prototype, negative pressures exist under almost all flow conditions with only lateral flow (see Fig. 53). The negative values are as low as -3.8 m. The addition of overtopping flow further decreases the pressure (see Fig. 54) to values as low as -6 m. The maximum negative values are 5.0 m and 11.3 m, which are respectively 11.7 per cent and 26.4 per cent of the dynamic head.

d. At tap C 18a, which would be 12 cm from the lip in the prototype, lateral flow creates no significant negative values, but with the addition of overtopping scattered values as low as -5.1 m are reached (see Figs. 53 and 54). The maximum negative ΔP values are 2.6 m and 10.0 m, which are 6.1 and 23.4 per cent respectively of the dynamic head.

e. In items a, b, and c above it should be noted that the taps discussed involve both "centerline" and wall conditions, but not with the individual taps in the same proximity to the lip. It appears in general that negative pressures are worse near the wall than at the "centerline." This implies that if tap C 18a had been near the wall, negative values lower than -5.1 m might have been found.

f. If pressure conditions are examined in a similar way for flow proceeding downstream from the lip, we observe first at tap C 18c, which would be 12.5 cm from the lip in the prototype. With only lateral flow this tap shows only positive pressures. With the

addition of overtopping flow, negative pressures are quite general and reach values as low as -3.3 m (see Fig. 55). The maximum negative ΔP value was 8.5 m, which is 19.8 per cent of the dynamic head.

g. At tap L 19, which would be at the wall and 50 cm downstream of the lip in the prototype, and with only lateral flow, very serious negative values are encountered (see Fig. 56). The pressures indicate prototype values as low as -14.1 m. Such values could not actually be reached in the prototype, since vaporization or major cavitation would limit the pressure to -9 or -10 m, the inherent vapor pressure limit of the water. With the addition of overtopping flows an even wider range of low negative pressures is reached (see Fig. 56). The area of tap L 19 is the most damage-prone disclosed in the model study. For the above lows the maximum negative ΔP values are 15.4 m and 13.6 m, which are 35.9 per cent and 31.8 per cent, respectively, of the dynamic head.

h. At tap C 19, which would be at the "centerline" and 50 cm downstream of the lip in the prototype, occasional negative pressures are again encountered with lateral flow. With the addition of overtopping flows a wider range of more negative pressures occurs with values to -8 m. The conditions at the "center" are not as severe as at the wall, but they are very serious (see Fig. 55). The maximum negative ΔP values for these conditions were 5.1 m and 13.9 m, or 11.9 and 32.5 per cent, respectively, of the dynamic head.

i. The average pressure values shown in the tables of Figs. 52 through 57 are in quite good agreement with the manometric values given in Figs. 18 through 23.

j. The large turbulence that causes dynamic pressure depression is due principally to the disturbance of the overtopping flow or to the rollers that tend to form at the end of the bucket under suitable tailwater conditions. A comparison of Figs. 52 and 53 indicates that lateral flow has considerable influence on the tailwater and consequently on the bucket roller contributions

to pressure fluctuations. From the foregoing pressure coefficient values it appears that the bucket rollers will in general contribute negative values of about 11.7 per cent of the dynamic head (one unique condition at tap L 19 does, however, show 35.9 per cent). The greater disturbance of the overtopping flow contributes up to 32.5 per cent.

k. In general, for any given discharge, increasing overtopping flows tend to slightly increase the average pressure and to substantially lower the minimum pressure near the lip.

The complex manner in which the potentially damaging negative pressure values relate to the flow conditions is difficult to ascertain from the tabular pressure data of Figs. 52 through 58. Accordingly, the data for the original sill configuration have been summarized graphically in Figs. 59 and 60. It should be noted that the discharge for these figures has been related to the flow in only one chute as an aid to operational use of the data.

It is quite obvious from Fig. 59 that the turbulence generated in low discharge flows by rollers generated with low tailwaters contributes moderately low negative pressures and in one instance causes a very severe negative pressure. The potential damage, as represented by low negative pressures, is markedly increased with overtopping of the side walls as shown in Fig. 60.

2. The Sill Extension

The dimensional changes represented by the added sill and taps are shown in Fig. 17 and the pertinent transient pressure fluctuation data for the velocity of 29 mps prototype in Figs. 44, 46, and 61. The data for the high stage velocity of 37 mps prototype are shown in Figs. 45, 47, and 62. These studies were confined to two pressure taps, C 18b and L 18b. Tap C 18b, which would be 12.5 cm upstream of the extension lip in the prototype, was located at the "centerline." Tap L 18b was similarly positioned, but at the wall. The significant points from the low speed data are discussed below. The high speed data are discussed separately later.

a. Lower pressures are again obtained at the wall taps than at the centerline. With lateral flow only, negative pressures occurred only at the wall and existed for a variety of flow

conditions. The low negative value was -3.0 m. The addition of overtopping flow diminishes the pressure values, and negative values were quite general, with the lowest peak being -6.8 m. For the above lows the maximum negative ΔP values are -4.4 m and -9.5 m, which are 10.3 per cent and 22.2 per cent, respectively, of the dynamic head. There was one unique condition at the "centerline" tap that with the overtopping flow produced a ΔP of 10.2 m, or a coefficient of 33.3 per cent.

b. In general, for a given discharge, increasing tailwater stages with increased overtopping tends to raise the pressures. However, this was not always true.

c. When compared to analogous pressure taps on the original sill, the values appear to be much the same. However, the static pressure diagrams suggest that the pressure gradient is steeper on the sill extension, and probably a smaller area of the lip is exposed to negative pressures.

d. The pressures on the downstream side of the triangular sill were not measured, but the shape is considered highly favorable for increasing the pressures in this area to positive values. It should be noted that the area on the original sill which would be 50 cm downstream of the lip showed extremely low negative values for a wide range of flow conditions.

3. The Sill Eroded Two Meters

Pressure fluctuation tests were run on the eroded sill to determine whether the potential for cavitation damage was diminishing to the point of becoming self-arresting. Data were taken for a range of discharges and tailwater stages and for lateral flow and overtopping flow. Fluctuation measurements were made at taps C 13a upstream of the lip on the "centerline," L 13a upstream of the lip at the side wall, and C 13b downstream of the lip on the "centerline." All taps are located a distance which would be 12.5 cm from the lip in the prototype. Pressure data for these taps are contained in Figs. 48 through 51 and 63 through 65. The following can be noted from these data:

a. With only lateral flow, tap C 13a showed a scattering of moderate negative pressures. The greatest of these was -3.6 m. Wall tap L 13a showed no negative values. Tap C 13b downstream of the lip also showed a scattering of moderate negative pressures, the greatest of which was -4.5 m.

b. With the addition of overtopping flow, tap C 13a shows further worsening of the negative pressures. The greatest of these was -7.0 m. Wall tap L 13a showed only a single moderate negative pressure value. Tap C 13b downstream of the lip generally showed negative values of considerable strength. The greatest of these was -6.1 m.

In order to provide for somewhat easier assimilation of these data, they have been summarized graphically in Figs. 66 and 67. It is quite obvious from these plottings that a considerable potential for cavitation damage continues to exist for the case of overtopping flows and a marginal potential exists with lateral flow without overtopping.

4. The Influence of Increased Dam Height

Only limited pressure fluctuation tests were made for the 37 mps velocity which should result with the ultimate dam height. These data are shown in Figs. 35, 37, and 58 for the original sill and Figs. 45, 47, and 62 for the sill extension.

Measurements made 12 cm upstream of the lip on the "centerline" with only lateral flow showed a maximum negative pressure of -1.7 m. The turbulence contribution to the ΔP value gave an effect of 4.5 m, which was 6.5 per cent of the dynamic head. For the case of lateral flow with overtopping this tap gave a maximum negative pressure of -1.9 m, or a turbulence ΔP contribution of 7.9 m or 11.5 per cent of the dynamic head.

Measurements made 25 cm upstream of the lip near the wall with only lateral flow showed a maximum negative pressure of -5.4 m, or a turbulence ΔP contribution of 5.5 m or 8.0 per cent of the dynamic head. For the case of lateral flow with overtopping this tap gave a maximum negative pressure of -7.4 m or a turbulence ΔP contribution of 10.0 m or 14.5 per cent of the dynamic head.

Since a negative static head of -4 m was reported earlier for conditions at tap 18a with a flow of 8000 cms, the combination of this value with the -2.5 m from turbulence effects at a flow of 8000 cms (see Fig. 58) and no lateral flow gives a total of -6.5 m. This is for the flow without overtopping. It is evident that protective measures will be necessary to prevent damage.

C. Training Wall Pressure Tests

The pressure conditions existing in the observed damage areas at the end of the training wall were measured with transducers mounted at two points on the model. Tap L 21 was located on the side wall a distance above tap L 18 equivalent to 50 cm in the prototype. Tap L 23 was mounted in the vicinity of maximum damage near the top of the wall. The approximate positions of these taps are shown in Fig. 17.

No static measurements were made at these taps, but transient transducer measurements were made under a range of test conditions with results as shown in Figs. 40, 41, and 57. The following points can be gathered from these data:

1. Static pressure conditions at tap L 21, which are approximated by the average transducer pressure, are roughly in accord with the hydrostatic pressure which would be generated by the tailwater stage. Slightly greater values occur when overtopping takes place.

2. Static pressures at tap L 23 near the top of the wall at elev. 123 are roughly 2 m less than those at L 21, which is again an approximation of hydrostatic tailwater stages.

3. With only lateral flow at L 21 the lowest negative pressure was -2.7 m and 4.4 m below the static pressure. The latter value is 10.3 per cent of the dynamic pressure head. With overtopping and lateral flow the maximum negative value was -4.3 m, 9.2 m below the static pressure. The latter value is 21.5 per cent of the dynamic pressure head.

4. The values at tap L 23 with only lateral flow gave a maximum negative pressure of -6.7 m, which is 5.3 m below the static value or 12.4 per cent of the dynamic head.

5. With lateral flow and overtopping at L 23 the maximum negative pressure was -7.0 m, 9.3 m below static pressure or 21.7 per cent of the dynamic head.

6. It is again apparent that overtopping flows contribute substantially to the negative pressures and that they should be eliminated by raising the walls.

7. The maximum negative pressures are substantially lower at L 23 than at L 21 and are of a level generally considered to be damaging. This is in essential agreement with the observed damage evidence in Fig. 12.

8. Tests were not made at the high dam velocity of 37 mps, but if it is assumed that the same percentage of the dynamic head would occur with the higher velocities, very serious damage pressures can be expected to result for most flow conditions.

9. No tests were made with the Type C ramp modification applied to the side wall, but its use should lead to much the same type of localization of negative pressures as occurs with its application to the sill. With armoring of this localized area, stabilization of erosion should result. The wall should probably be eliminated downstream of the wall ramp and the ramp should be an extension of the sill ramp.

D. Bucket Lip Cavitation Erosion Tests

The occurrence of vapor cavitation in a flow on a hydraulic structure is the result of high velocity and curvilinear flow paths. On most structures the critical regions of three-dimensional curvilinear flow are too complex to be analytically predicted. They can, however, be located visually on a suitable model which actually cavitates, and the model can be experimentally altered to improve or eliminate the cavity as a source of trouble. There is an extensive history of use of such models to study many hydraulic flow problems.

In order to achieve reasonable simulation of the prototype cavities, such a model must be operated under a similar cavitation environment condition as measured by the cavitation parameter σ (see Appendix B). Since a model must be operated with velocities which are only a fraction of those

in the prototype, the environment pressure must also be suitably reduced to permit the attainment of a suitable σ value. Variable pressure test facilities permit this kind of control. In addition to this control the model conditions must reasonably simulate the existence of small gas bubbles which serve as the cavity nuclei, and surface tension effects and adequate time ratios must be provided in the model. If all these conditions can be reasonably simulated, the model becomes a useful tool in diagnosing and solving the cavitation problem.

Problems involving surface damage due to cavitation impose an additional requirement relative to model diagnosis. This is because not all cavities in a flow create boundary damage, only those whose trailing ends collapse in the immediate vicinity of a boundary. Isolation of this type of cavitation is accomplished most directly in a model whose surfaces are treated to indicate the presence of physical damage due to the cavity collapse action.

In view of the above, the Guri model was built to operate in a test facility which could provide reasonably high velocity and reduced pressures, and the region of the model known to sustain damage was built so as to show evidence of cavity collapse forces. For this purpose the model was built to fit in the largest variable pressure facility at St. Anthony Falls. This facility, which was described earlier and is shown in Fig. 13, permitted the use of a model of 1:78.7 size. The sill of the structure, which sustained the critical damage at Guri, was made of an annealed soft aluminum. These procedures, which had resulted in an effective model test in an earlier study at St. Anthony Falls [4], were employed in the first exploratory tests of the Guri structure.

Subsequent operation of this model established that cavitation could not be satisfactorily modeled. Later non-cavitating studies of the model using pressure taps pointed up two reasons why the cavitation model did not act as effectively here as in the earlier study [4]:

1. The reduced pressure regions which were actually low enough to support cavitation at Guri existed in a flow distance on the lip which was probably no longer than about 20 cm in the prototype. At a scale of 1:78.7 this distance would be only about 3 mm in the model.

2. Cavitation is a process which requires a suitable gas nucleus to pass through the lower pressure region. A cavity grows by vaporization as the nucleus enters the low pressure field and collapses as it condenses on leaving the low pressure field. This thermodynamic process of vaporization and condensation requires a certain minimum time span if it is to occur at all. In the brief time required to pass through the negative pressure region of the Guri model these thermodynamic processes apparently were not developed adequately, and vapor cavitation failed to occur.

In contrast, the relative success of cavitation modeling in the earlier study [4] can be attributed to a model with relatively large regions of negative pressure and a basic model ratio of about 1 to 8 as compared to the ratio of 1 to 78.7 employed in the Guri model.

In view of the failure to simulate cavitation in the Guri model, the remainder of the tests resorted to boundary pressure measurements on a non-cavitating model. This is a more time-consuming method of locating the cavitation, but had to be employed when true cavitation could not be properly generated.

V. CONCLUSIONS AND RECOMMENDATIONS

It is quite apparent from the earlier descriptions that the flow conditions which caused damage to the bucket lip at Guri were of a very complex form and sequence as a result of operating conditions. Since documented records of operating conditions were not available, it must be recognized that a laboratory investigation of cause and effect is necessarily somewhat speculative in nature. There are, however, certain logical reasons why damage by cavitation may occur, and those reasons were found to exist at Guri. Moreover, the limited and specific areas of the model which were found in laboratory tests to be capable of supporting cavitation damage were in general quite closely correlated with those regions which were actually damaged at Guri. While this agreement or correlation between model and prototype has been quite good, the model is not an exact simulation of the prototype, and the laboratory findings should be used conservatively. The following conclusions are believed to be a reasonable assessment of the model findings in combination with the known mechanics of cavitation.

1. It is the experience of various investigators that concrete structures exposed to high velocity flow will exhibit erosion in those areas in which the transient boundary pressure frequently falls below approximately one-half atmosphere (-4 to -5 meters of relative water head) and subsequently rises to a higher value. The erosion is generally caused by the formation and subsequent collapse of vapor cavities traveling close to a boundary. In the region of rising pressure, where the cavity ultimately collapses, a very small but intense pressure blow is delivered to the boundary. Most materials can be exposed to many thousands of cycles of blows before material erosion begins. Brief exposures to cavitation are usually not serious, but sustained exposure can prove very erosive.

2. In the flip bucket spillway at Guri, the only areas that exhibited significant erosive damage were those in which the laboratory pressure tests disclosed a capability to produce pulsing negative pressure values greater than approximately one-half atmosphere.

3. Vapor cavities which form in a low pressure region and collapse in a higher pressure region are the result of a combination of three sources of low pressure. The negative pressure dip of this combination of pressure sources is inherently transient in nature. This combination of three low pressures must occur in close proximity to a boundary if damage is to take place on the boundary.

4. The small-scale vorticity is inherent in any turbulent flow, but the powerful large-scale eddies that pulse on the boundary are the result of major upstream disturbances in the flow. These disturbances are generally impinging streams, hydraulic jumps or rollers, or separation vorticity shed by some upstream boundary irregularity.

5. In the Guri flip bucket two flow conditions appear to contribute powerful large upstream eddies near the bucket lip. These are (a) the impinging stream resulting from flow overtopping the wall and (b) the formation of a partial jump or roller when a high tailwater begins to back a low flow down into the bucket.

6. The turbulence due to flow overtopping the bucket side wall appears to be the strongest factor contributing to the negative pressure pulsations. An increase in the height of the walls to eliminate overtopping flow is a simple and practical solution to the reduction or elimination of this low pressure source, and it is recommended.

7. The presence of the very turbulent partial jump or roller in the downstream end of the bucket can be largely eliminated by (a) operating with a deeper flow in the bucket, thus sweeping the budding jump out of the bucket despite the high tailwater, or (b) depressing the tailwater stage so that back-up is reduced or eliminated. In addition to sweeping out the jump, a deeper flow in the bucket also tends to suppress the cavitation potential by increasing the static boundary

pressure contributed by the centrifugal action on the curved bucket. Cavitation damage can be minimized for a given discharge and tailwater stage by routing the flow via a reduced number of chutes to increase the flow depth. With adequate flow depth, sweepout of the jet can be achieved. A guide to these preferred operating conditions is shown in Fig. 59, which defines the areas in which the negative pressures occur. In general practice a negative pressure not lower than -3 m (-10 ft) is acceptable.

8. Lowering of the tailwater to reduce back-up in the bucket will substantially reduce the potential for cavitation damage. It is probable that natural degradation will, in the course of time, tend to lower the bed and the tailwater. However, this cannot be expected to provide early benefits. To the extent that it is practical, reduction of tailwater stages by downstream dredging is recommended.

9. Tailwater back-up effects can also be reduced by rebuilding the bucket to raise the lip above all normal tailwater stages. This is an expensive alternative that should be approached with caution. It should be noted (Fig. 22) that even with the tailwater pool completely removed, a velocity of 29 mps, corresponding to the existing dam head, produced a static lip pressure of -2 m, and a velocity of 37 mps, corresponding to the ultimate dam height, produced -4 m (not shown). Both of these were at a discharge of 8000 cms. If for a corresponding discharge a dynamic negative pressure of -2.0 m is taken from Fig. 52 for $V = 29$ mps and -2.5 m is taken from Fig. 58 for $V = 37$ mps, the total negative values are about -4 m and -6.5 m, respectively. Both of these are potentially damaging pressure values. If discharges less than 8000 cms had been included in the data, it is probable that even lower negative totals would have resulted.

It should be noted that raising the bucket lip above the existing elevation of 121.23 m would involve substantial changes in the dimensions and shape of the bucket exit. Such changes would require additional experimental model studies for clarification of their performance characteristics.

10. Early damage evidences as shown in Fig. 10 indicate that some damage did occur initially near the center of the lip. Such damage is well away from the side walls and probably beyond the region of turbulence pulse generation by wall overtopping flows. This damage could be due to turbulence generated by rollers in the bucket, but since it occurred only in certain areas along the sill, it may be associated with certain patterns of upstream flow. This suggests that wave actions and separation vortices from the crest gates and piers (see Figs. 1, 4, 5, and 6) may in some instances create sufficient localized turbulence in the bucket to support damage. Hence it is recommended that in field operations, the number of gates and the gate openings be selected to minimize the generation of discrete waves and turbulence centers. The damage alleviation measures suggested in items 7, 8, and 9 are also applicable to center sill damage.

11. In addition to the foregoing transient sources of negative pressures, consideration must be given to minimizing those boundary areas which inherently possess low mean static pressures as a consequence of high velocity flow. Damage evidence, together with analytical studies of boundary pressures, indicates that the only boundary region having a potential for low static pressure is the lip of the bucket. In this region, the protective high centrifugal pressures of the curved bucket end quite abruptly, and transition must be made to the pressure of the atmosphere. The test data indicate that, with one exception, the pressures in this region never become subatmospheric. The one exception is the extreme end of the lip when low flows are discharged with the lip above tailwater. In this instance, a subatmospheric pressure of about -2 m occurred for a chute velocity of 29 mps, and approximately -4 m of negative pressure occurred for the chute velocity of 37 mps consistent with the ultimate dam height.

12. Tests indicate that provision of a lip piece which presses slightly into the flow as shown in Fig. 17, Type C, will generate sufficient positive dynamic pressure to suppress the normal negative transients and confine them to the extreme lip of the extension. The lip shape reforms the flow for an appreciable distance upstream. The new form of flow generates substantially higher static pressures on the upstream boundary to alleviate cavitation damage.

13. To doubly protect the critical lip area, it is suggested that the reshaped lip piece be fabricated of a metal known to have high resistance to cavitation pitting and adequate resistance to the water conditions at Guri. A suitable stainless steel is recommended.

14. Although the extent of the lip area which is subjected to cavitation erosion is very small, it is important that erosion be prevented from forming at the initial edge of the lip. This is true because of the progressive nature of the erosion once it starts. This non-arresting or progressive nature is demonstrated by both the history of erosion in field observations and the continuing presence of low negative lip pressures in the model studies of eroded lips. The model studies confirm the field observations that cavitation damage potential was greater for a sill eroded down 4 m than for the original sill configuration.

15. A very large vortex in the tailwater pool generates a strong lateral flow across the end of the spillway. The complex flow which exists under the jet sheet as it leaves the bucket lip is not fully understood, but the presence of the lateral flow moderately depresses pressures on the bucket lip and probably contributes to the cavitation damage. There appears to be no simple way in which this flow can be significantly reduced.

Elevation of the sill to a position above the tailwater can, however, nullify the influence of the lateral flow.

16. In the model studies of the original sill configuration, damaging low pressures were found on the bucket immediately upstream of the lip. However, the transient pressures on the sill and just a short distance downstream of the lip and near the wall were even lower. The static pressures at sill tap L 19 were positive when only lateral flow existed, but became moderately negative when overtopping flows were added. However, when these same flows were examined for their transient dips, very severe negative pressure values were observed. They constitute the pressures of greatest potential damage for the entire spillway and are the source of the very low pressure dip shown in Figs. 59 and 60.

The triangular extension was added to the sill primarily to correct the low negative pressures on the bucket floor. However, the sloped ramp on the downstream side of the sill extension should enhance sill pressures in a manner similar to that achieved by the upstream ramp. However, the very complex nature of the tailwater flow over the sill precludes any decisive speculation as to the resulting sill pressure.

17. An attempt to model the actual formation and collapse of vapor cavities was unsuccessful in these tests. In retrospect, this has been traced to the very small flow length to which the expansion and collapse of the cavities at Guri must be confined. The pressure diagrams (such as Fig. 20) indicate that the physical length of the negative boundary pressure region in the prototype is probably less than 1/10 m long. At a scale of 78.7, this region is probably less than a few millimeters in the model. Since cavity formation and collapse require a definite time span for the thermodynamics of vaporization and condensation, cavities should not be generated with the conditions prevailing in the small Guri model. Successful modeling of cavitation has been achieved with other, larger models in the

cavitation facility at St. Anthony Falls, but the duration of negative pressures proved too brief with the lip conditions prevailing on the Guri model.

18. Pressure measurements on the training wall for the low dam velocity indicate that near the top of the wall damaging levels of negative pressure generally exist with overtopping flows and exist for many flow conditions even without overtopping. At a level near the sill, damaging negative pressures exist with overtopping flow, but are probably not serious without overtopping. However, at the ultimate high dam velocity, damage would probably occur at most flow conditions even without overtopping. It appears that the damaging conditions on the side wall would be alleviated by the same measures which might alleviate damage on the bucket, to which conclusions 7 through 15 apply. It is recommended that the revised wall be terminated at a line beginning at the bucket sill and rising from the sill at an angle. The angle should be 45° with the horizontal, sloping upstream. The end of the wall should be fitted with the same form of extension as was recommended for the sill in conclusions 12 through 14.

19. The model pressure tests with the sill eroded to two and four meters below the original configuration continued to show negative pressures equal to or greater than those found in tests of the original sill. In other words, there was no evidence that cavitation would become self-arresting as erosion proceeded. This was true for test conditions both with and without wall overtopping flows. Negative pressure conditions were not too severe with the sill eroded two meters, but were very severe when it was lowered to four meters, and high rates of erosion are probable.

VI. ACKNOWLEDGMENTS

The investigation at the St. Anthony Falls Hydraulic Laboratory of the University of Minnesota was conducted for the Harza Engineering Company of Chicago serving as consulting engineers for the Corporacion Venezolana de Guayana of the Republic of Venezuela.

John F. Ripken and Warren Q. Dahlin served as principal investigators for the Laboratory. The motion picture record of the tests was prepared by Warren Q. Dahlin with the assistance of William M. Dingman. Narration of the film was by Edward Silberman.

David S. Louie and Hans Hasen represented the Harza Engineering Company in the many consultations which were held at the St. Anthony Falls Hydraulic Laboratory.

A briefing on the investigation was held at the Laboratory on October 28, 1971. In addition to Laboratory staff members, G. Chavarri of the Corporacion Venezolana de Guayana and David S. Louie, Hans Hasen, and Russell S. Roddy, Jr., of the Harza Engineering Company attended this meeting.

LIST OF REFERENCES

[1] Anderson, A. G. and Charbonneau, A. L., Guri Hydroelectric Project Report on the Second Stage Diversion and Flow Characteristics of the Spillway, Project Report No. 79, St. Anthony Falls Hydraulic Laboratory, University of Minnesota, 1966.

[2] Balloffet, A., "Pressure on Spillway Buckets," Journal of the Hydraulics Division, ASCE, Vol. 87, No. HY5, September 1961.

[3] Lenau, C. W. and Cassidy, J. J., "Flow through Spillway Flip Bucket," Journal of the Hydraulics Division, ASCE, Vol. 95, No. HY2, March 1969.

[4] Ripken, J. F. and Hayakawa, N., "Cavitation in High-Head Conduit Control Dissipators," Journal of the Hydraulics Division, ASCE, Vol. 98, No. HY1, January 1972.

LIST OF FIGURES

Figure

Figure

Figure

Figure

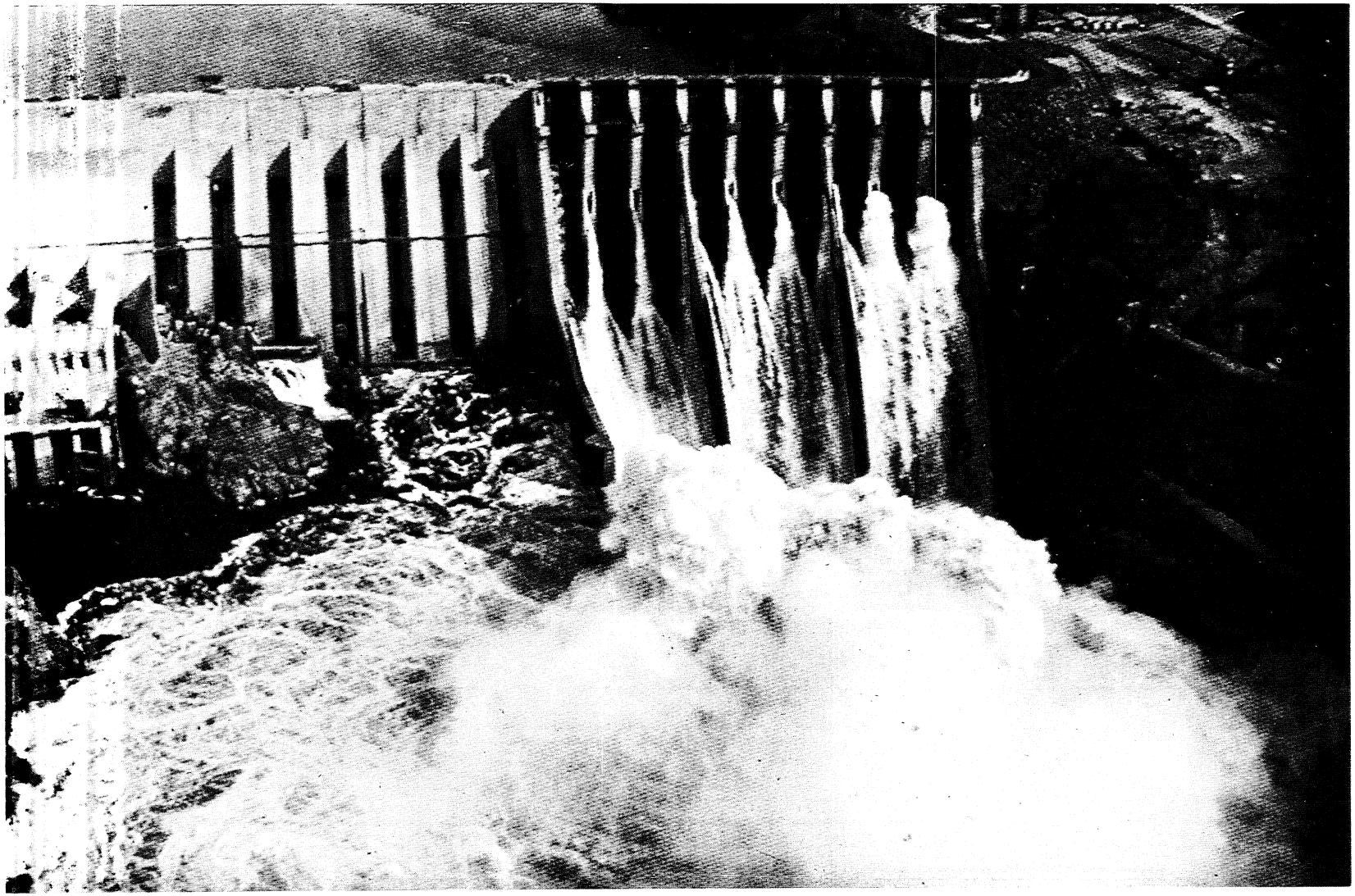

Fig. 1 - Air View of the Guri Spillway in Operation (from Engineering News-Record)

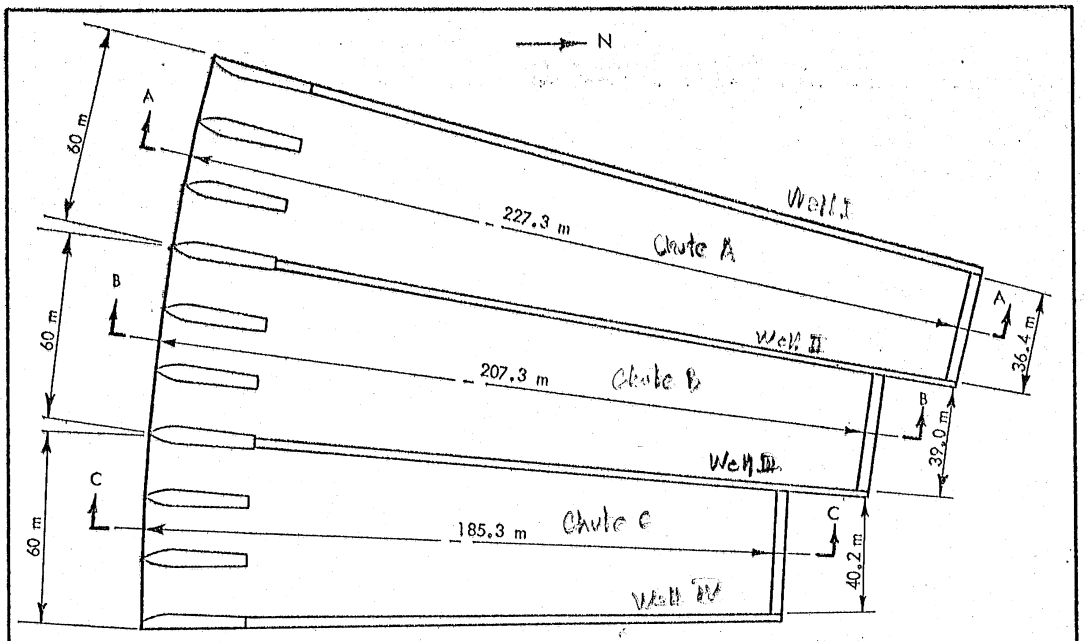

Fig. 2 - Plan View and Pertinent Dimensions of the Guri Spillway

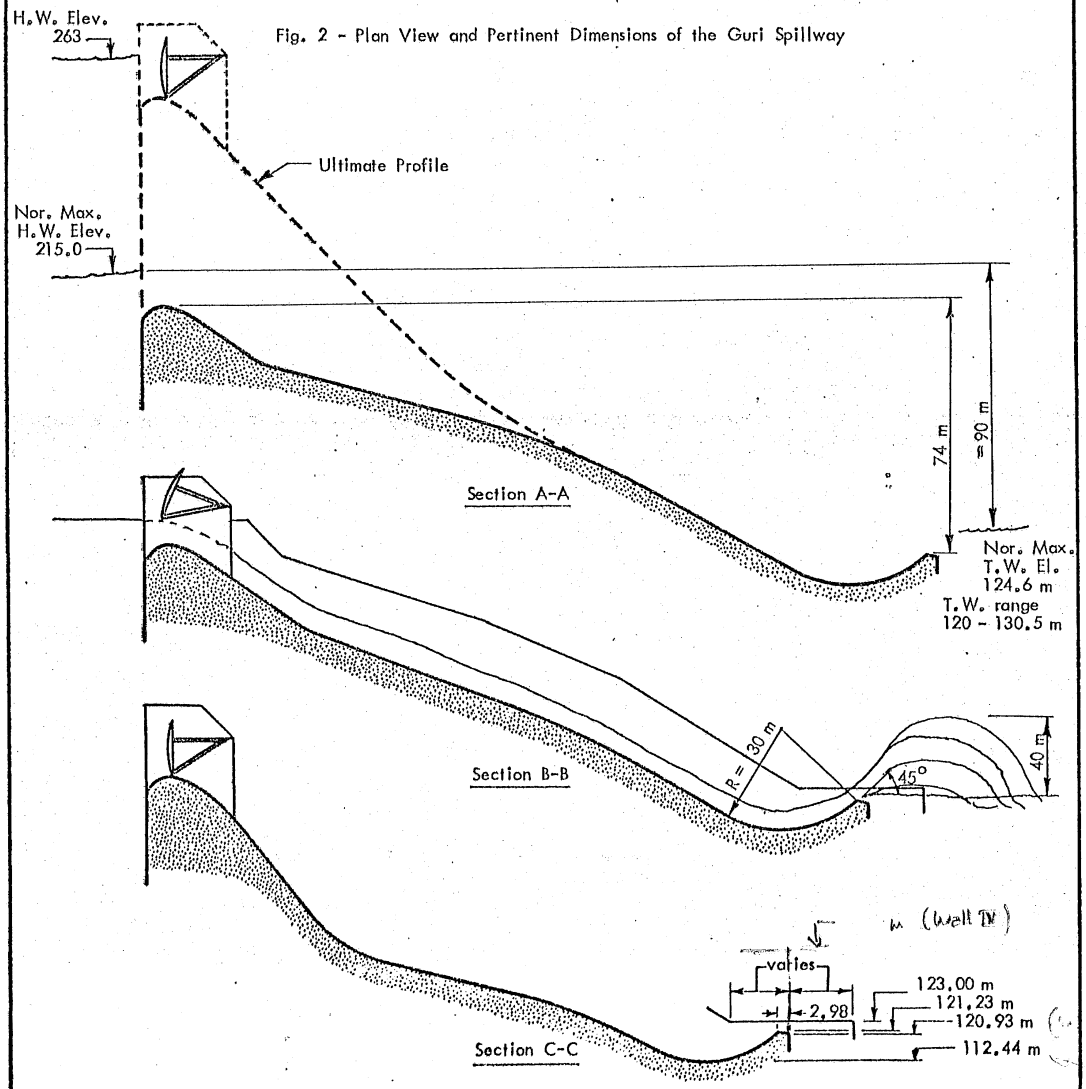

Fig. 3 - Chute Profiles and Pertinent Dimensions of the Guri Spillway

Figs. 2 and 3

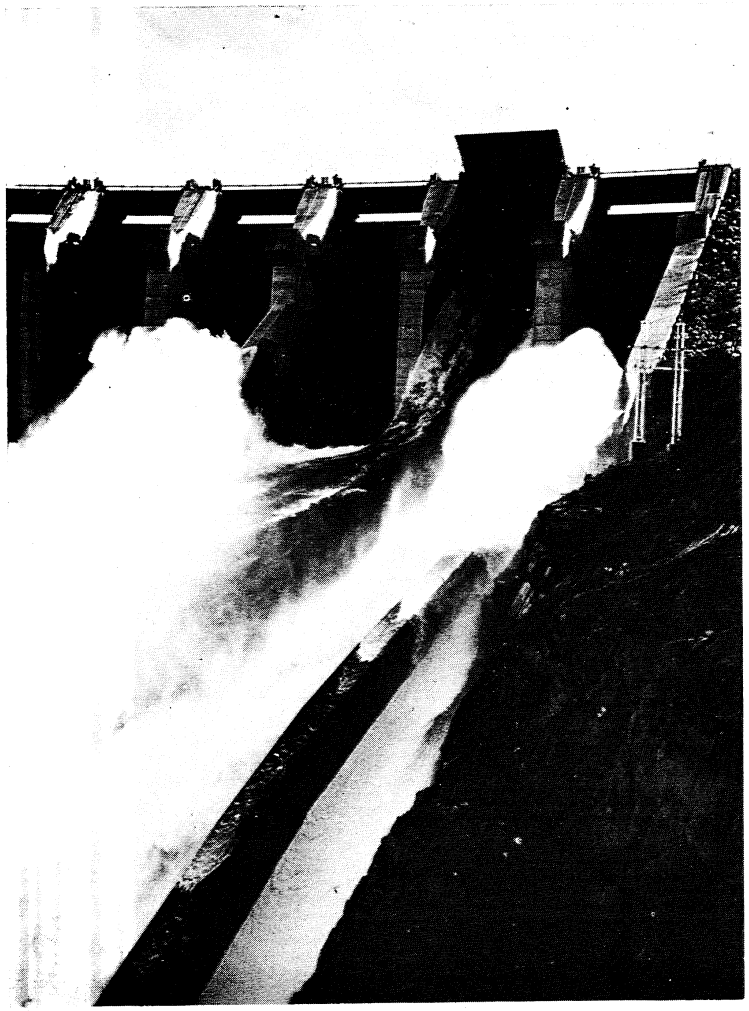

Fig. 4 - Spillway Discharge in the West Chute with Release from One Gate (Harza Engineering Co.)

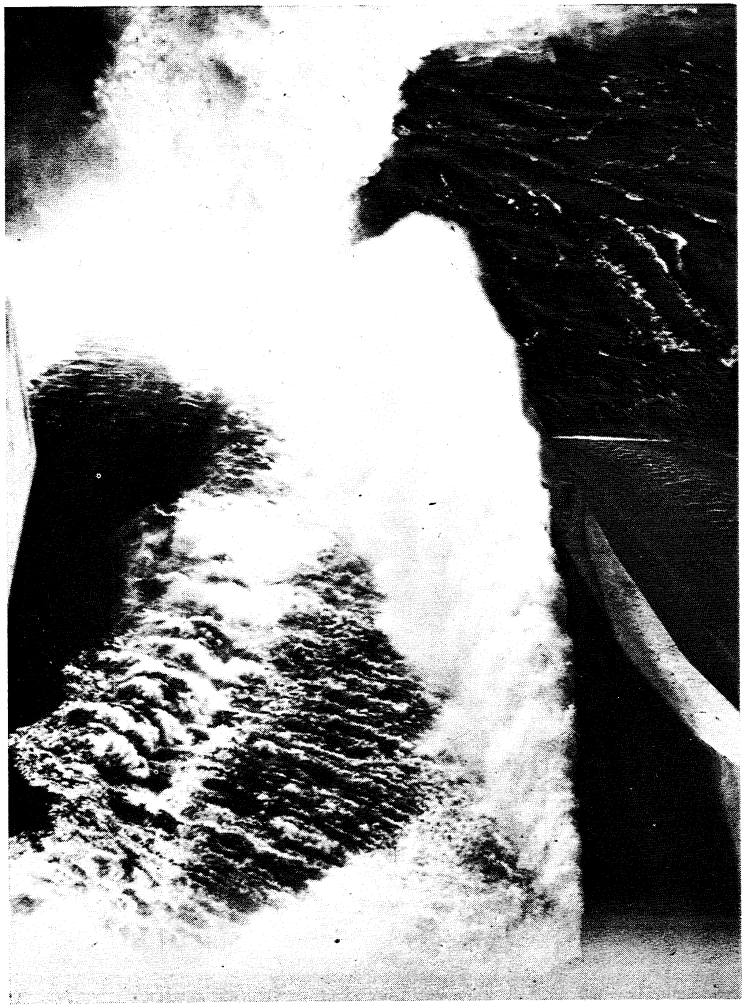

Fig. 5 - Spillway Discharge in One Chute as viewed from the Crest with Release from One Gate (Harza Engineering Co.)

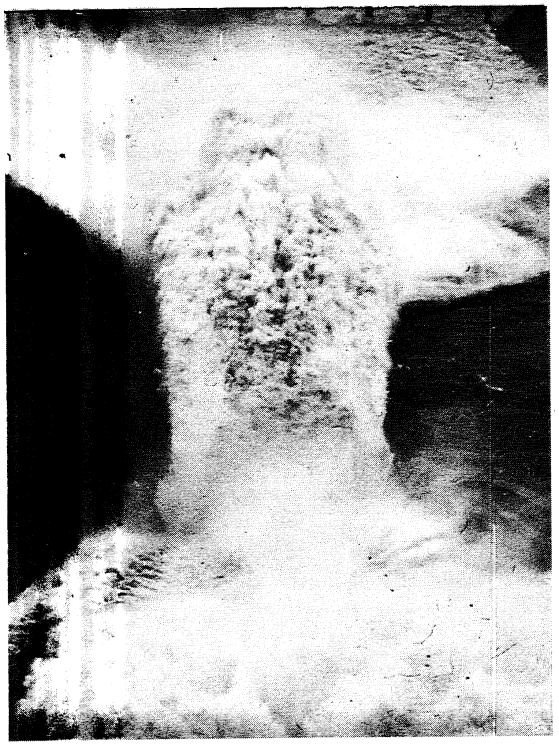

Fig. 6 - Spillway Discharge in the West Chute as viewed from the Crest with Release from Three Gates (Harza Engineering Co.)

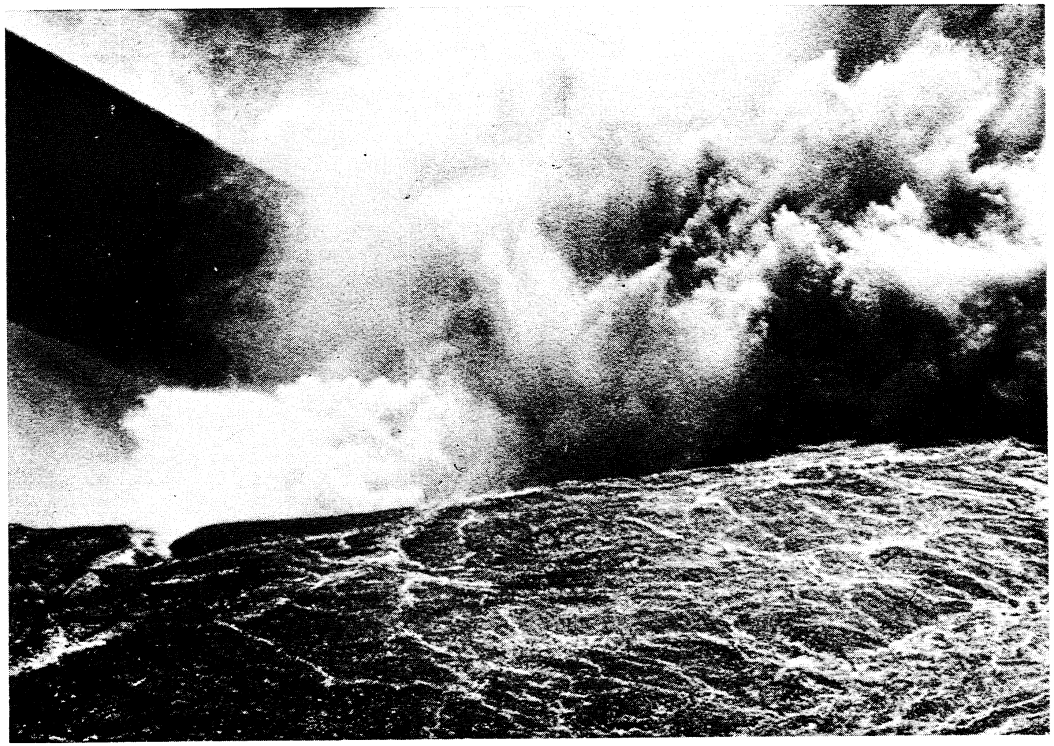

Fig. 7 - Flip Bucket Discharge from the Center Chute with Flow Overtopping the Lower East Training Wall about 3.5 meters (Harza Engineering Co.)

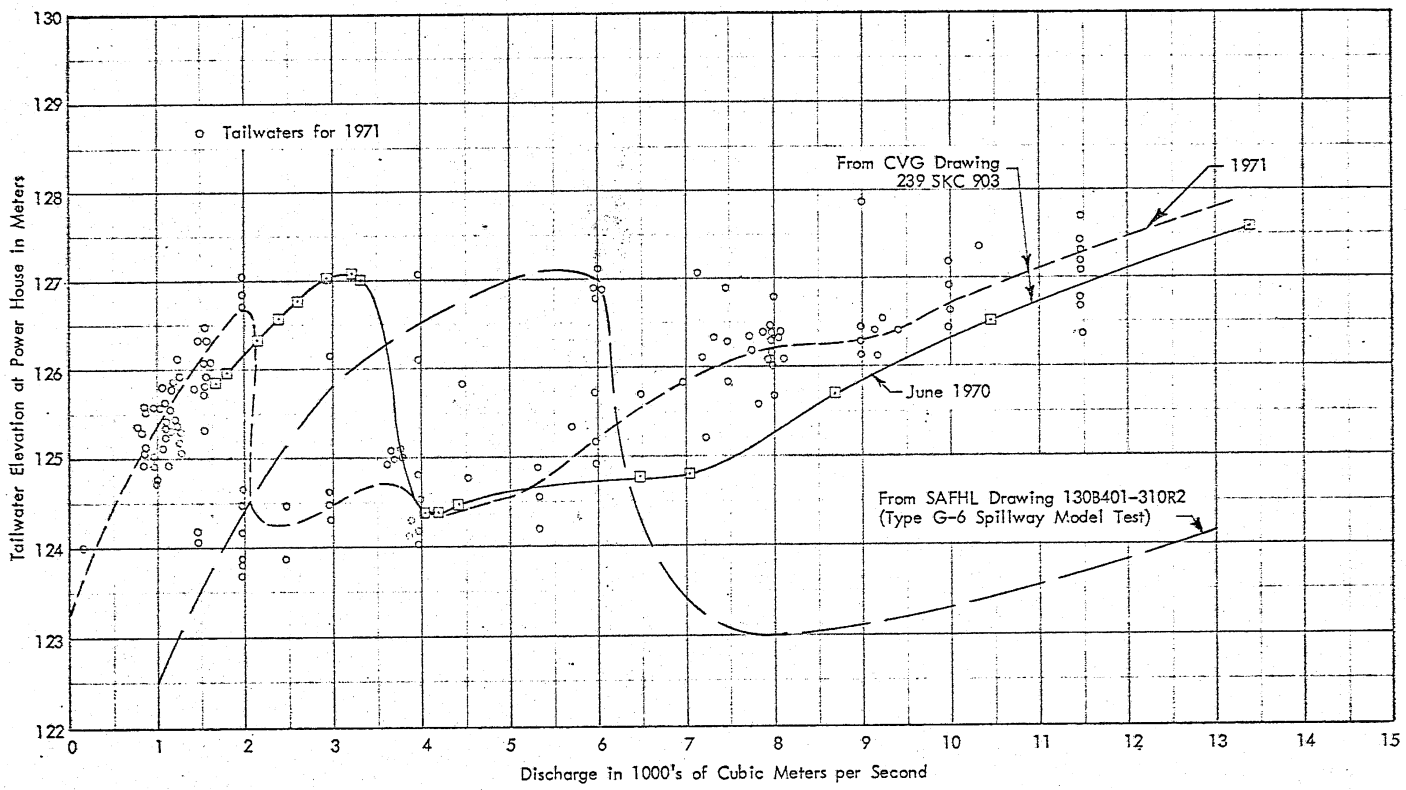

Fig. 8 – Tailwater Stages vs. Smaller Discharges at the Guri Powerhouse

Fig. 8

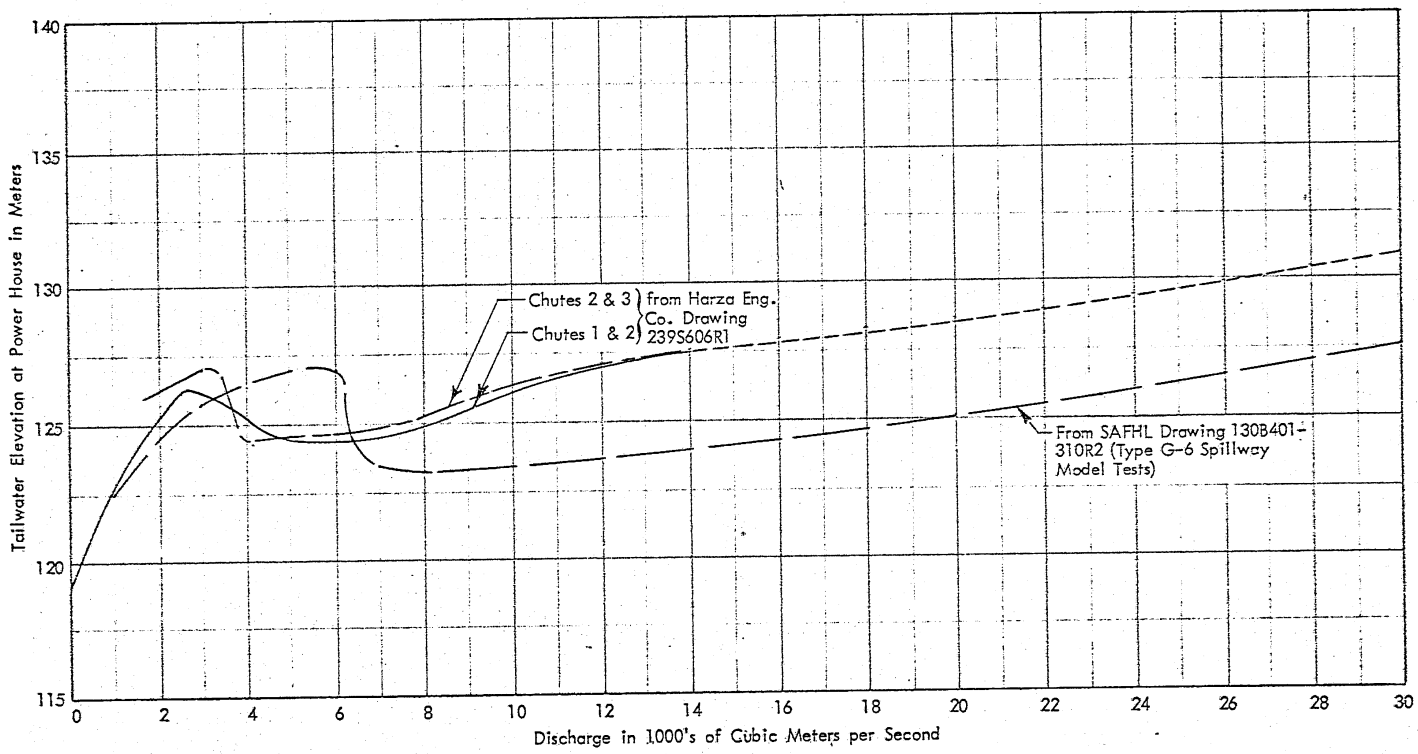

Fig. 9 – Tailwater Stages vs. Larger Discharges at the Guri Powerhouse

Fig. 9

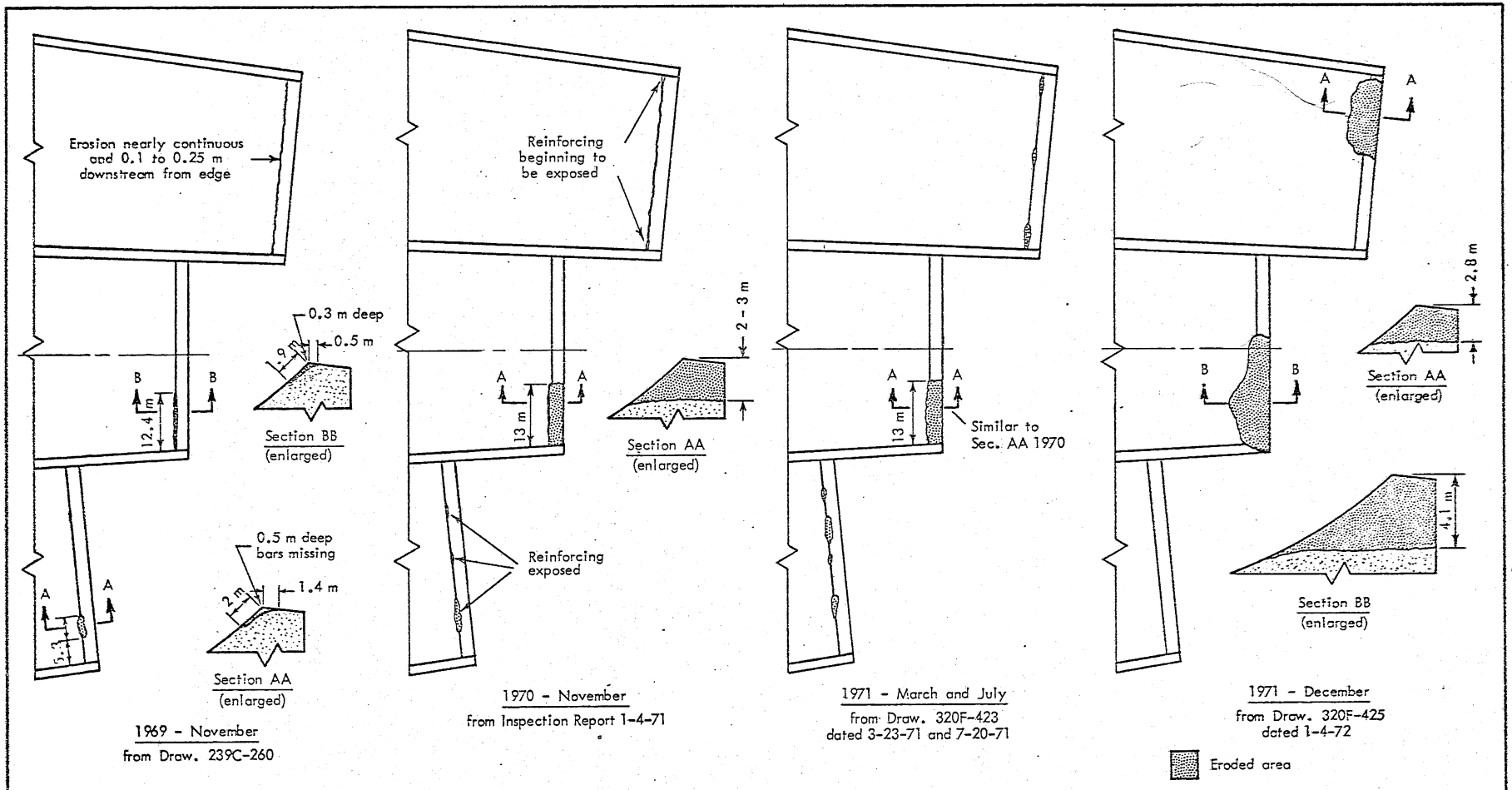

Fig. 10 - Plan and Sectional Views of the Location and Extent of Erosive Damage on the Spillway Bucket Lip

Fig. 10

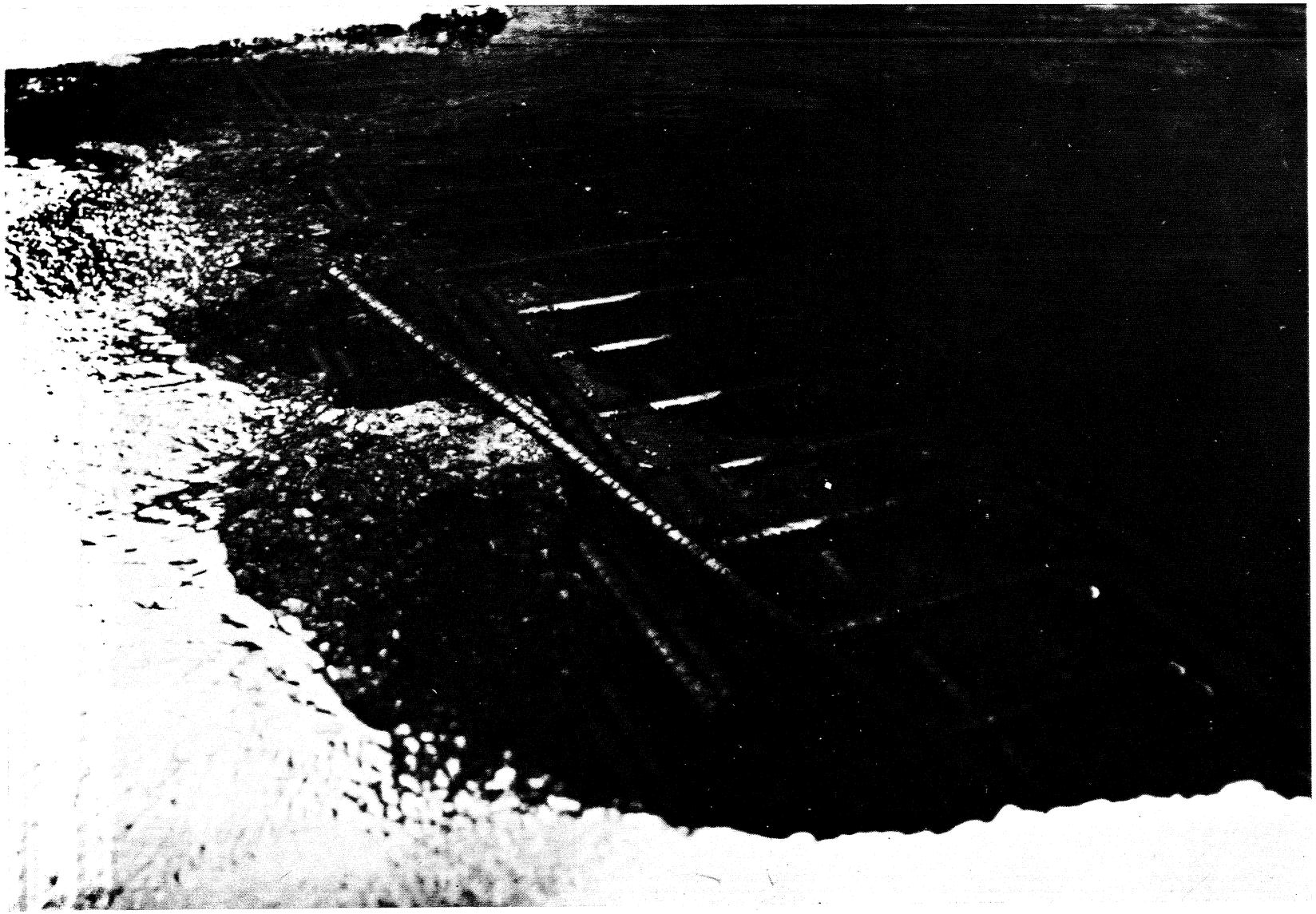

Fig. 11 - Photo of the Damage Sustained by the Sill of the East Chute in 1969 - Normal Flow from Right to Left (Harza Engineering Co.)

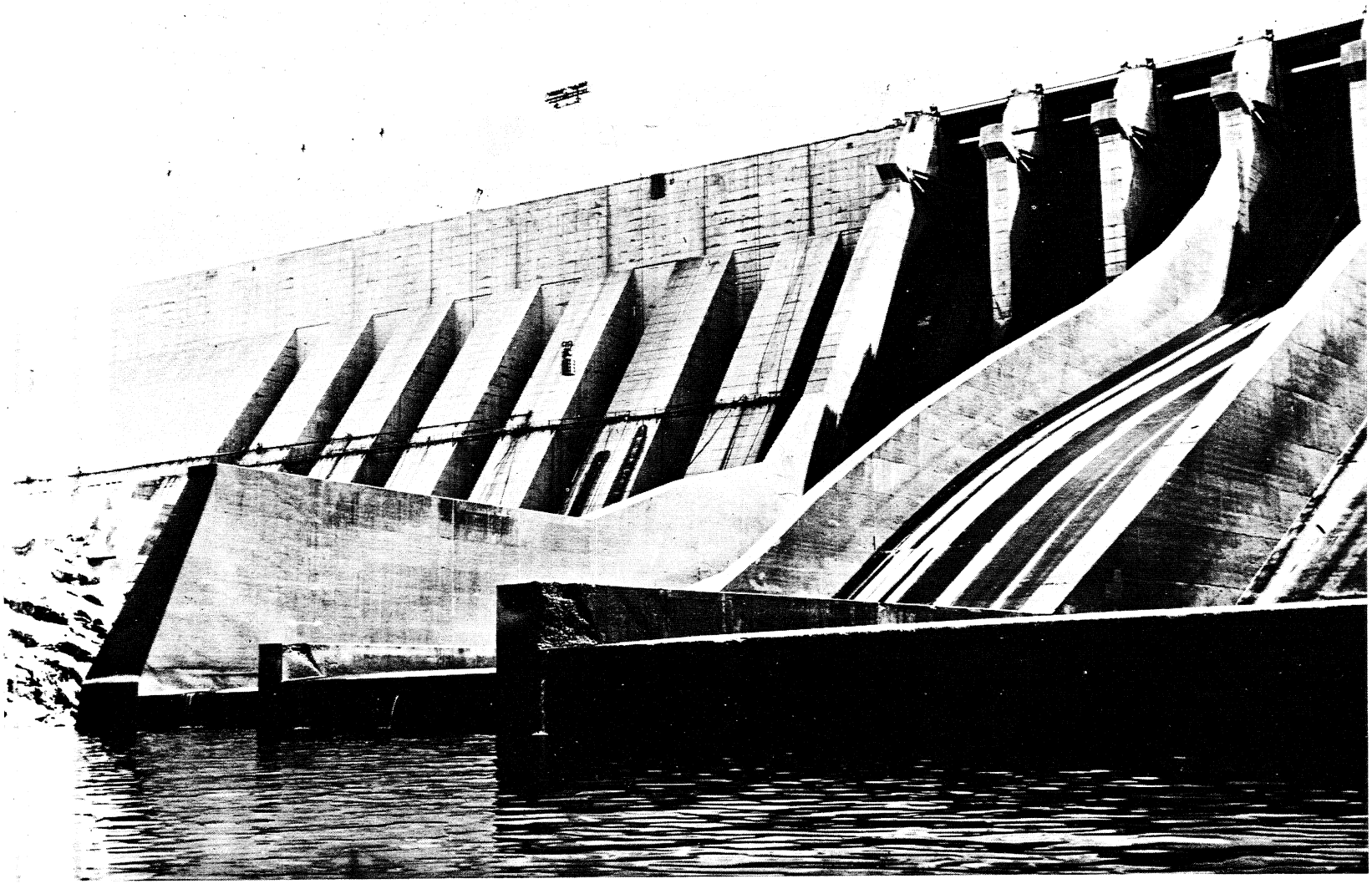

Fig. 12 - Downstream View of the Spillway Sill showing Erosive Damage on the Training Walls (Harza Engineering Co.)

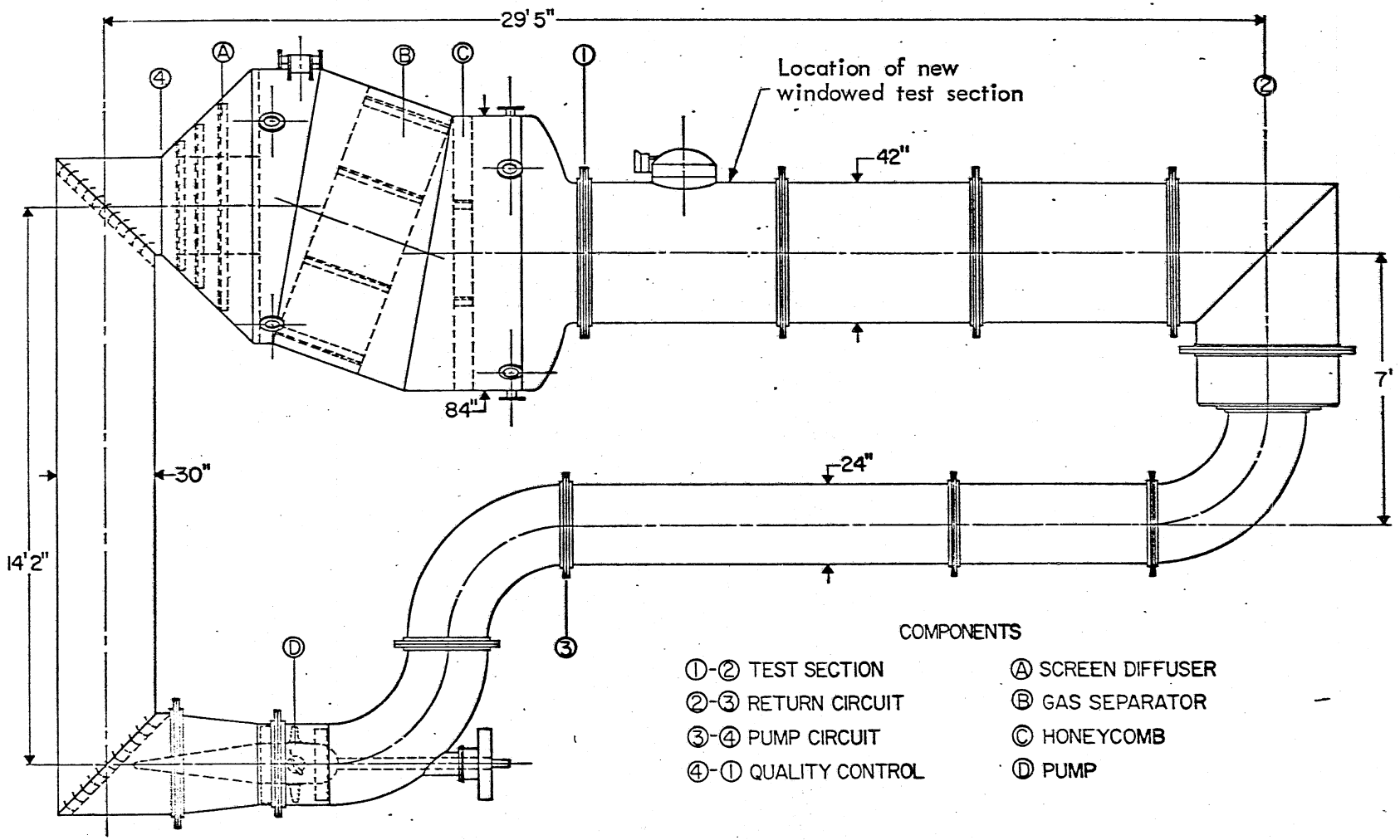

Fig. 13 - The 108 cm (42 inch) Recirculating, Variable Pressure Water Tunnel at St. Anthony Falls

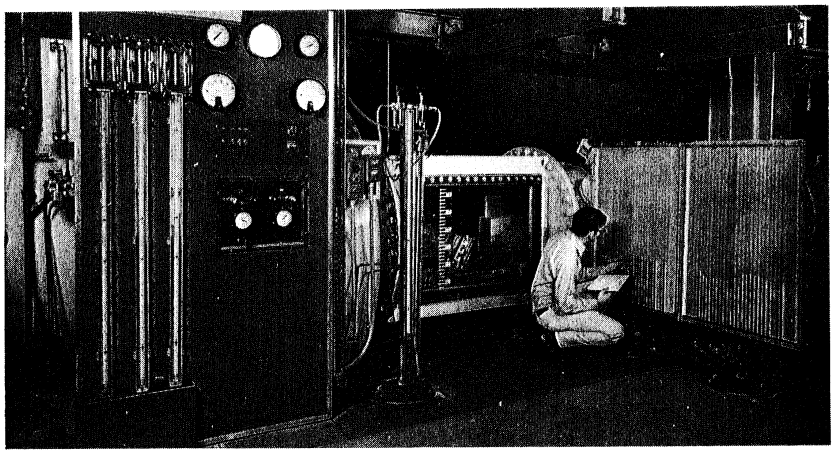

Fig. 14 - (Ser. No. 130-963) The Tunnel with Rectangular Windowed Test Section and Mounted Spillway Model connected for Manometric Static Pressure Readout

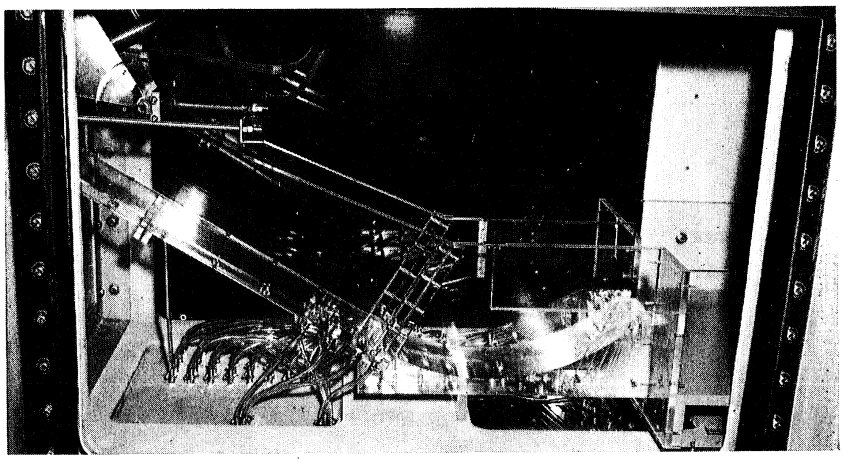

Fig. 15 - (Ser. No. 130-960) The Flip Bucket Model as seen through the Test Section Window

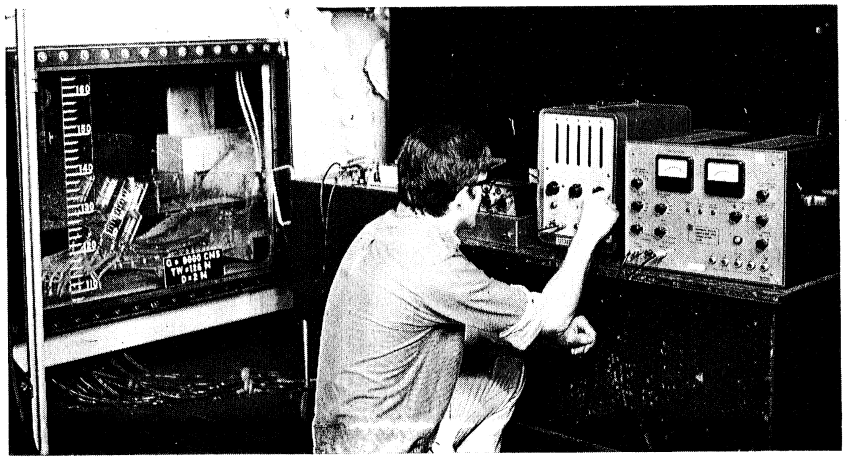

Fig. 16 - (Ser. No. 130-967) The Operating Flip Bucket Model Equipped for Electronic Readout of Transient Pressures

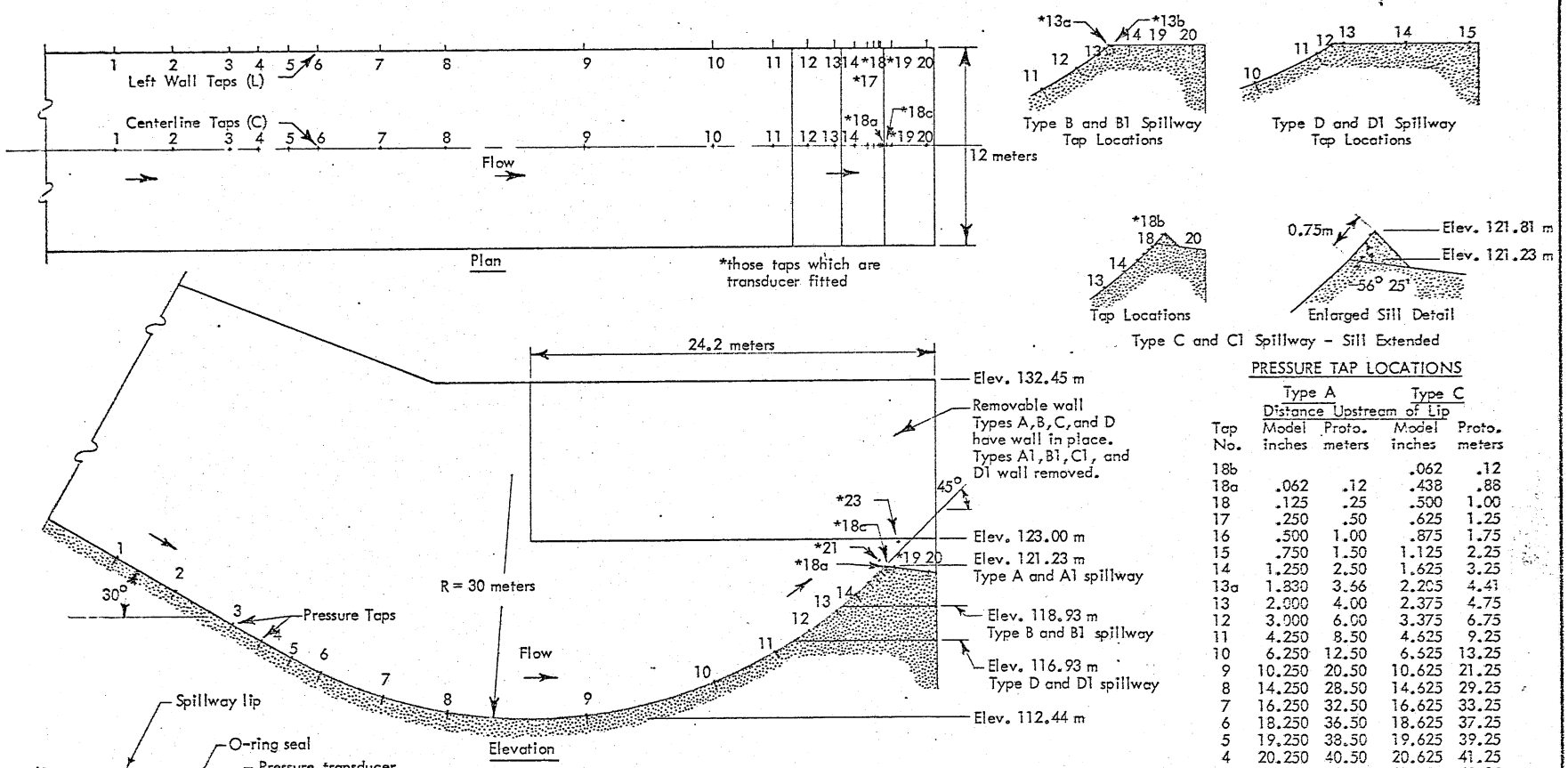

Fig. 17 - Sill and Wall Configurations and Pressure Tap Locations for the Various Types of Spillway Test Arrangements Modeled

PRESSURE TAP LOCATIONS

Tap No.	Type A Distance Upstream of Lip Model inches	Type A Proto. meters	Type C Model inches	Type C Proto. meters
18b			.062	.12
18a	.062	.12	.438	.88
18	.125	.25	.500	1.00
17	.250	.50	.625	1.25
16	.500	1.00	.875	1.75
15	.750	1.50	1.125	2.25
14	1.250	2.50	1.625	3.25
13a	1.830	3.66	2.205	4.41
13	2.000	4.00	2.375	4.75
12	3.000	6.00	3.375	6.75
11	4.250	8.50	4.625	9.25
10	6.250	12.50	6.625	13.25
9	10.250	20.50	10.625	21.25
8	14.250	28.50	14.625	29.25
7	16.250	32.50	16.625	33.25
6	18.250	36.50	18.625	37.25
5	19.250	38.50	19.625	39.25
4	20.250	40.50	20.625	41.25
3	21.250	42.50	21.625	43.25
2	23.250	46.50	23.625	47.25
1	25.250	50.50	25.625	51.25
	Distance Downstream of Lip			
18c	.062	.12		
19	.250	.50		
20	1.250	2.50	1.150	2.30

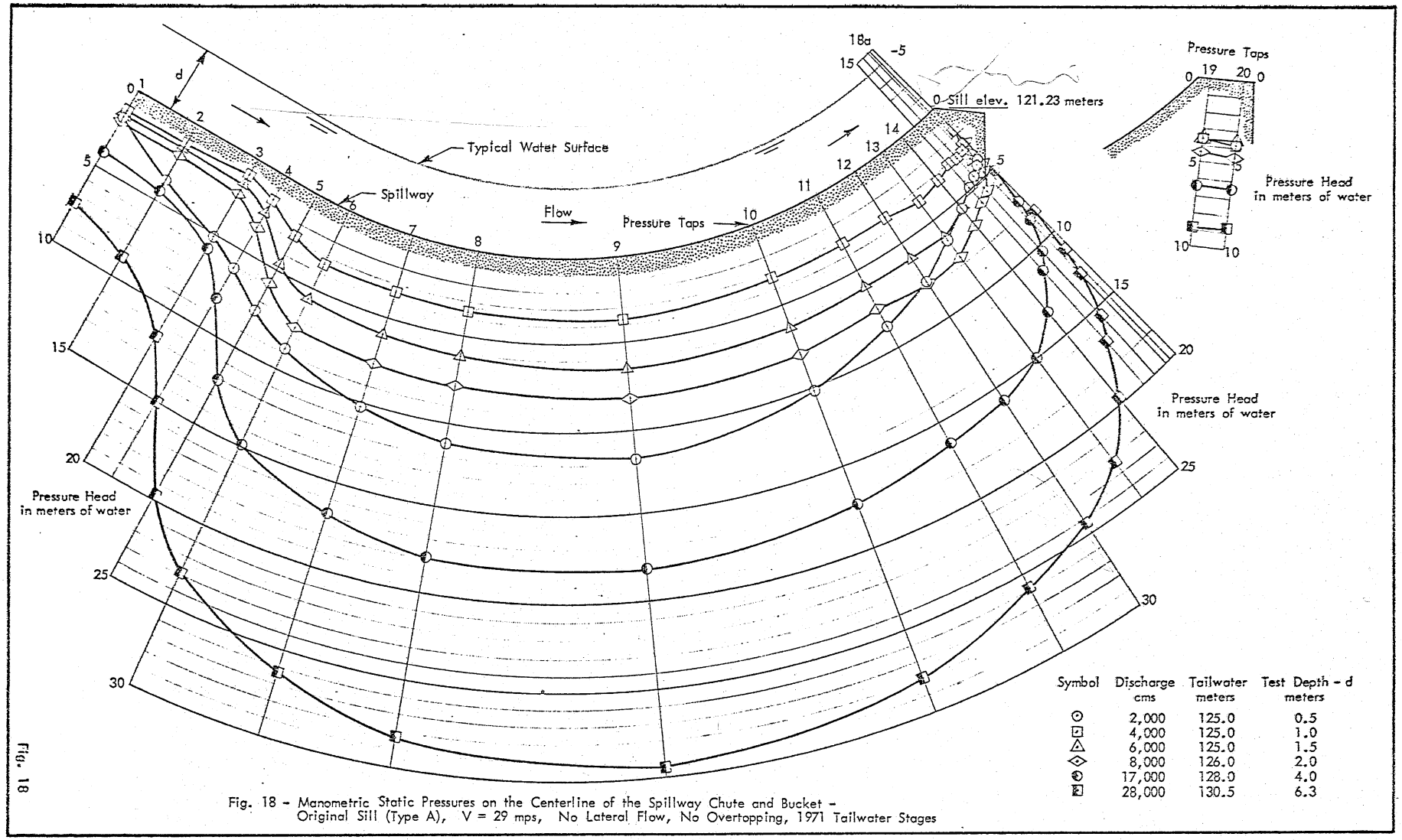

Fig. 18 - Manometric Static Pressures on the Centerline of the Spillway Chute and Bucket - Original Sill (Type A), V = 29 mps, No Lateral Flow, No Overtopping, 1971 Tailwater Stages

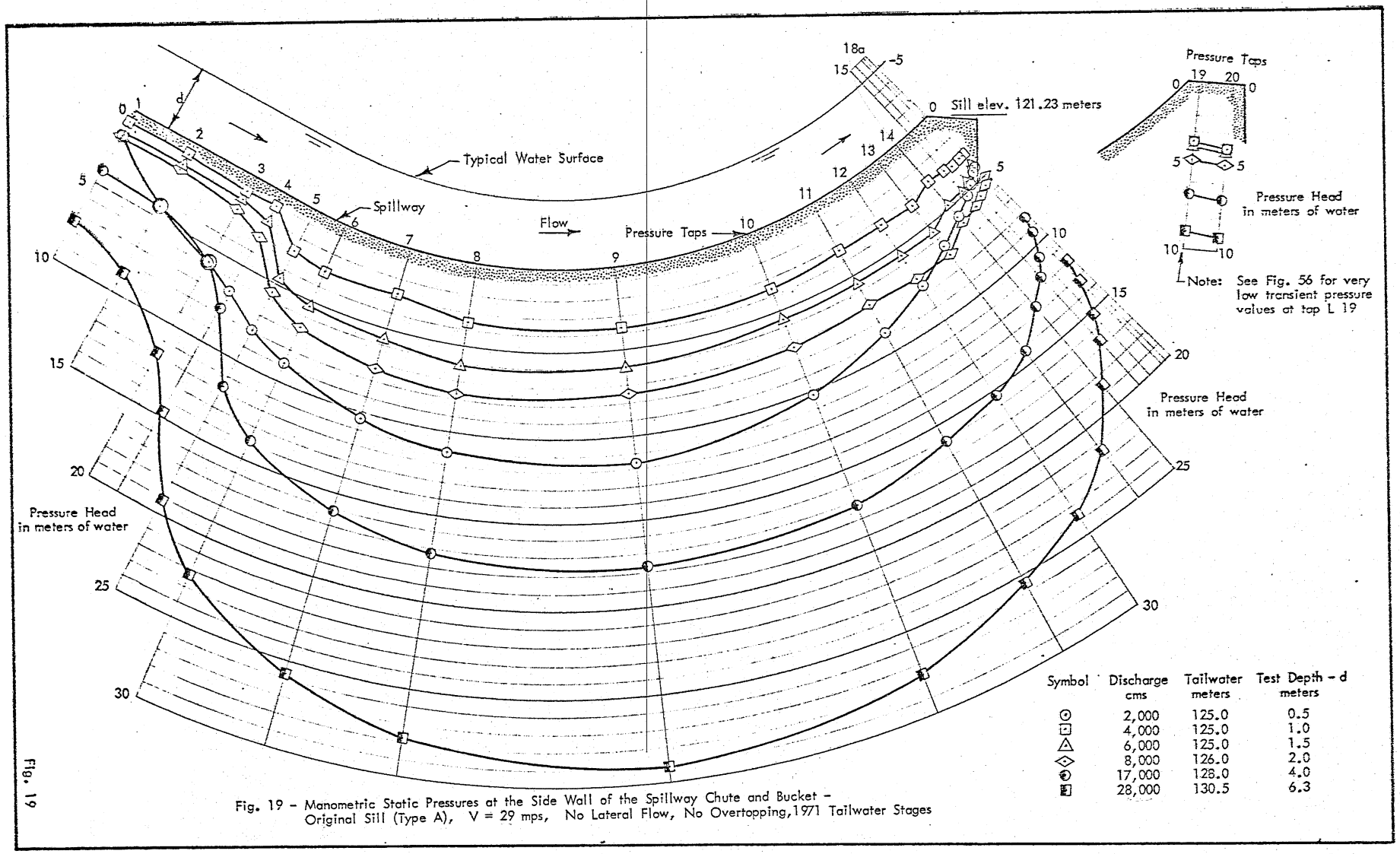

Fig. 19 - Manometric Static Pressures at the Side Wall of the Spillway Chute and Bucket - Original Sill (Type A), V = 29 mps, No Lateral Flow, No Overtopping, 1971 Tailwater Stages

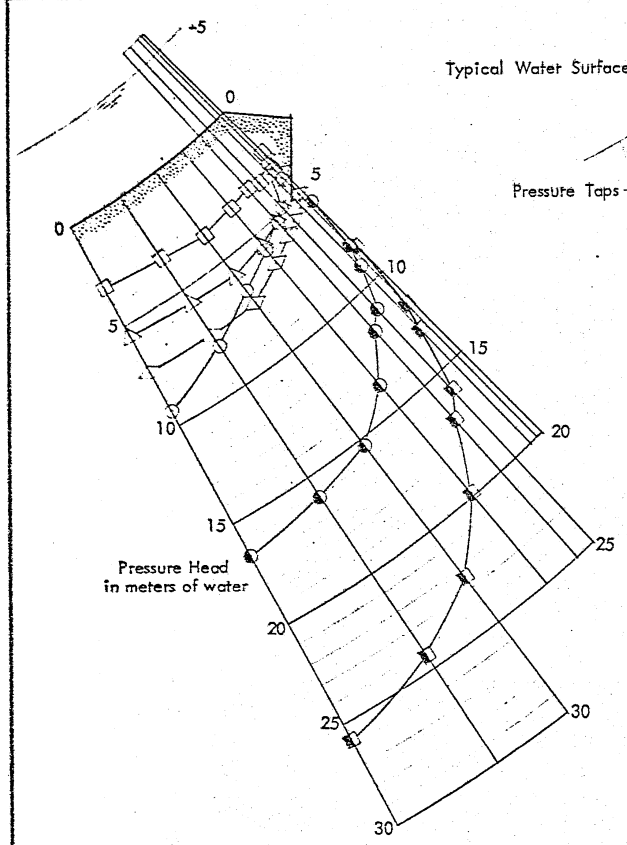

Type A Spillway - With Lateral Flow

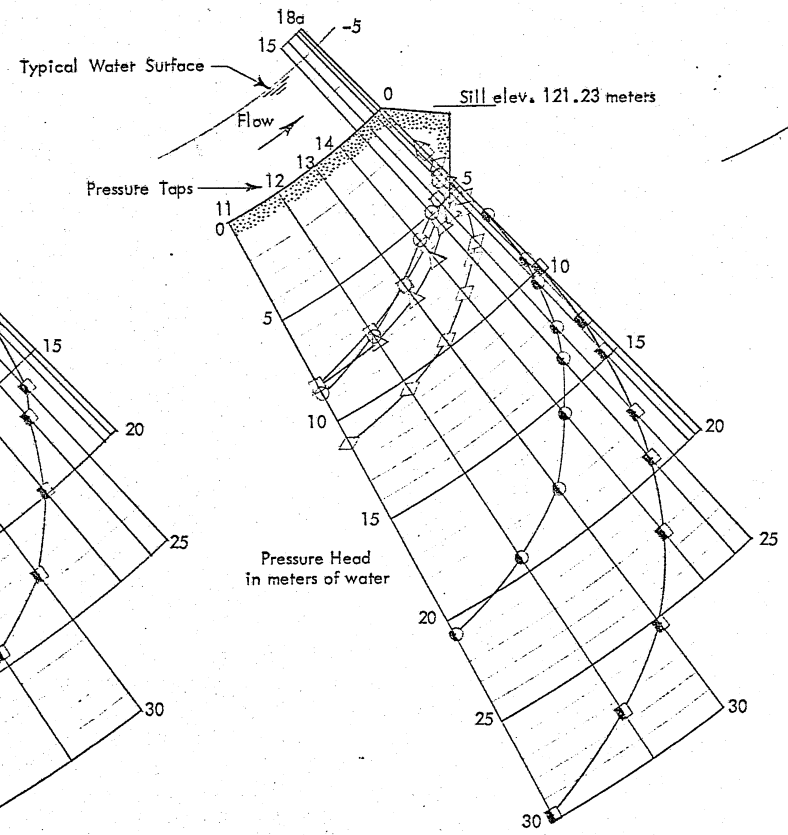

Type A1 Spillway - Overtopping

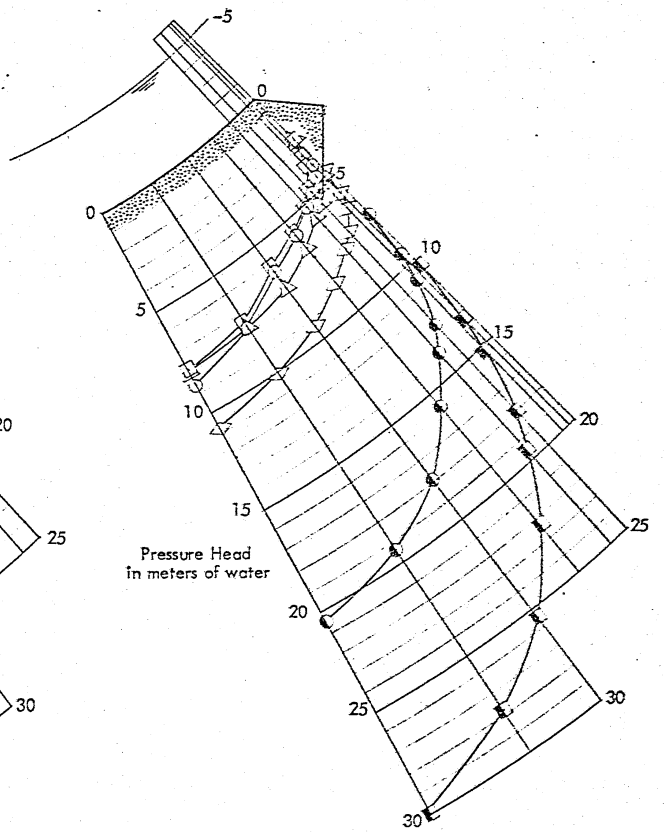

Type A1 Spillway - Overtopping with Lateral Flow

Symbol	Discharge cms	Tailwater meters	Test Depth - d meters
⊙	2,000	125.0	0.5
⊡	4,000	125.0	1.0
△	6,000	125.0	1.5
◇	8,000	126.0	2.0
⊙	17,000	128.0	4.0
⊞	28,000	130.5	6.3

Fig. 20 - Manometric Static Pressures on the Centerline of the Bucket Exit - Original Sill (Type A), V = 29 mps, Lateral Flow, Overtopping, 1971 Tailwater Stages

Fig. 20

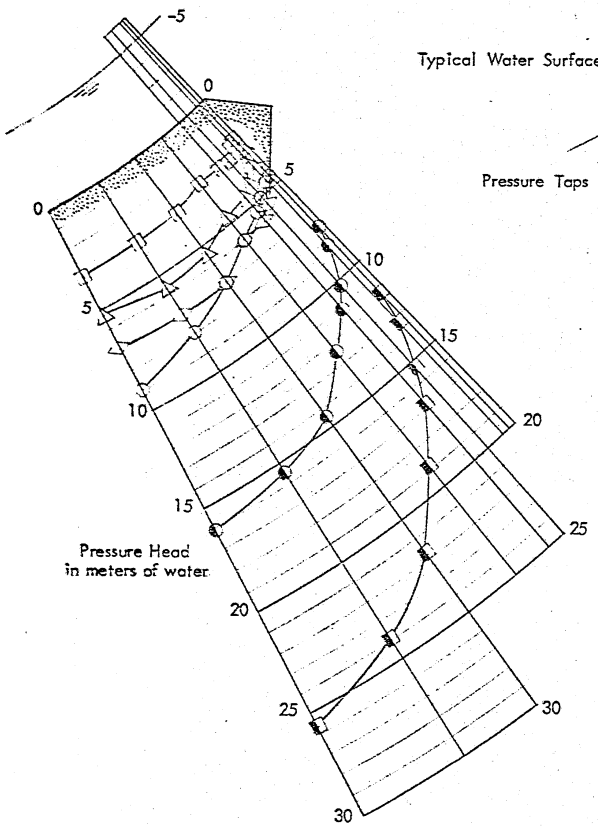

Type A Spillway - With Lateral Flow

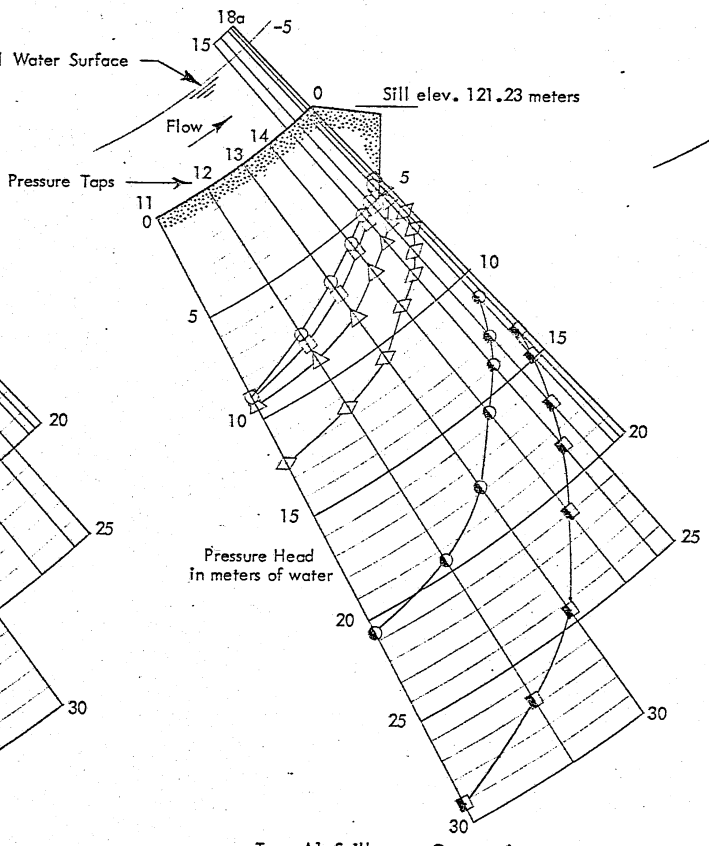

Type A1 Spillway - Overtopping

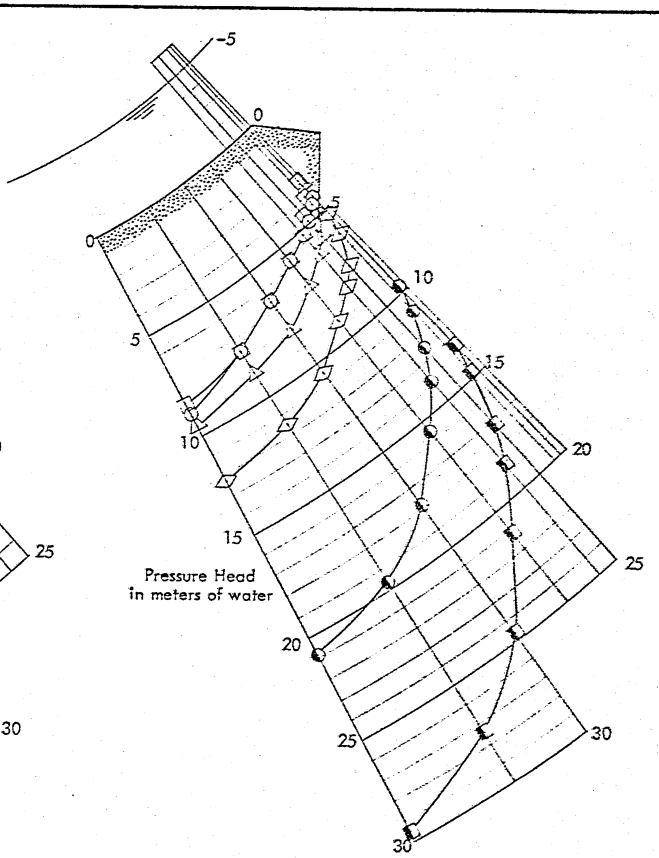

Type A1 Spillway - Overtopping with Lateral Flow

Symbol	Discharge cms	Tailwater meters	Test Depth - d meters
⊙	2,000	125.0	0.5
⊡	4,000	125.0	1.0
△	6,000	125.0	1.5
◇	8,000	126.0	2.0
⊖	17,000	128.0	4.0
◧	28,000	130.5	6.3

Fig. 21 - Manometric Static Pressures at the Side Wall of the Bucket Exit - Original Sill (Type A), V = 29 mps, Lateral Flow, Overtopping, 1971 Tailwater Stages

Fig. 21

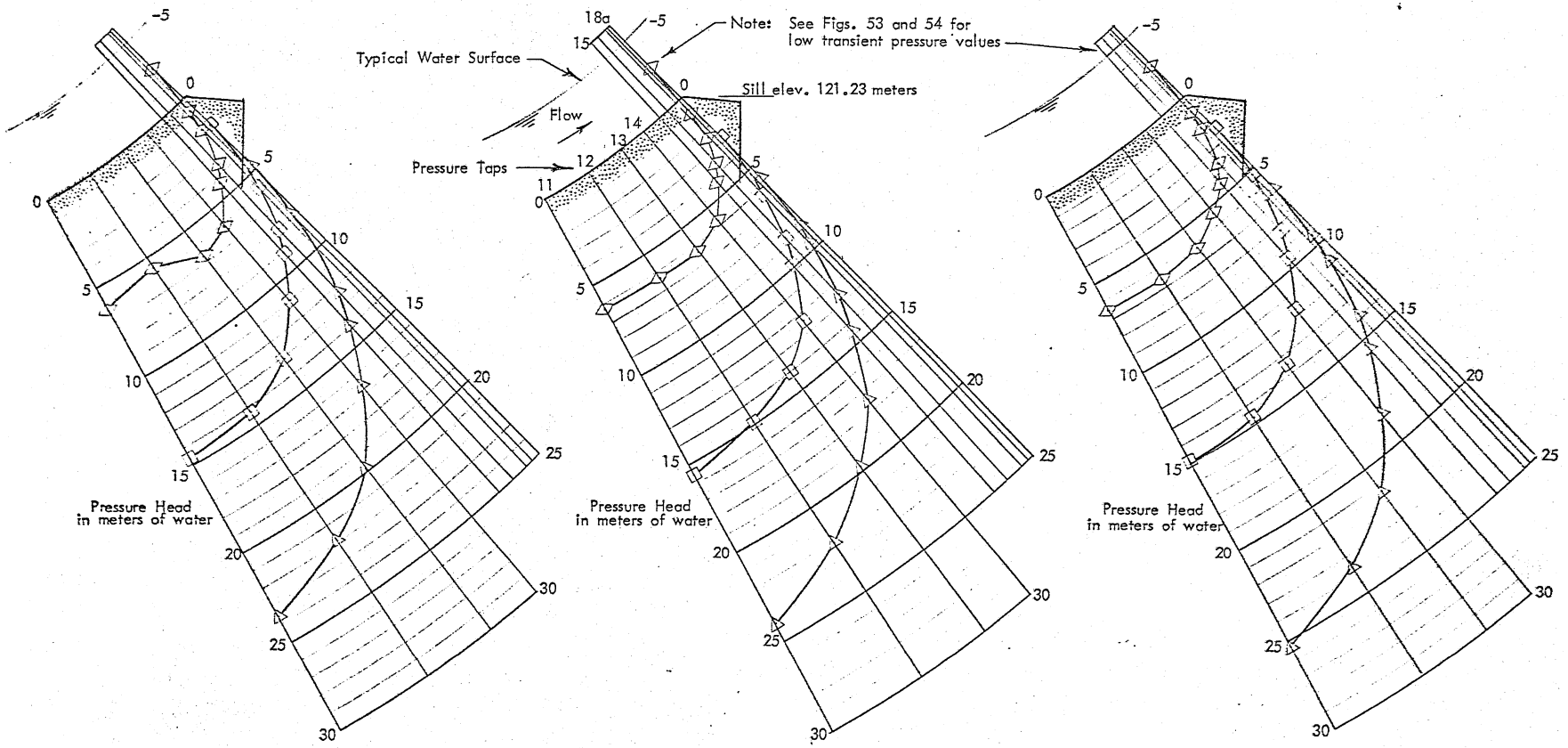

Type A Spillway - No Lateral Flow

Type A Spillway - With Lateral Flow

Type A1 Spillway - Overtopping

Symbol	Discharge cms	Tailwater meters	Test Depth - d meters
◇	8,000	120.0	2.0
⊡	17,000	124.6	4.0
△	28,000	127.0	6.3

Fig. 22 - Manometric Static Pressures on the Centerline of the Bucket Exit - Original Sill (Type A), V = 29 mps, Lateral Flow, Overtopping, Low Tailwater Stages

Fig. 22

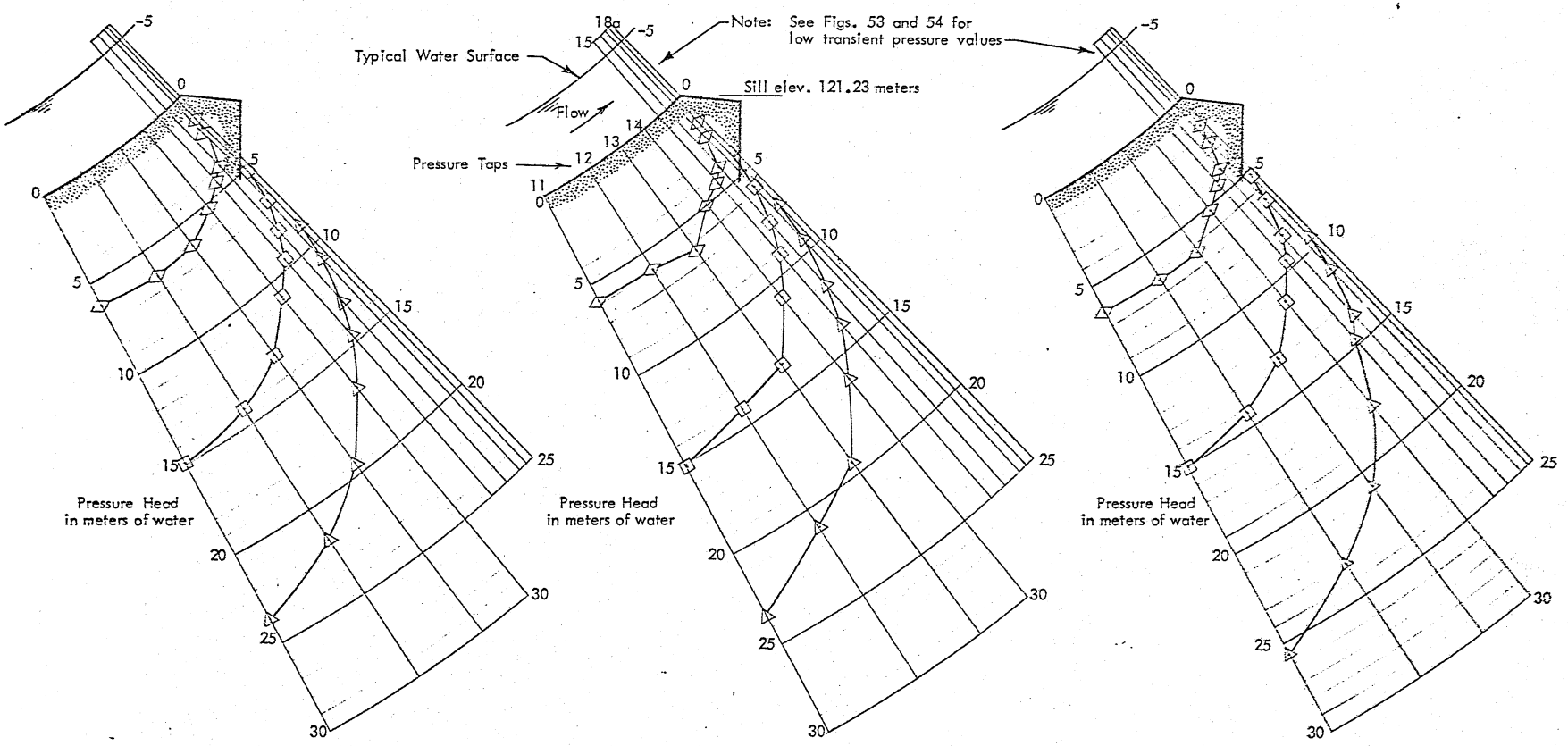

Type A Spillway - No Lateral Flow

Type A Spillway - With Lateral Flow

Type A1 Spillway - Overtopping

Symbol	Discharge cms	Tailwater meters	Test Depth - d meters
◇	8,000	120.0	2.0
⊡	17,000	124.6	4.0
△	28,000	127.0	6.3

Fig. 23 - Manometric Static Pressures at the Side Wall of the Bucket Exit - Original Sill (Type A), V = 29 mps, Lateral Flow, Overtopping, Low Tailwater Stages

Fig. 23

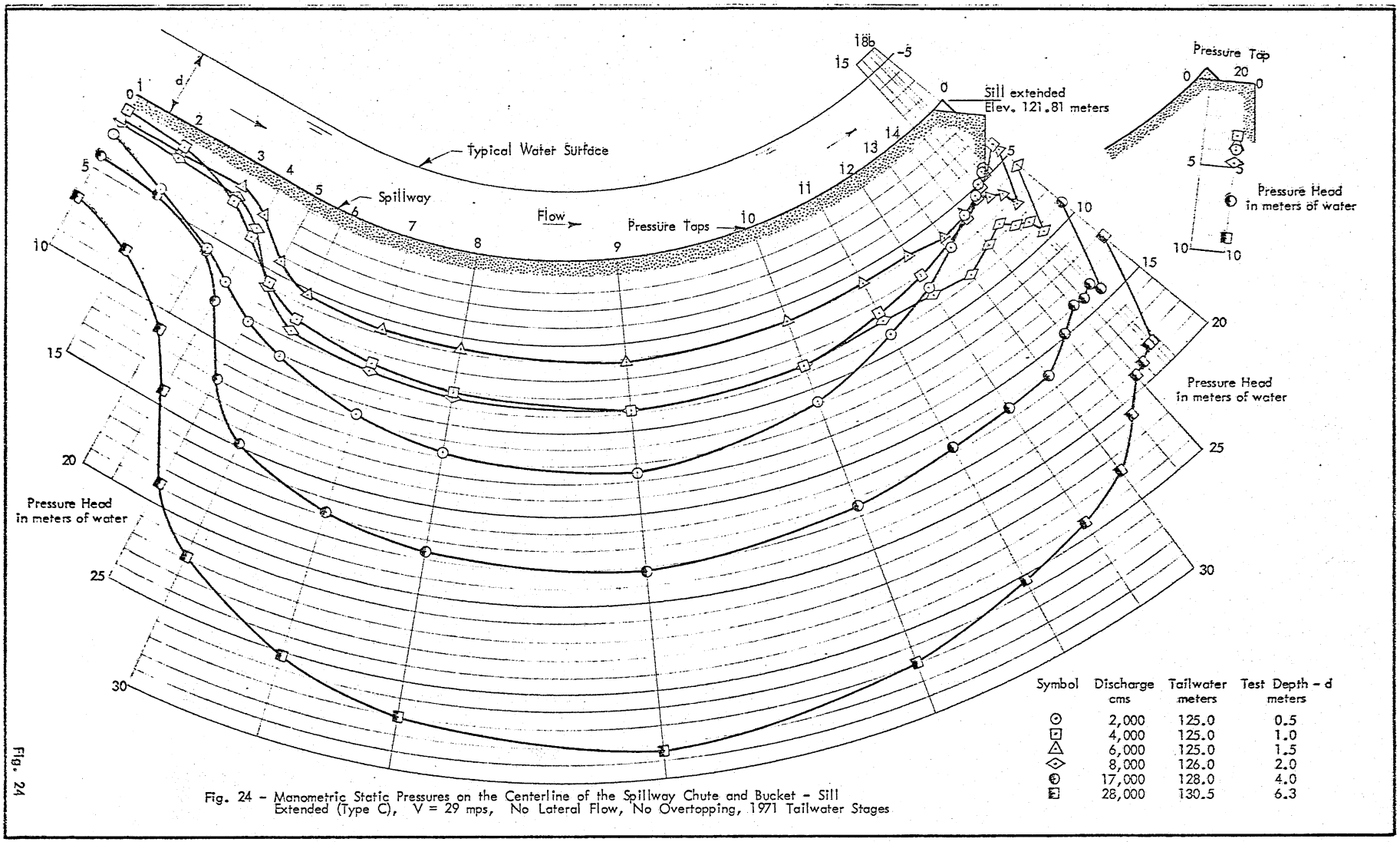

Fig. 24 - Manometric Static Pressures on the Centerline of the Spillway Chute and Bucket - Sill Extended (Type C), V = 29 mps, No Lateral Flow, No Overtopping, 1971 Tailwater Stages

Fig. 24

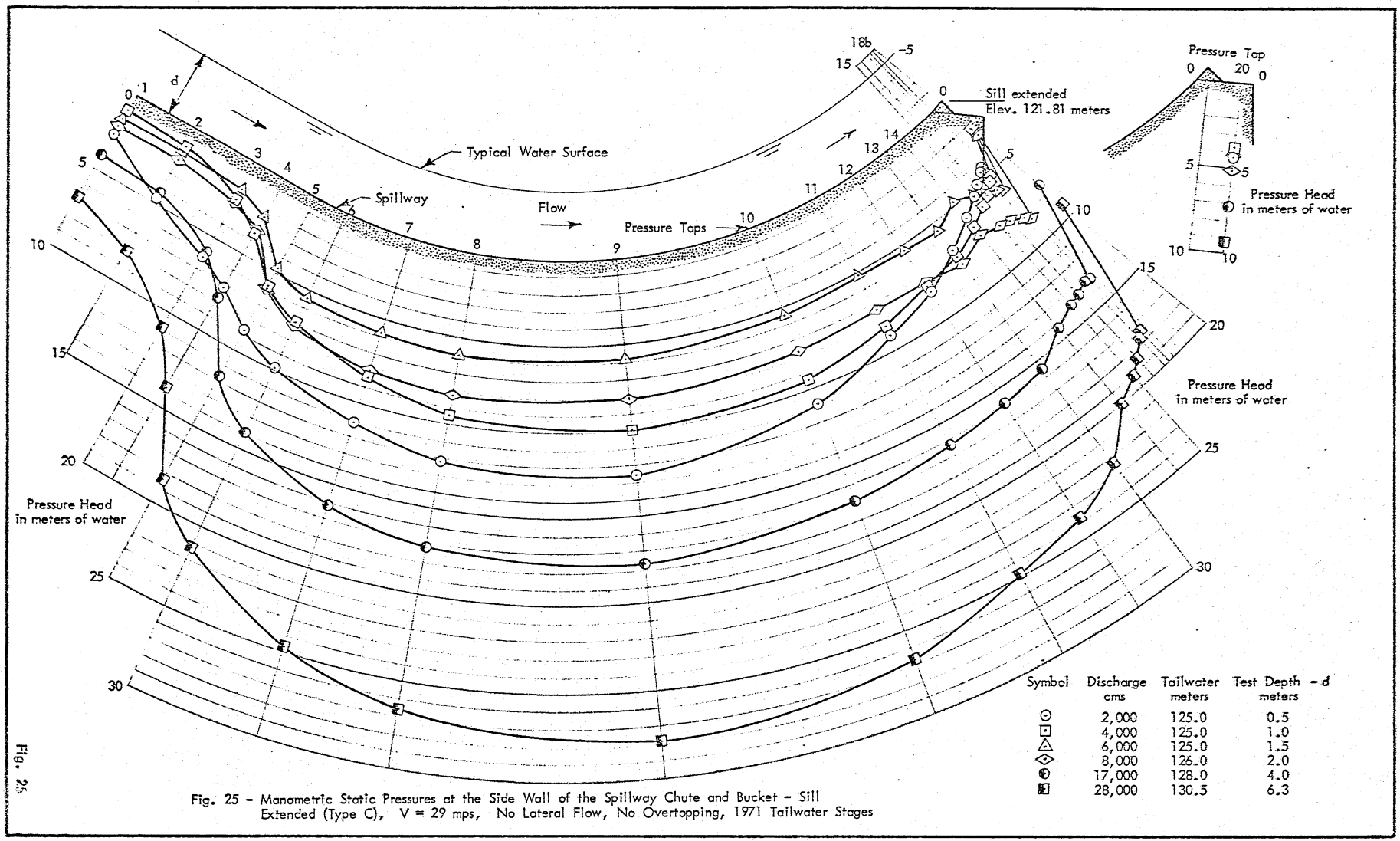

Fig. 25 - Manometric Static Pressures at the Side Wall of the Spillway Chute and Bucket - Sill Extended (Type C), V = 29 mps, No Lateral Flow, No Overtopping, 1971 Tailwater Stages

Fig. 25

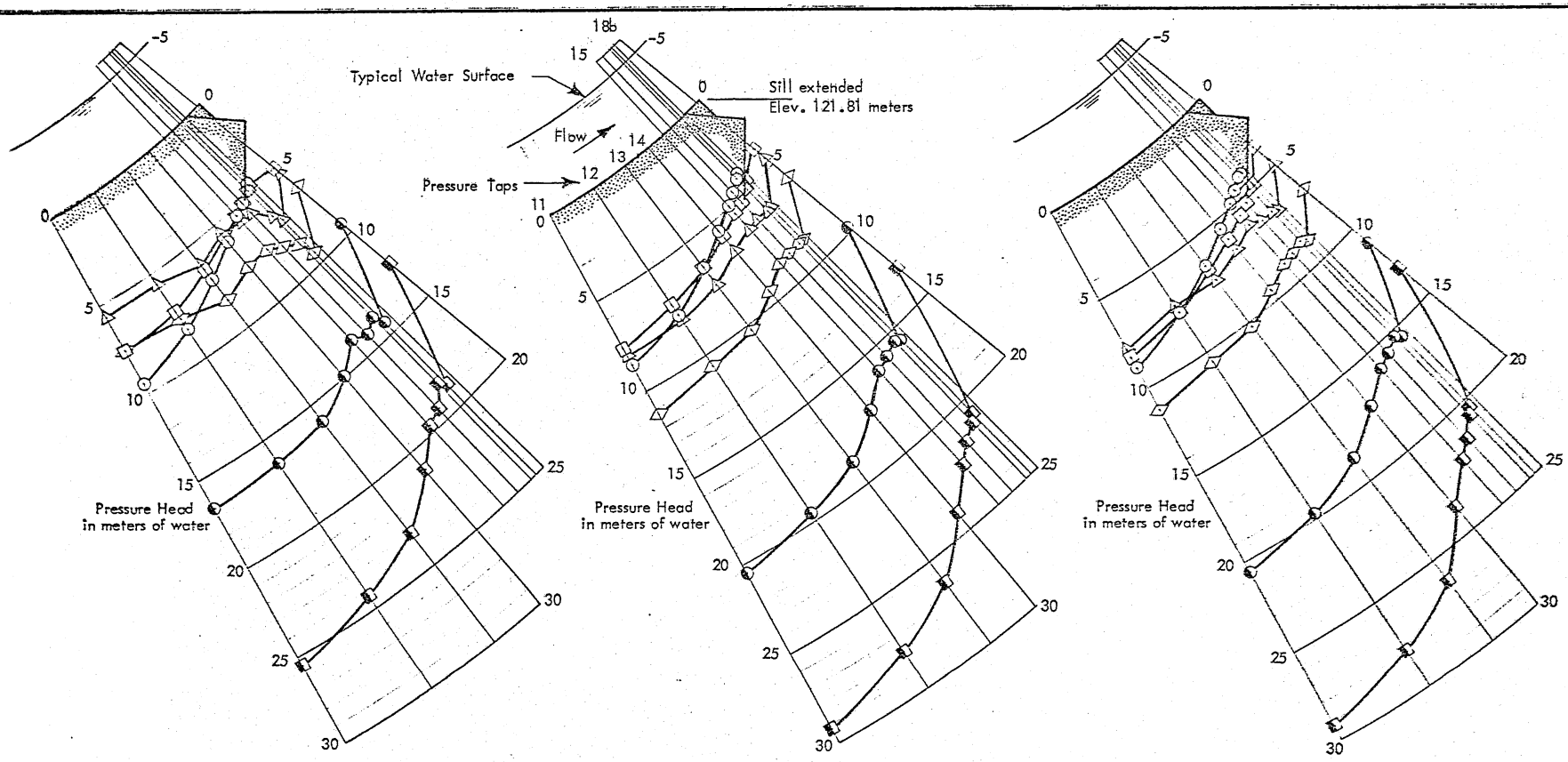

Type A Spillway - With Lateral Flow

Type A1 Spillway - Overtopping

Type A1 Spillway - Overtopping with Lateral Flow

Symbol	Discharge cms	Tailwater meters	Test Depth - d meters
⊙	2,000	125.0	0.5
⊡	4,000	125.0	1.0
△	6,000	125.0	1.5
◇	8,000	126.0	2.0
◐	17,000	128.0	4.0
◪	28,000	130.5	6.3

Fig. 26 - Manometric Static Pressures on the Centerline of the Bucket Exit - Sill Extended (Type C), V = 29 mps, Lateral Flow, Overtopping, 1971 Tailwater Stages

Fig. 26

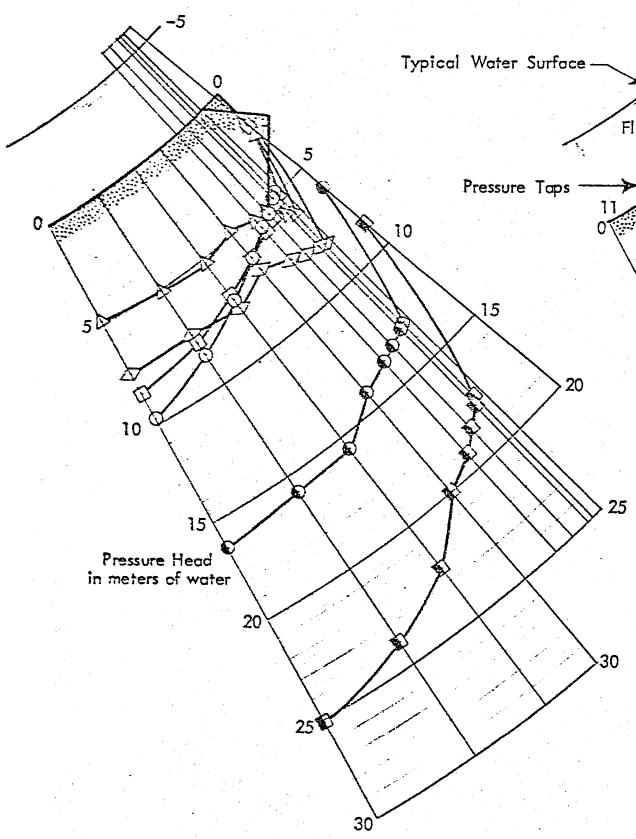

Type A Spillway - With Lateral Flow

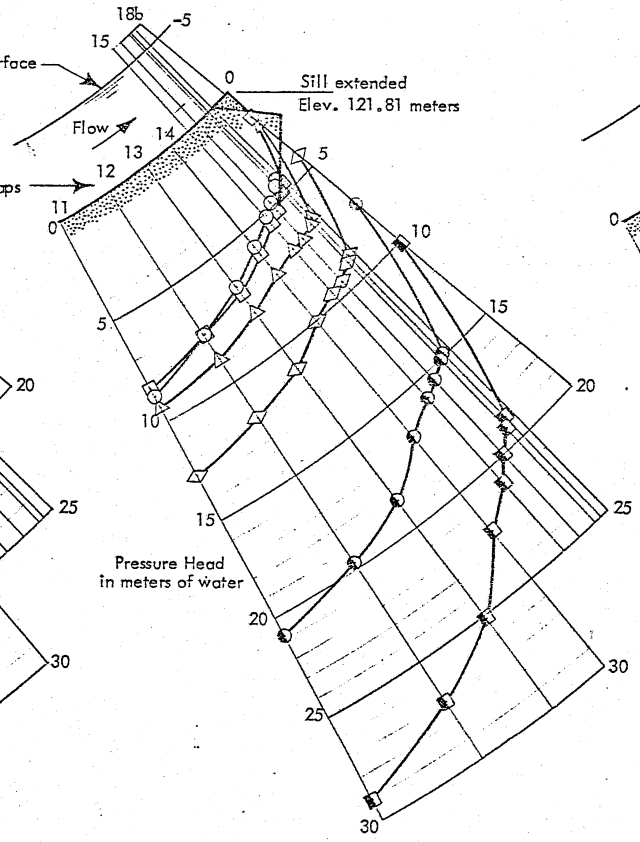

Type A1 Spillway - Overtopping

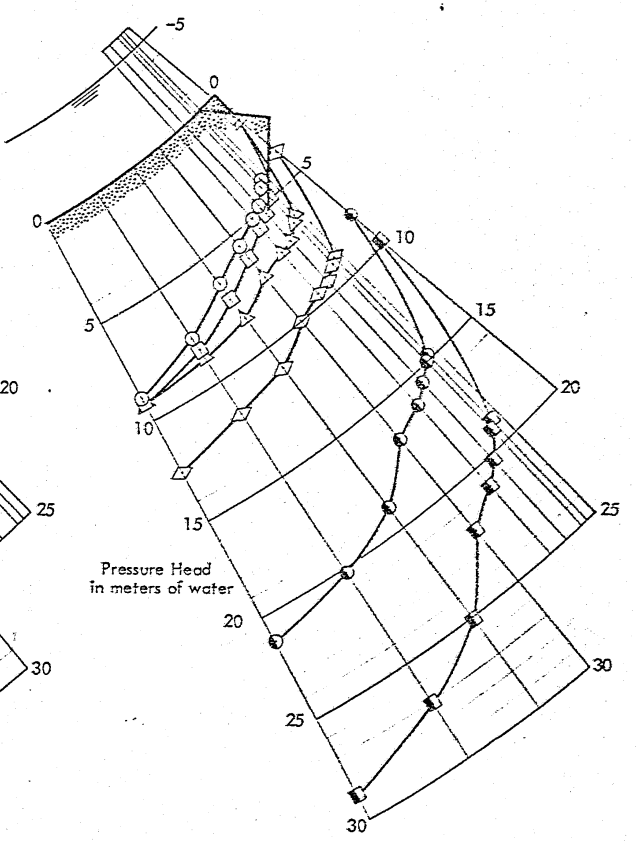

Type A1 Spillway - Overtopping with Lateral Flow

Symbol	Discharge cms	Tailwater meters	Test Depth - d meters
⊙	2,000	125.0	0.5
⊡	4,000	125.0	1.0
△	6,000	125.0	1.5
◇	8,000	126.0	2.0
◐	17,000	128.0	4.0
◧	28,000	130.5	6.3

Fig. 27 - Manometric Static Pressures at the Side Wall of the Bucket Exit - Sill Extended (Type C), V = 29 mps, Lateral Flow, Overtopping, 1971 Tailwater Stages

Fig. 27

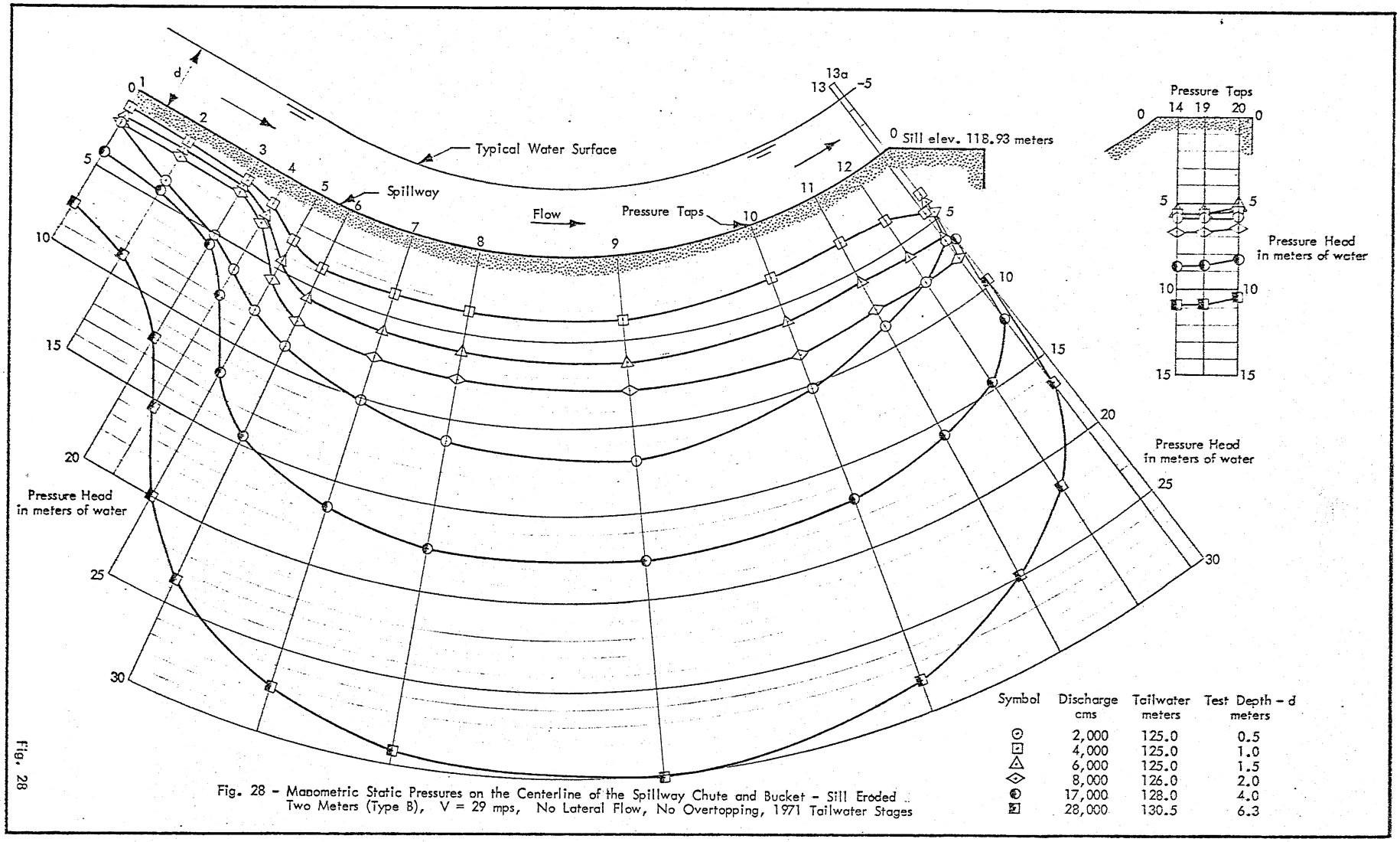

Fig. 28 – Manometric Static Pressures on the Centerline of the Spillway Chute and Bucket – Sill Eroded Two Meters (Type B), V = 29 mps, No Lateral Flow, No Overtopping, 1971 Tailwater Stages

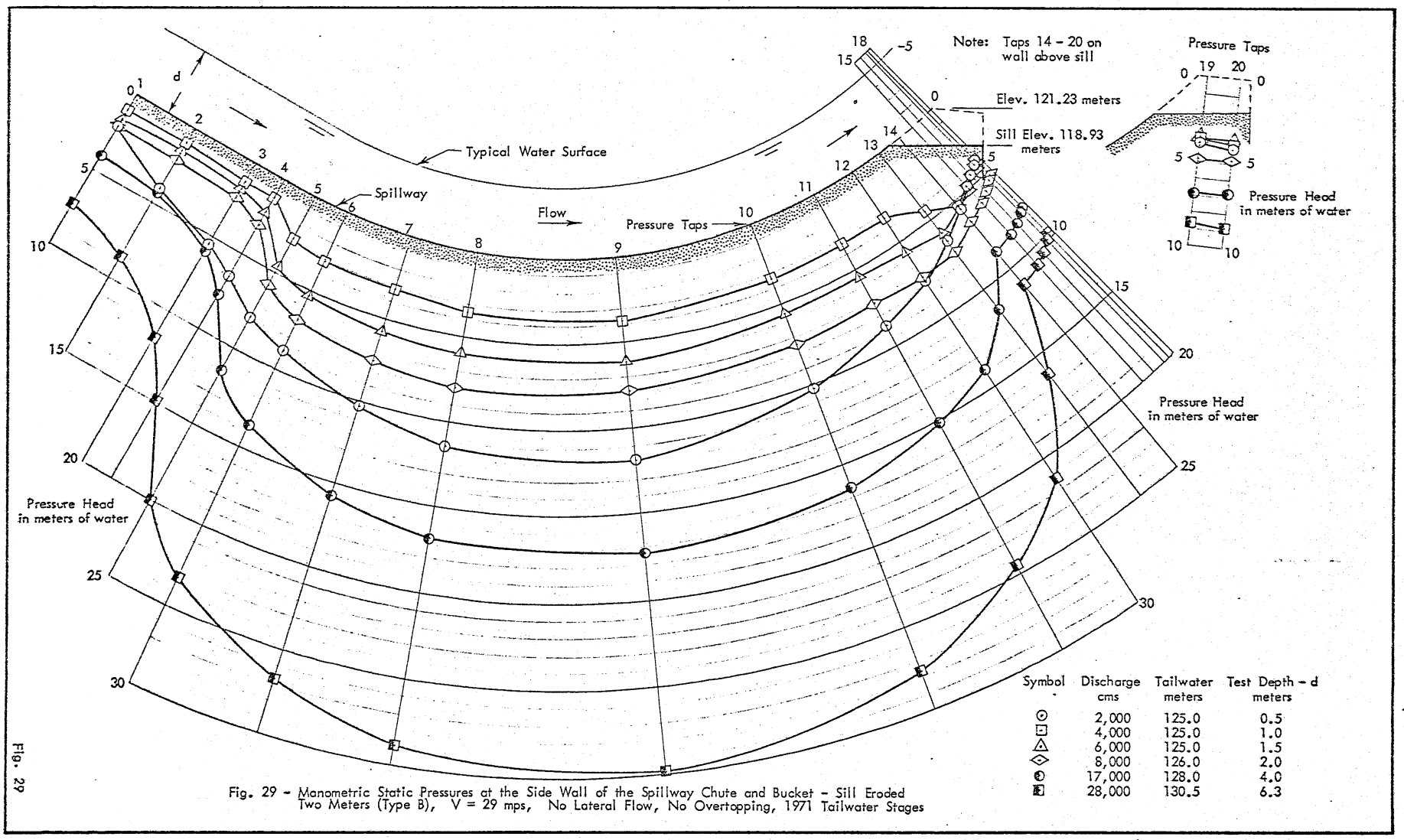

Fig. 29 - Manometric Static Pressures at the Side Wall of the Spillway Chute and Bucket - Sill Eroded Two Meters (Type B), V = 29 mps, No Lateral Flow, No Overtopping, 1971 Tailwater Stages

Fig. 29

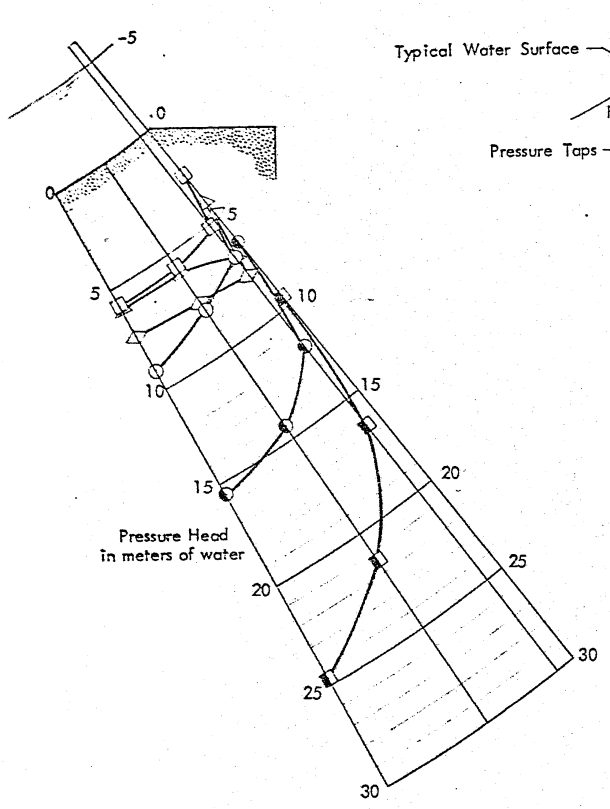

Type B Spillway - With Lateral Flow

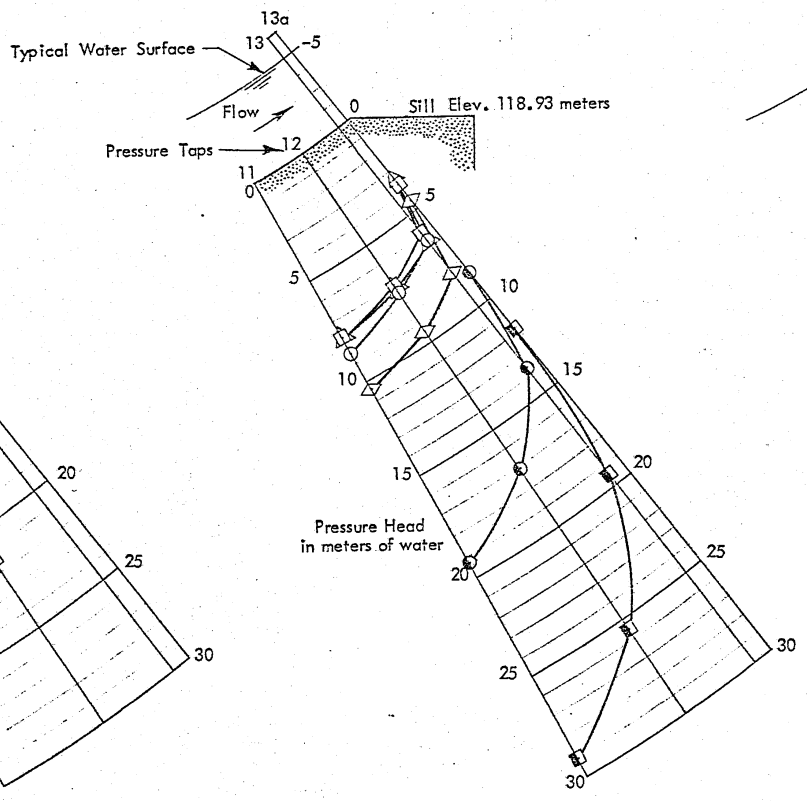

Type B1 Spillway - Overtopping

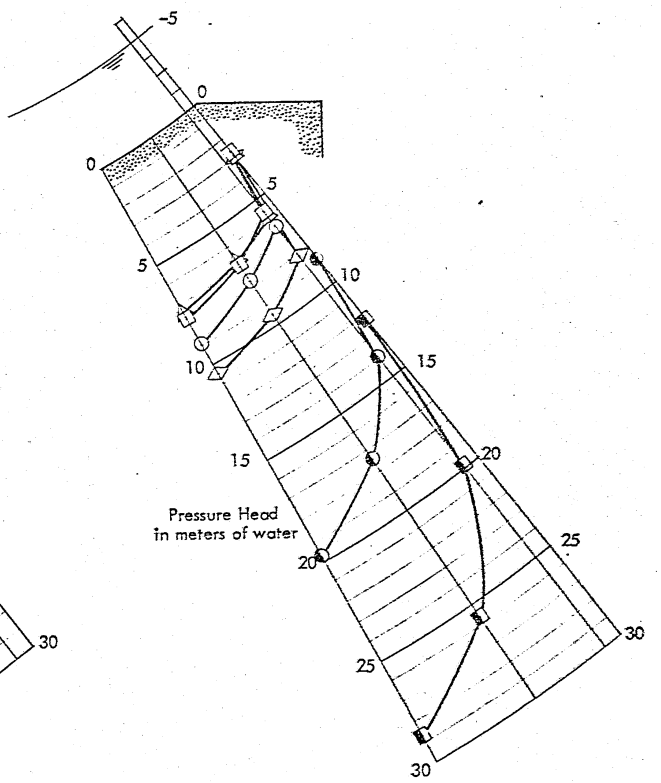

Type B1 Spillway - Overtopping with Lateral Flow

Symbol	Discharge cms	Tailwater meters	Test Depth - d meters
⊙	2,000	125.0	0.5
⊡	4,000	125.0	1.0
△	6,000	125.0	1.5
◇	8,000	126.0	2.0
⊕	17,000	128.0	4.0
▣	28,000	130.5	6.3

Fig. 30 - Manometric Static Pressures on the Centerline of the Bucket Exit - Sill Eroded Two Meters (Type B), V = 29 mps, Lateral Flow, Overtopping, 1971 Tailwater Stages

Fig. 30

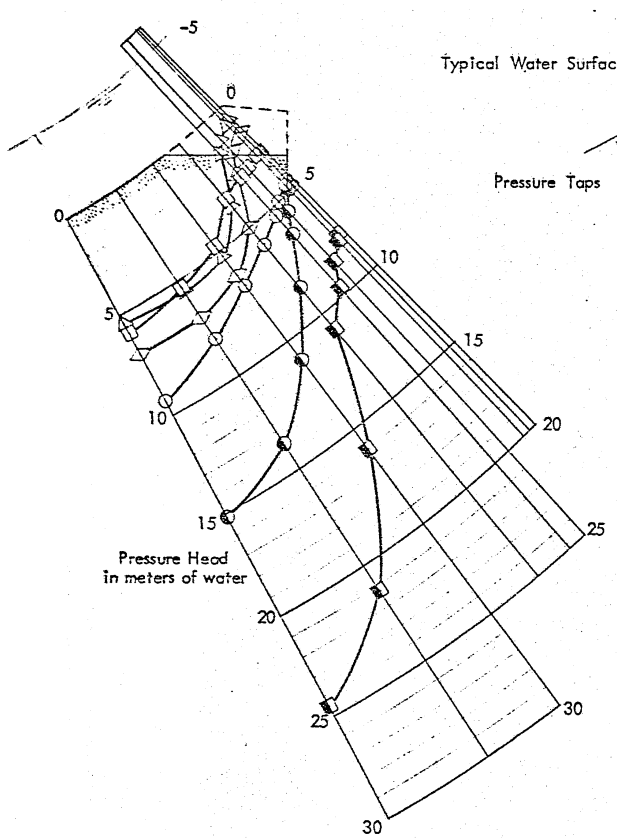

Type B Spillway - With Lateral Flow

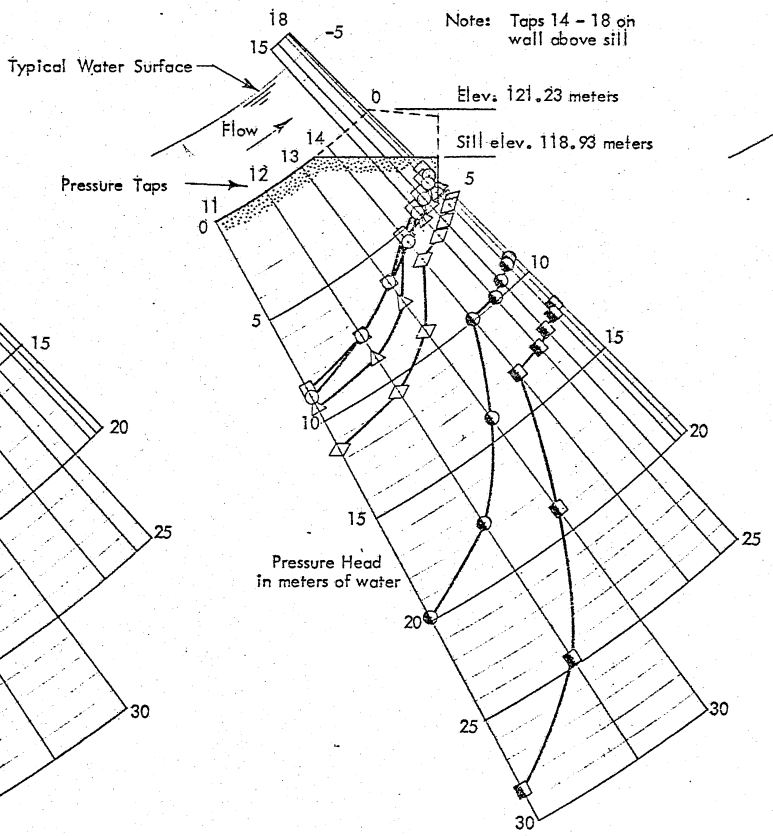

Type B1 Spillway - Overtopping

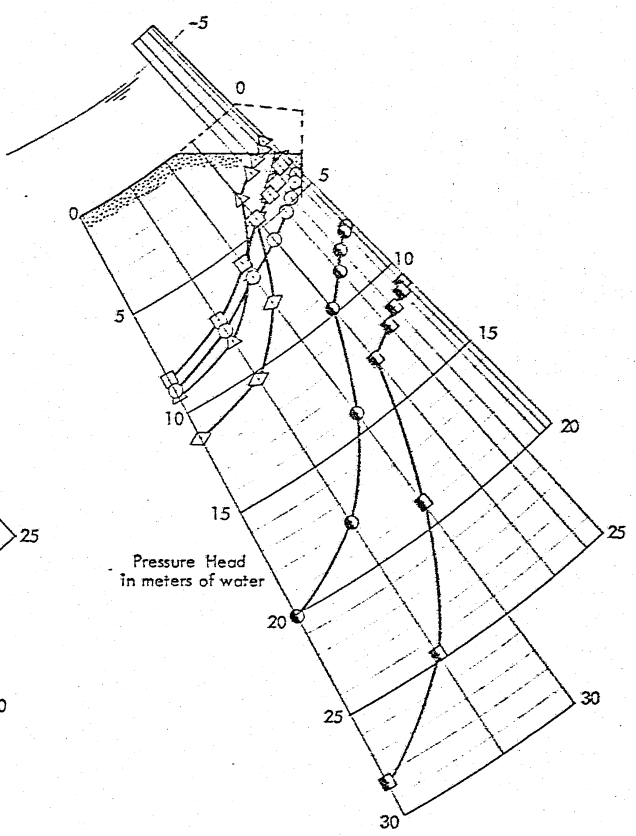

Type B1 Spillway - Overtopping with Lateral Flow

Symbol	Discharge cms	Tailwater meters	Test Depth - d meters
⊙	2,000	125.0	0.5
⊡	4,000	125.0	1.0
△	6,000	125.0	1.5
◇	8,000	126.0	2.0
◐	17,000	128.0	4.0
◙	28,000	130.5	6.3

Fig. 31 - Manometric Static Pressures at the Side Wall of the Bucket Exit - Sill Eroded
Two Meters (Type B), V = 29 mps, Lateral Flow, Overtopping, 1971 Tailwater Stages

Fig. 31

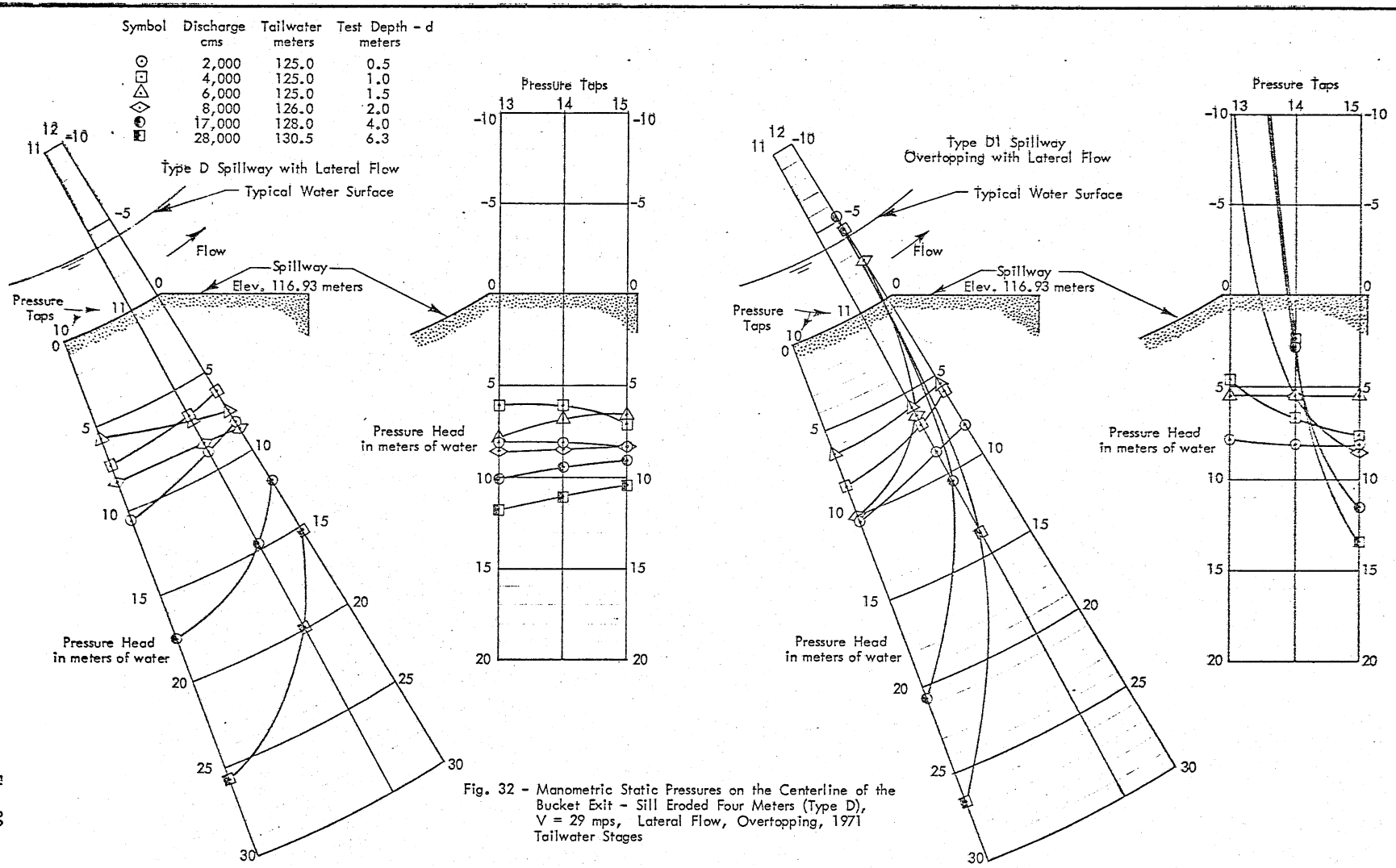

Fig. 32 - Manometric Static Pressures on the Centerline of the Bucket Exit - Sill Eroded Four Meters (Type D), V = 29 mps, Lateral Flow, Overtopping, 1971 Tailwater Stages

Fig. 32

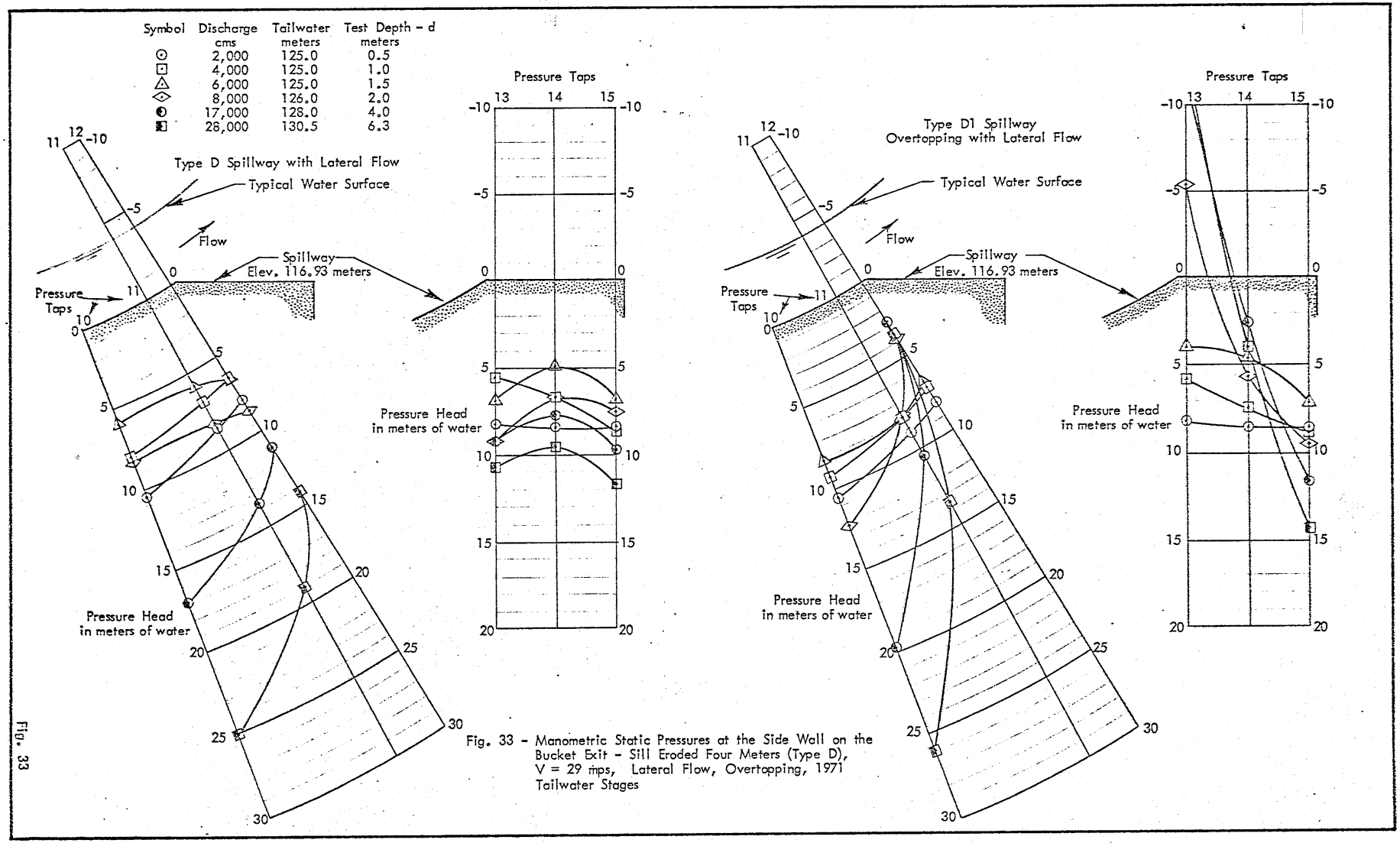

Fig. 33 – Manometric Static Pressures at the Side Wall on the Bucket Exit – Sill Eroded Four Meters (Type D), V = 29 mps, Lateral Flow, Overtopping, 1971 Tailwater Stages

Fig. 33

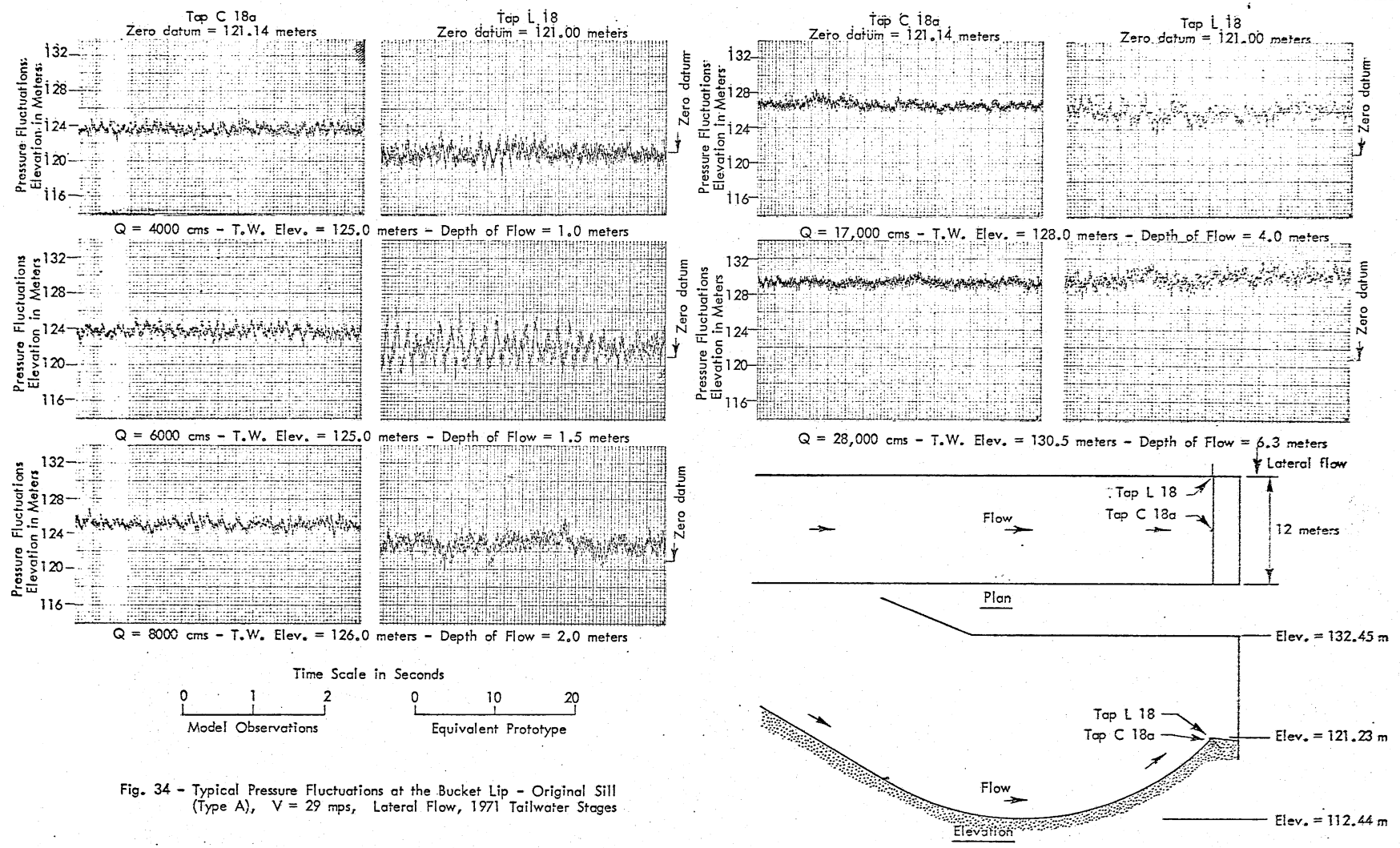

Fig. 34 - Typical Pressure Fluctuations at the Bucket Lip - Original Sill (Type A), V = 29 mps, Lateral Flow, 1971 Tailwater Stages

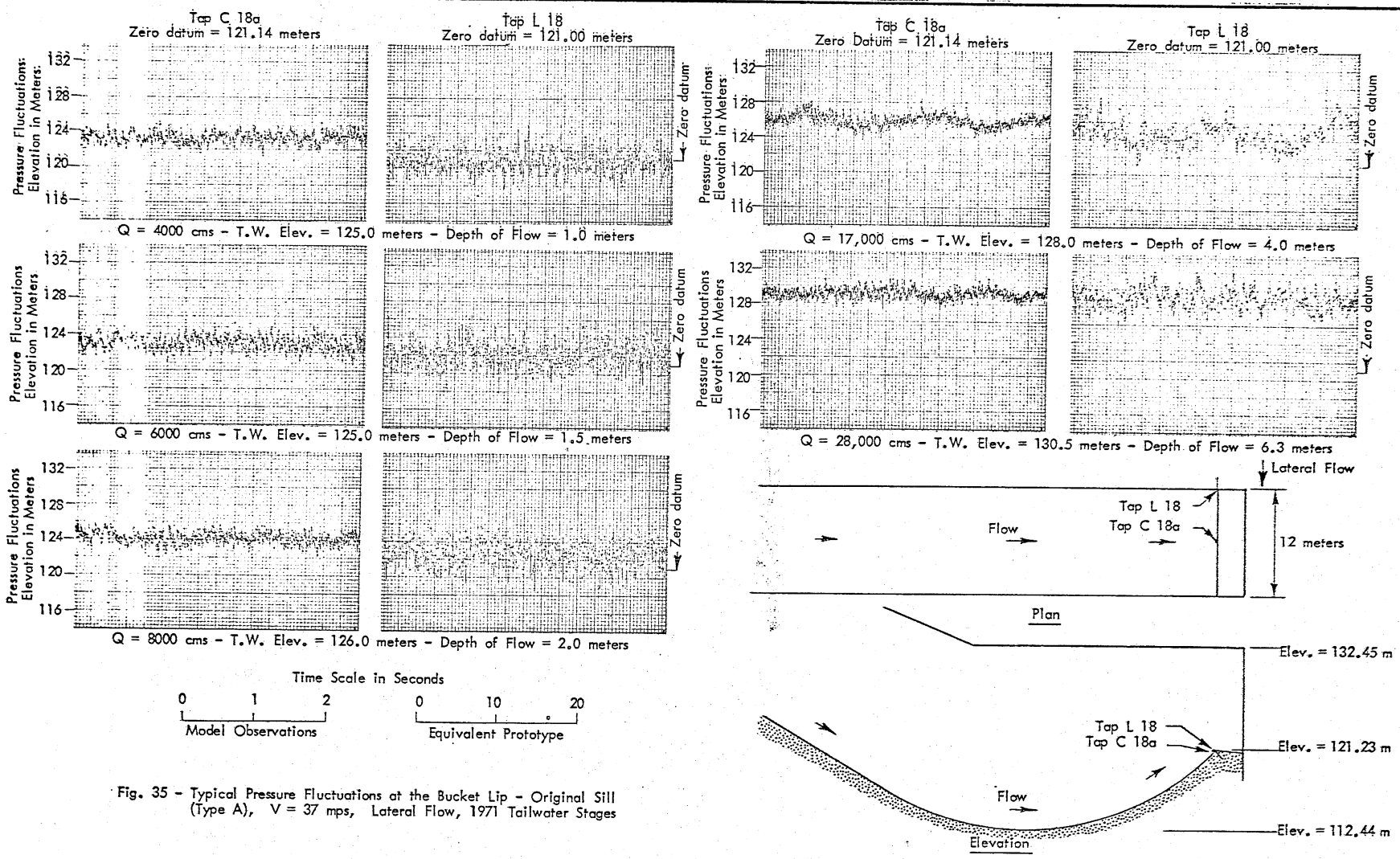

Fig. 35 - Typical Pressure Fluctuations at the Bucket Lip - Original Sill (Type A), V = 37 mps, Lateral Flow, 1971 Tailwater Stages

Fig. 35

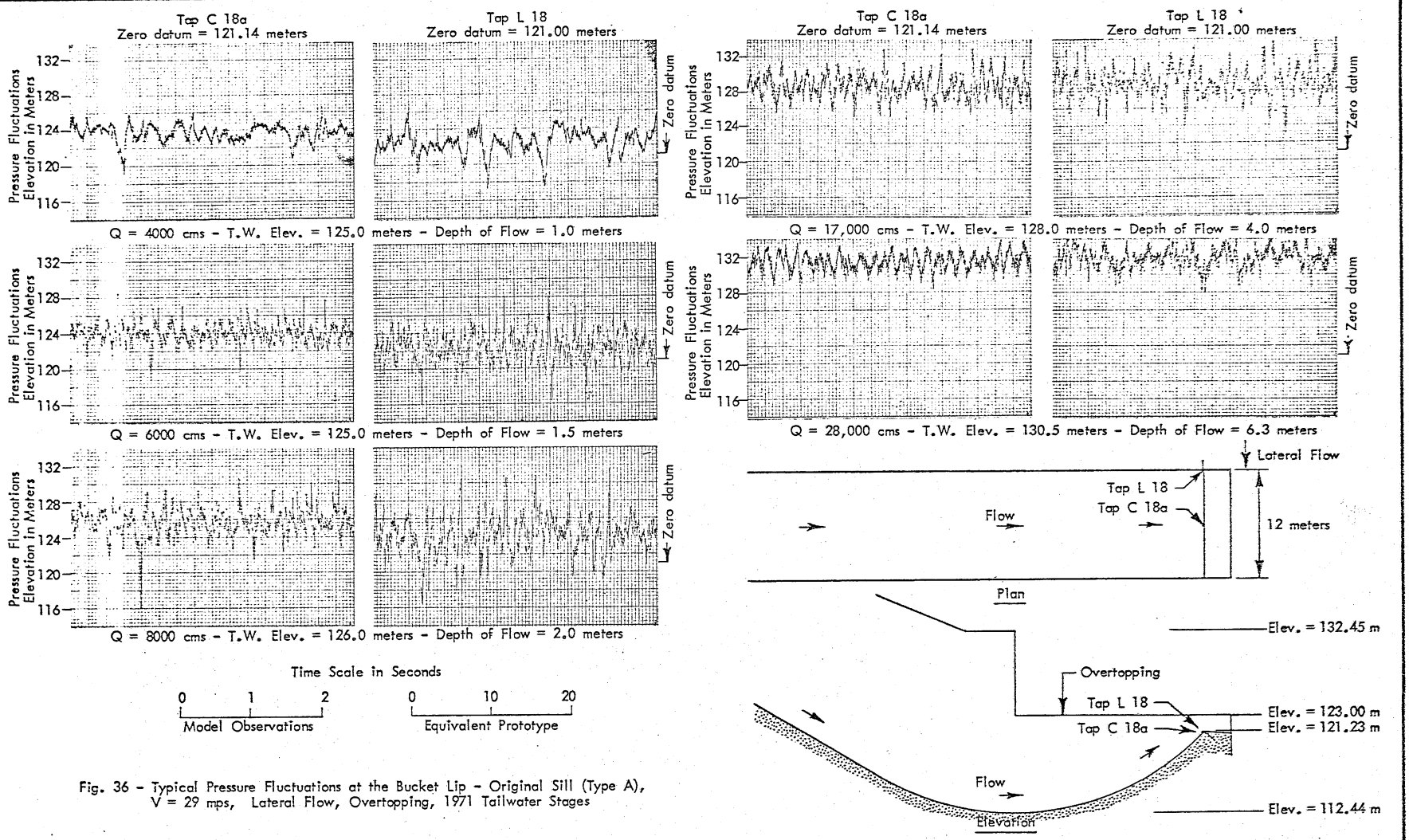

Fig. 36 - Typical Pressure Fluctuations at the Bucket Lip - Original Sill (Type A), V = 29 mps, Lateral Flow, Overtopping, 1971 Tailwater Stages

Fig. 36

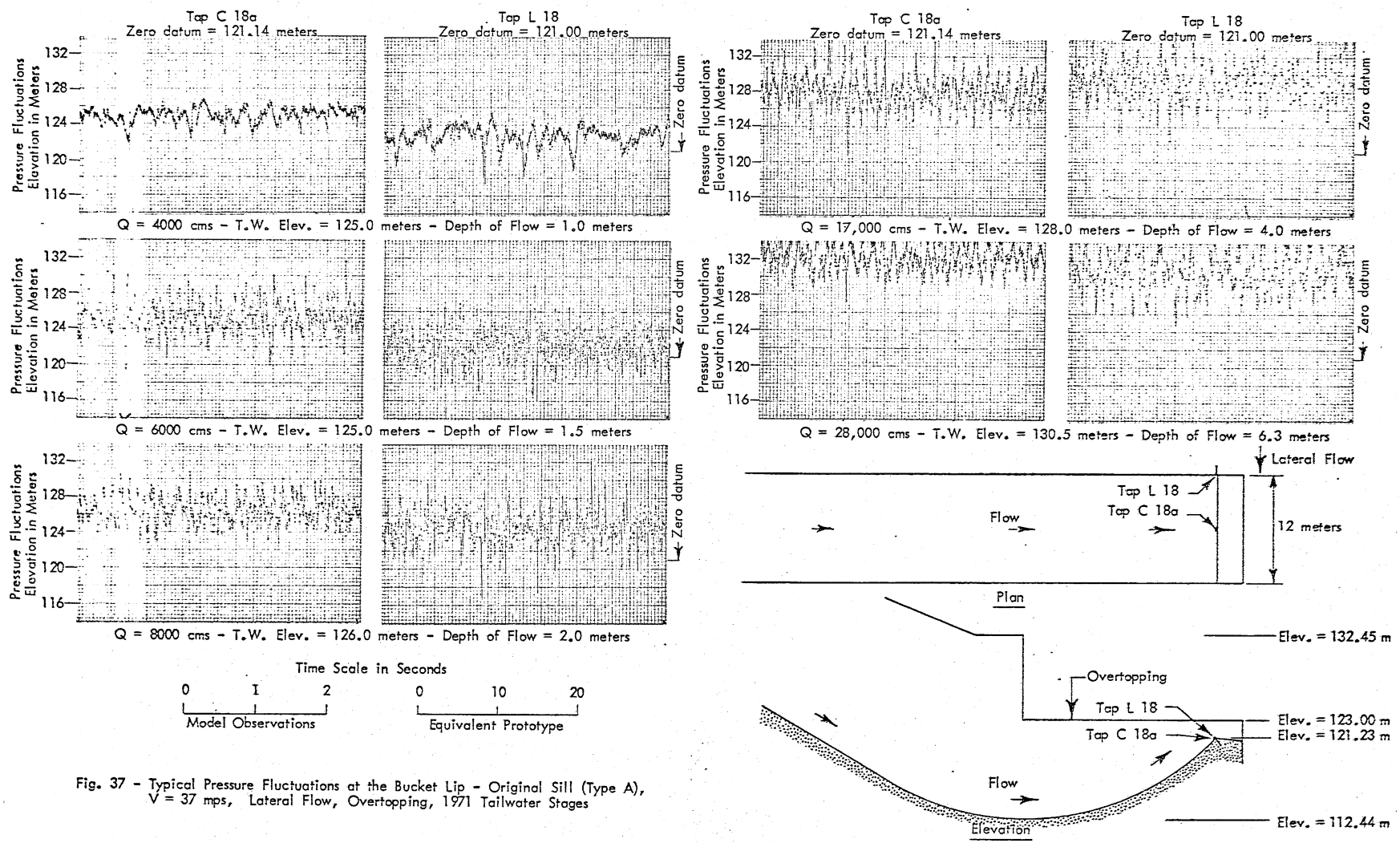

Fig. 37 - Typical Pressure Fluctuations at the Bucket Lip - Original Sill (Type A), V = 37 mps, Lateral Flow, Overtopping, 1971 Tailwater Stages

Fig. 37

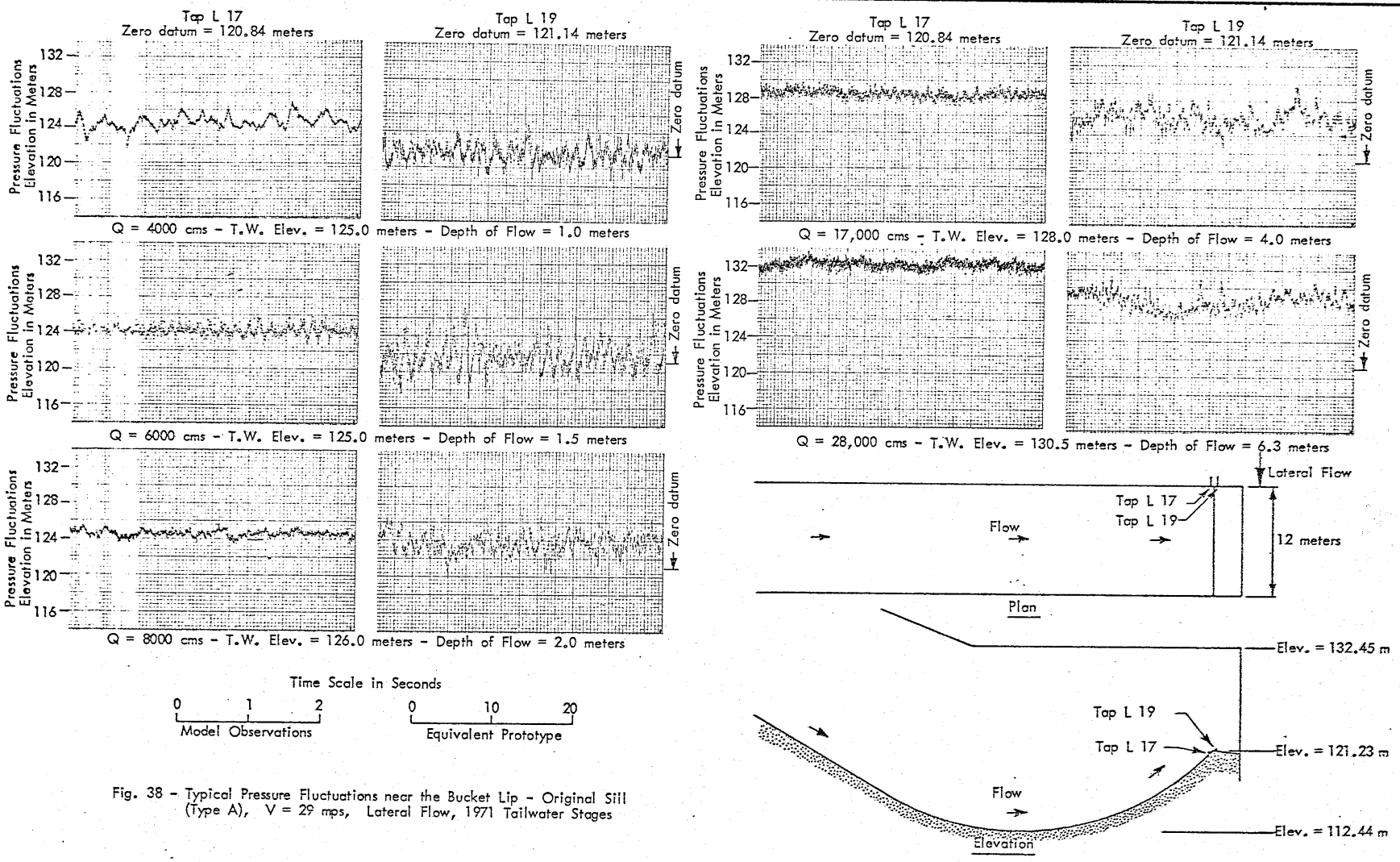

Fig. 38 - Typical Pressure Fluctuations near the Bucket Lip - Original Sill (Type A), V = 29 mps, Lateral Flow, 1971 Tailwater Stages

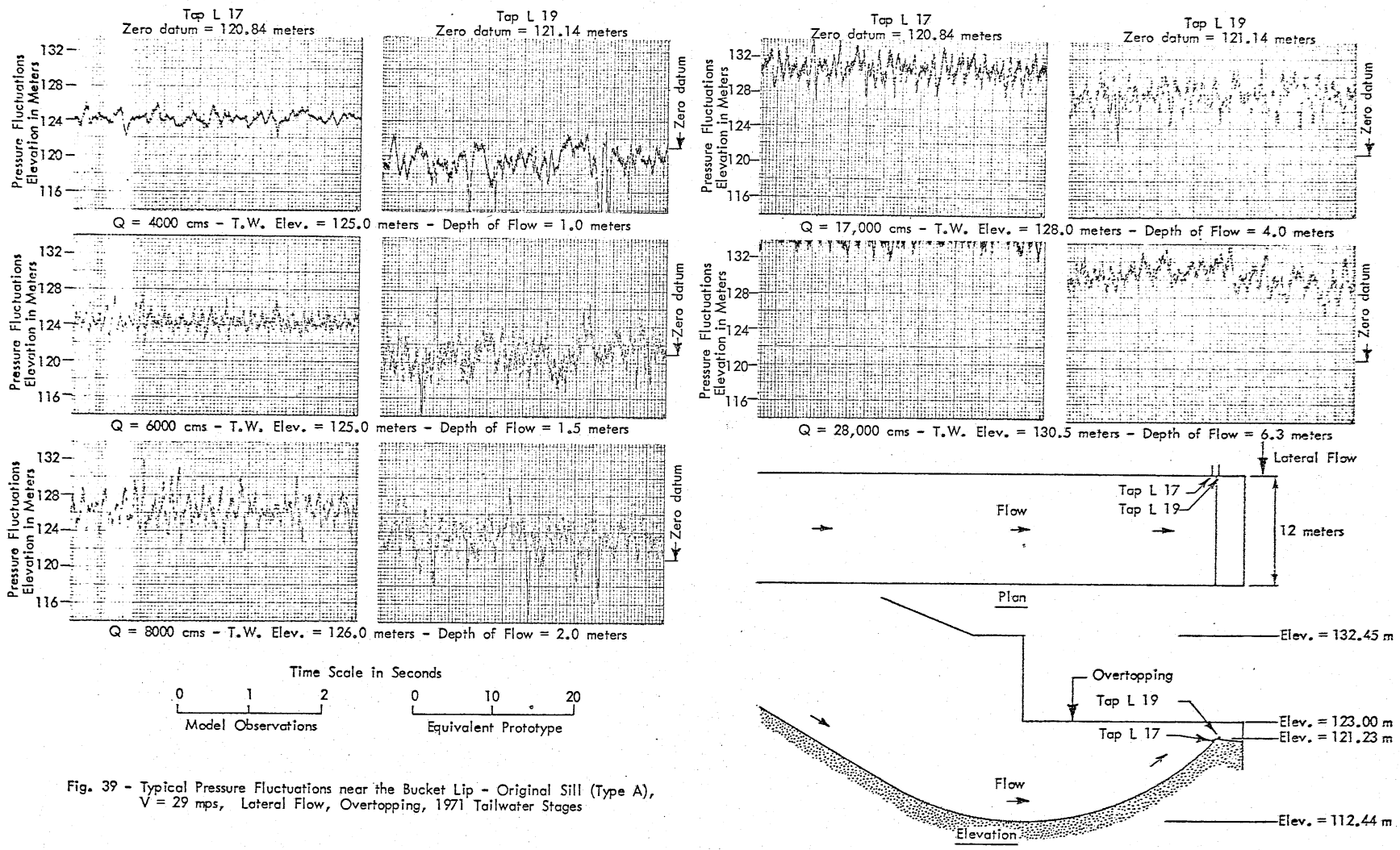

Fig. 39 - Typical Pressure Fluctuations near the Bucket Lip - Original Sill (Type A), V = 29 mps, Lateral Flow, Overtopping, 1971 Tailwater Stages

Fig. 39

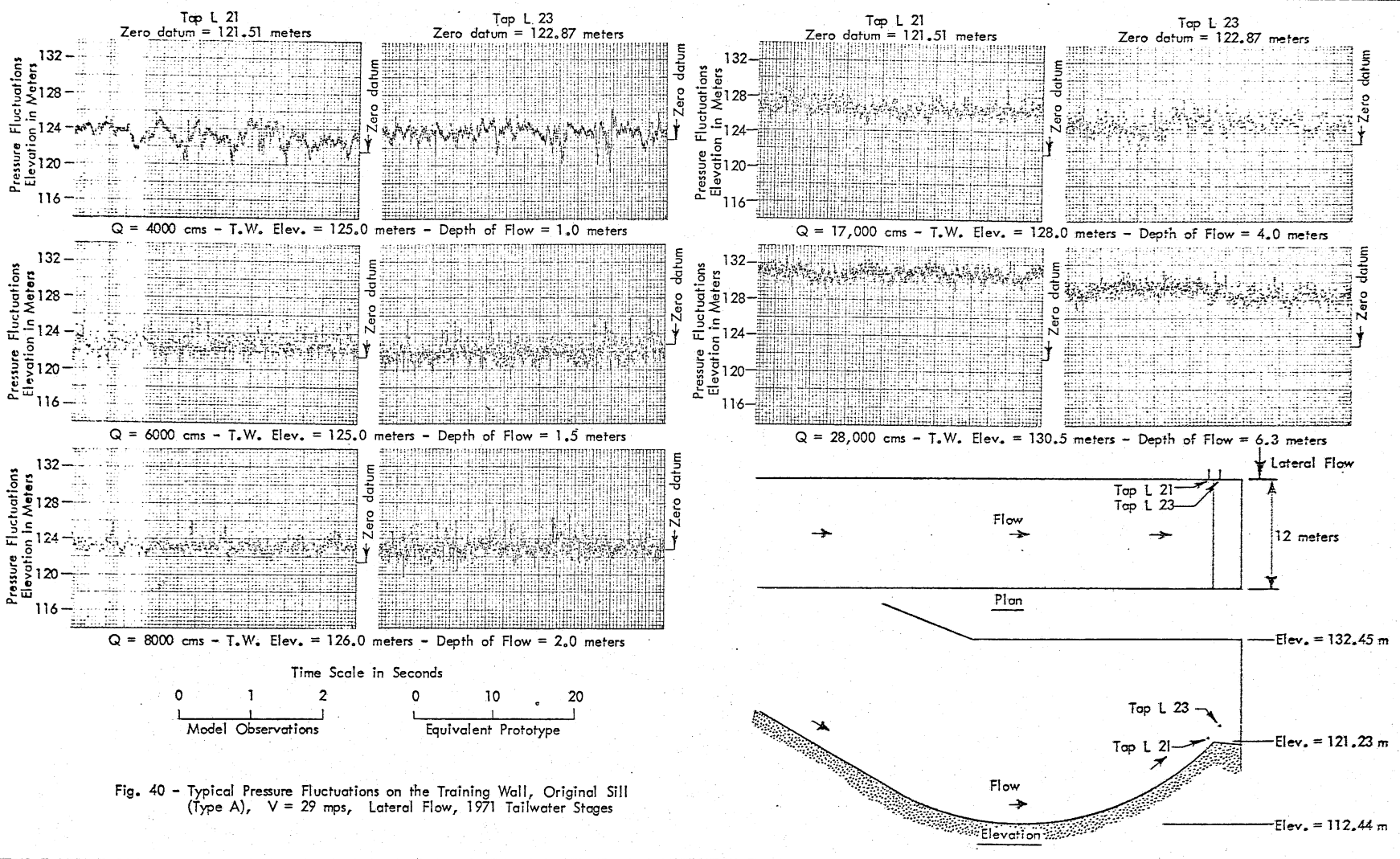

Fig. 40 - Typical Pressure Fluctuations on the Training Wall, Original Sill (Type A), V = 29 mps, Lateral Flow, 1971 Tailwater Stages

Fig. 40

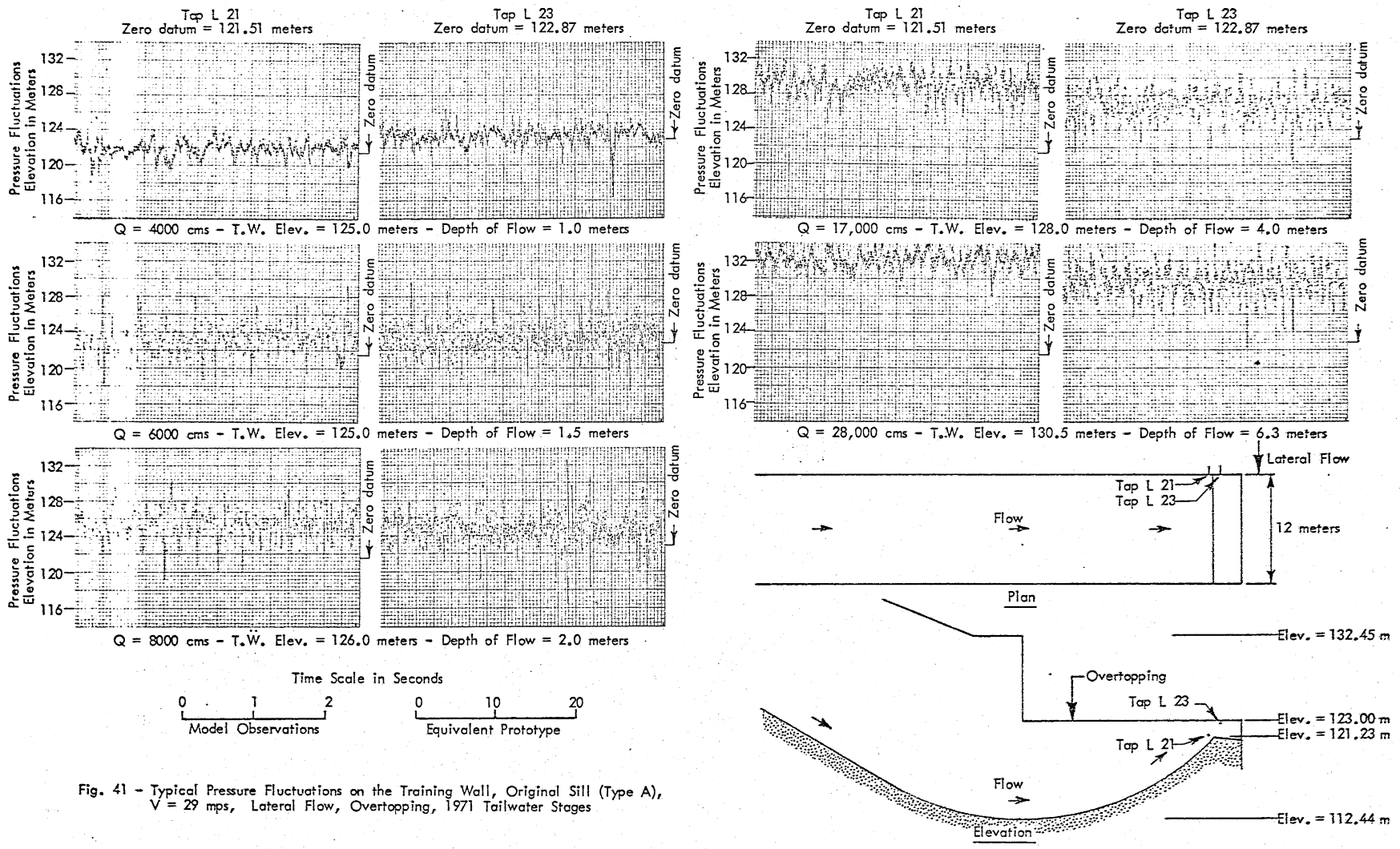

Fig. 41 - Typical Pressure Fluctuations on the Training Wall, Original Sill (Type A), V = 29 mps, Lateral Flow, Overtopping, 1971 Tailwater Stages

Fig. 41

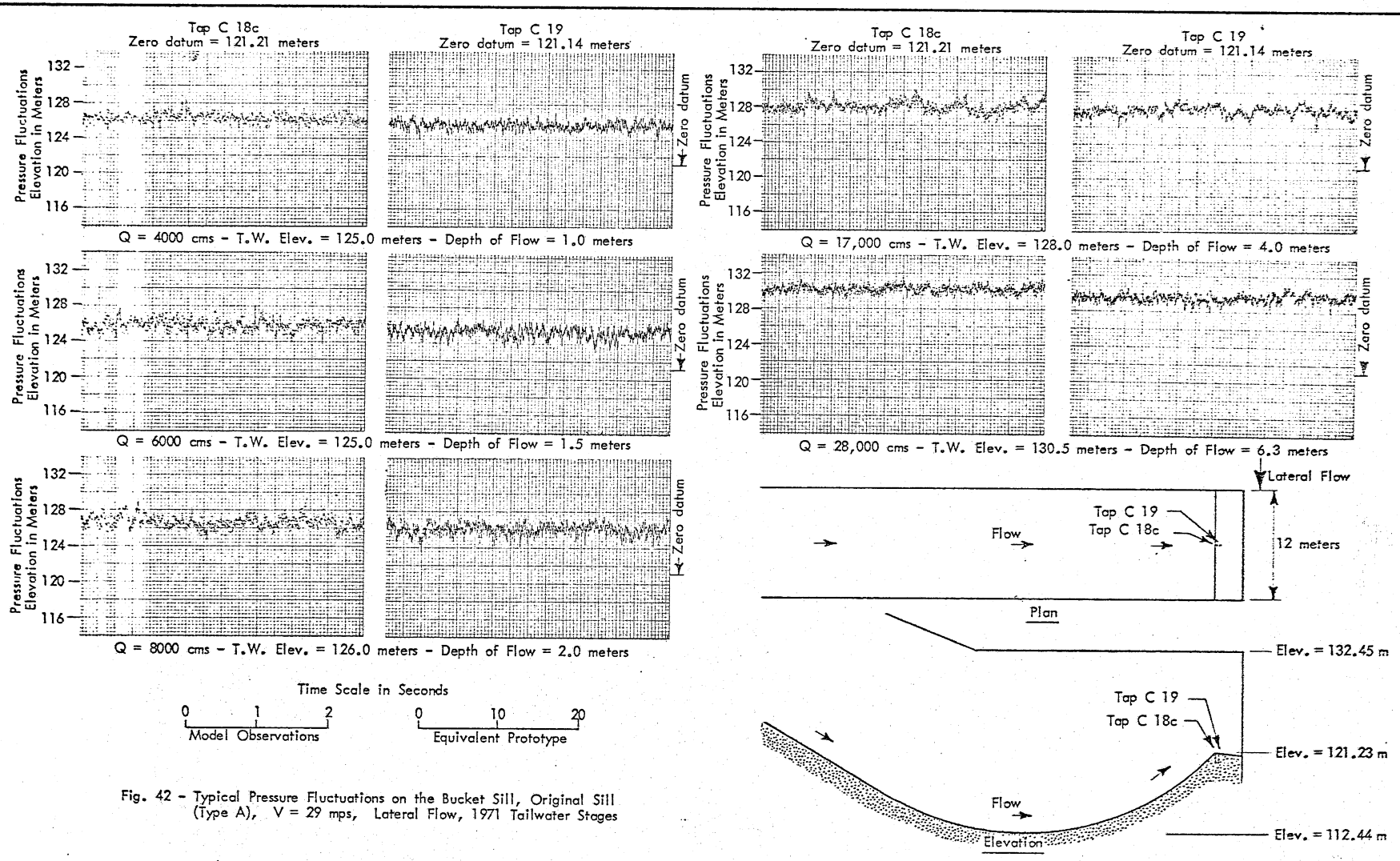

Fig. 42 - Typical Pressure Fluctuations on the Bucket Sill, Original Sill (Type A), V = 29 mps, Lateral Flow, 1971 Tailwater Stages

Fig. 42

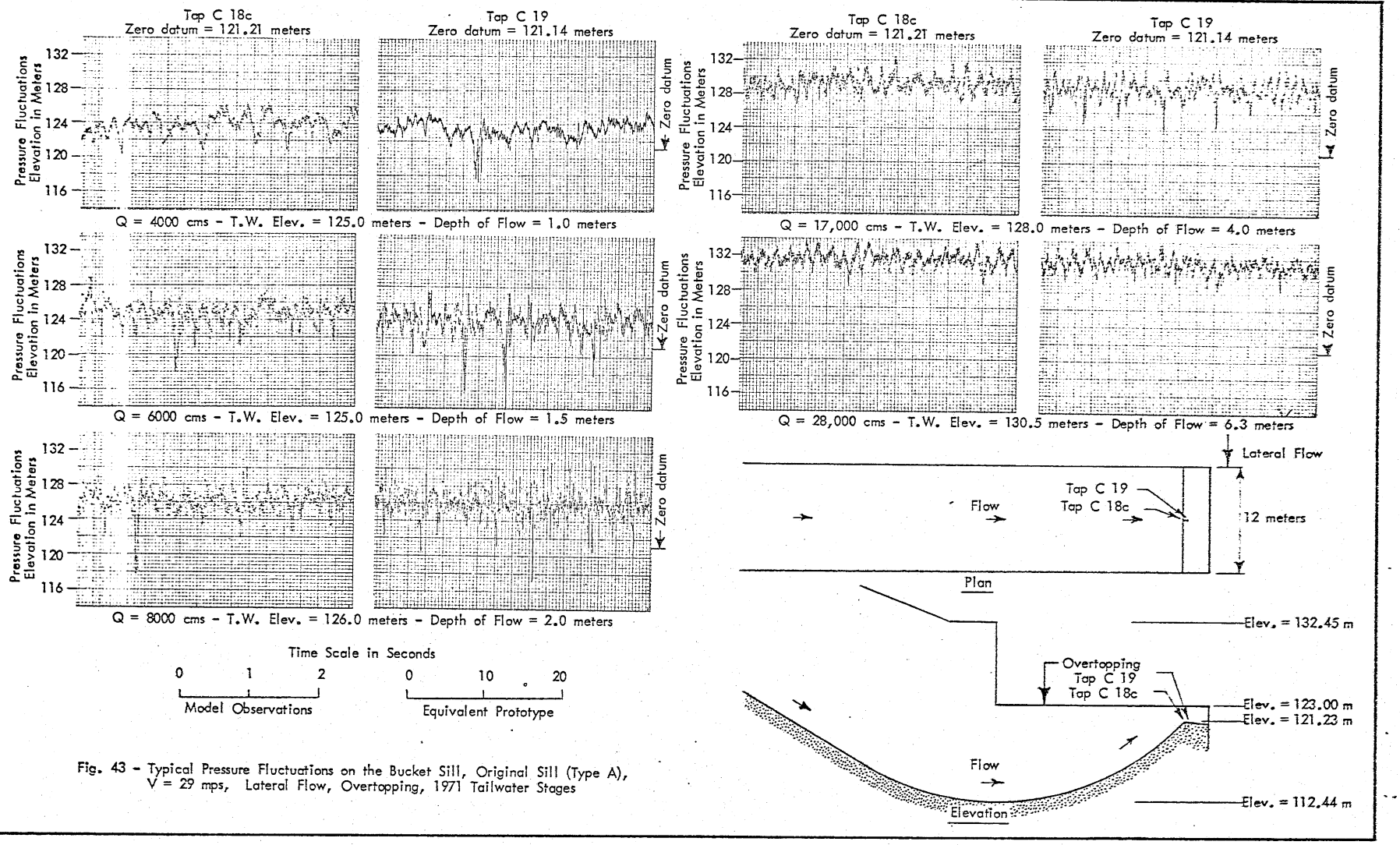

Fig. 43 - Typical Pressure Fluctuations on the Bucket Sill, Original Sill (Type A), V = 29 mps, Lateral Flow, Overtopping, 1971 Tailwater Stages

Fig. 43

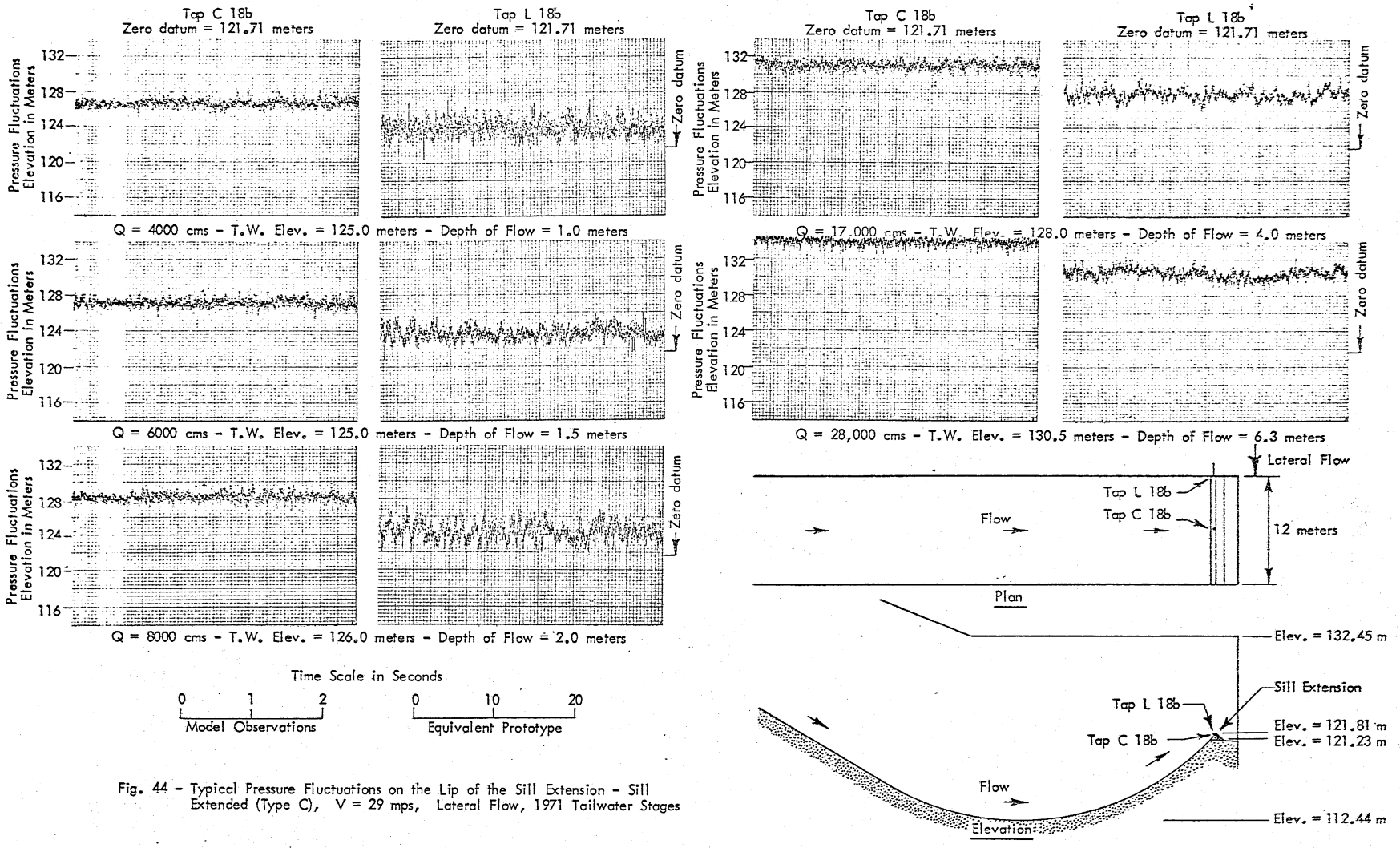

Fig. 44 - Typical Pressure Fluctuations on the Lip of the Sill Extension - Sill Extended (Type C), V = 29 mps, Lateral Flow, 1971 Tailwater Stages

Fig. 44

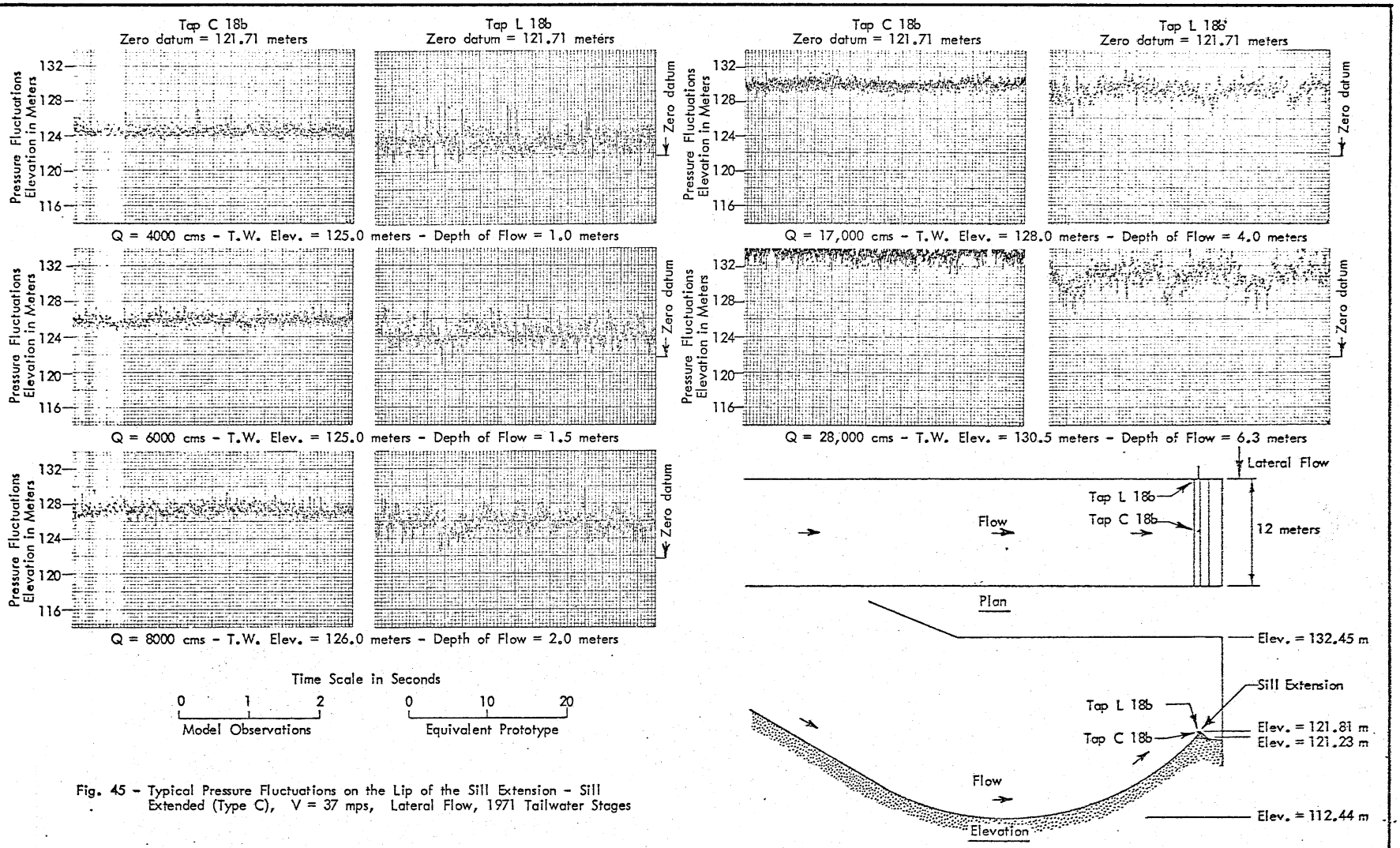

Fig. 45 - Typical Pressure Fluctuations on the Lip of the Sill Extension - Sill Extended (Type C), V = 37 mps, Lateral Flow, 1971 Tailwater Stages

Fig. 45

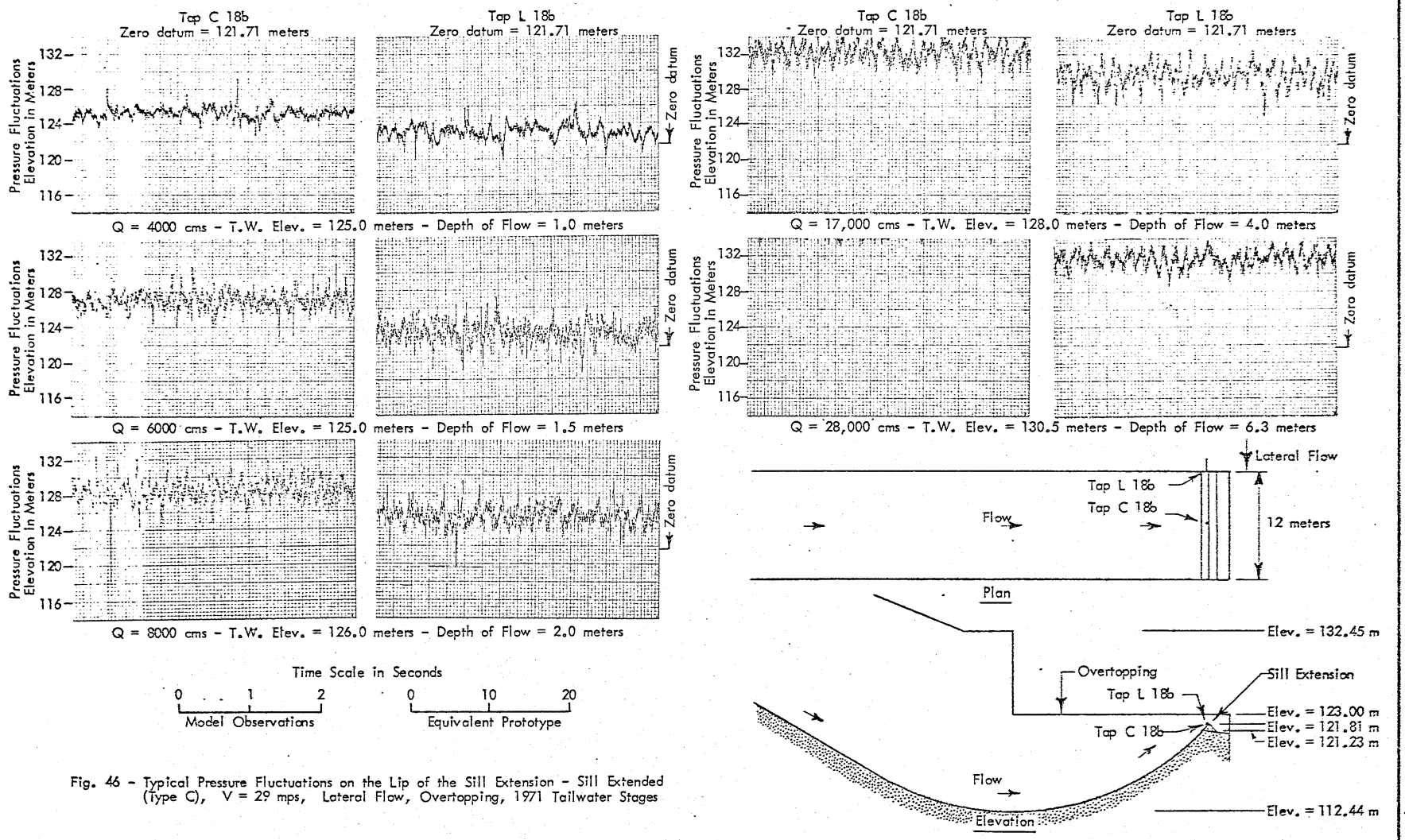

Fig. 46 - Typical Pressure Fluctuations on the Lip of the Sill Extension - Sill Extended (Type C), V = 29 mps, Lateral Flow, Overtopping, 1971 Tailwater Stages

Fig. 46

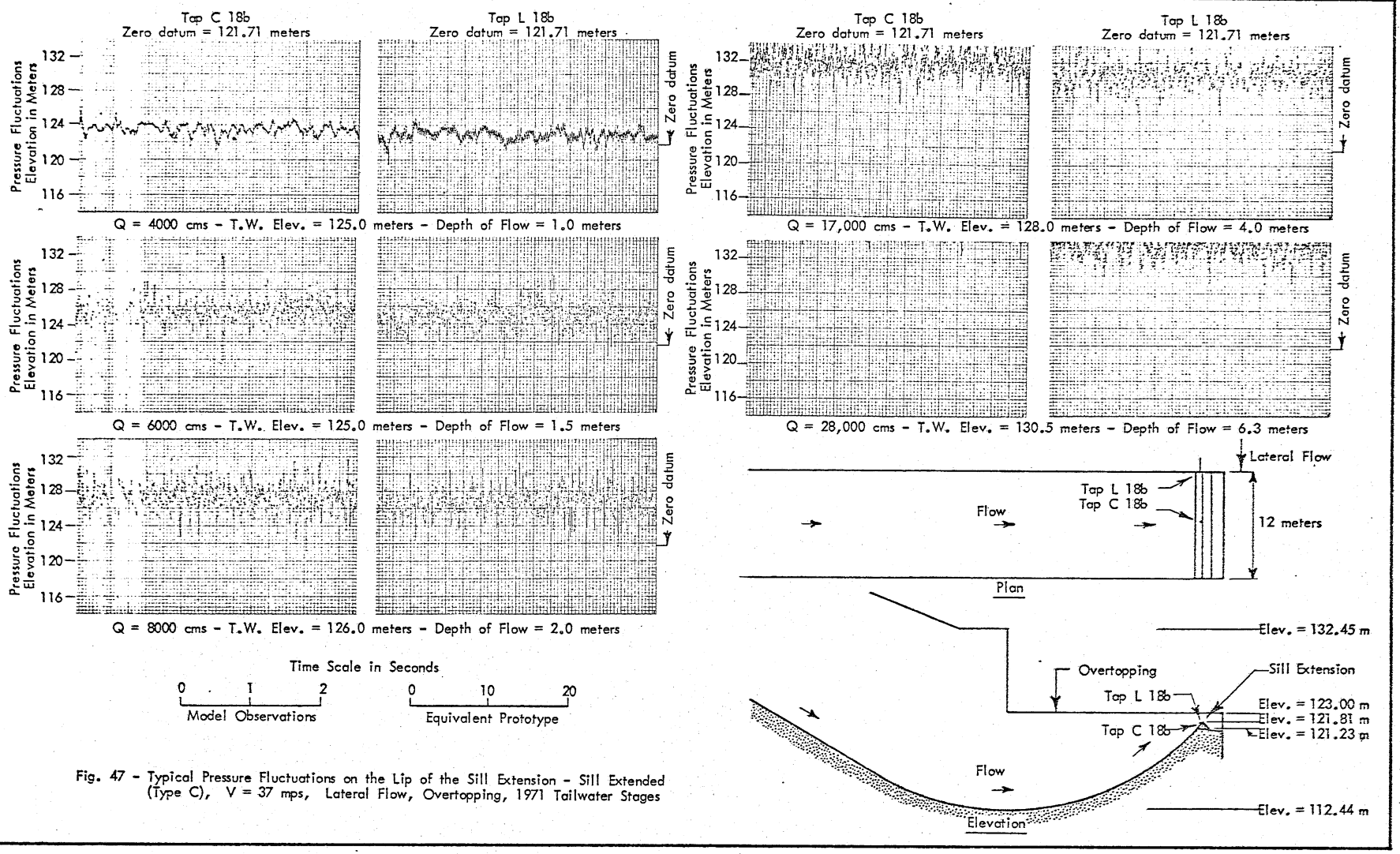

Fig. 47 - Typical Pressure Fluctuations on the Lip of the Sill Extension - Sill Extended (Type C), V = 37 mps, Lateral Flow, Overtopping, 1971 Tailwater Stages

Fig. 47

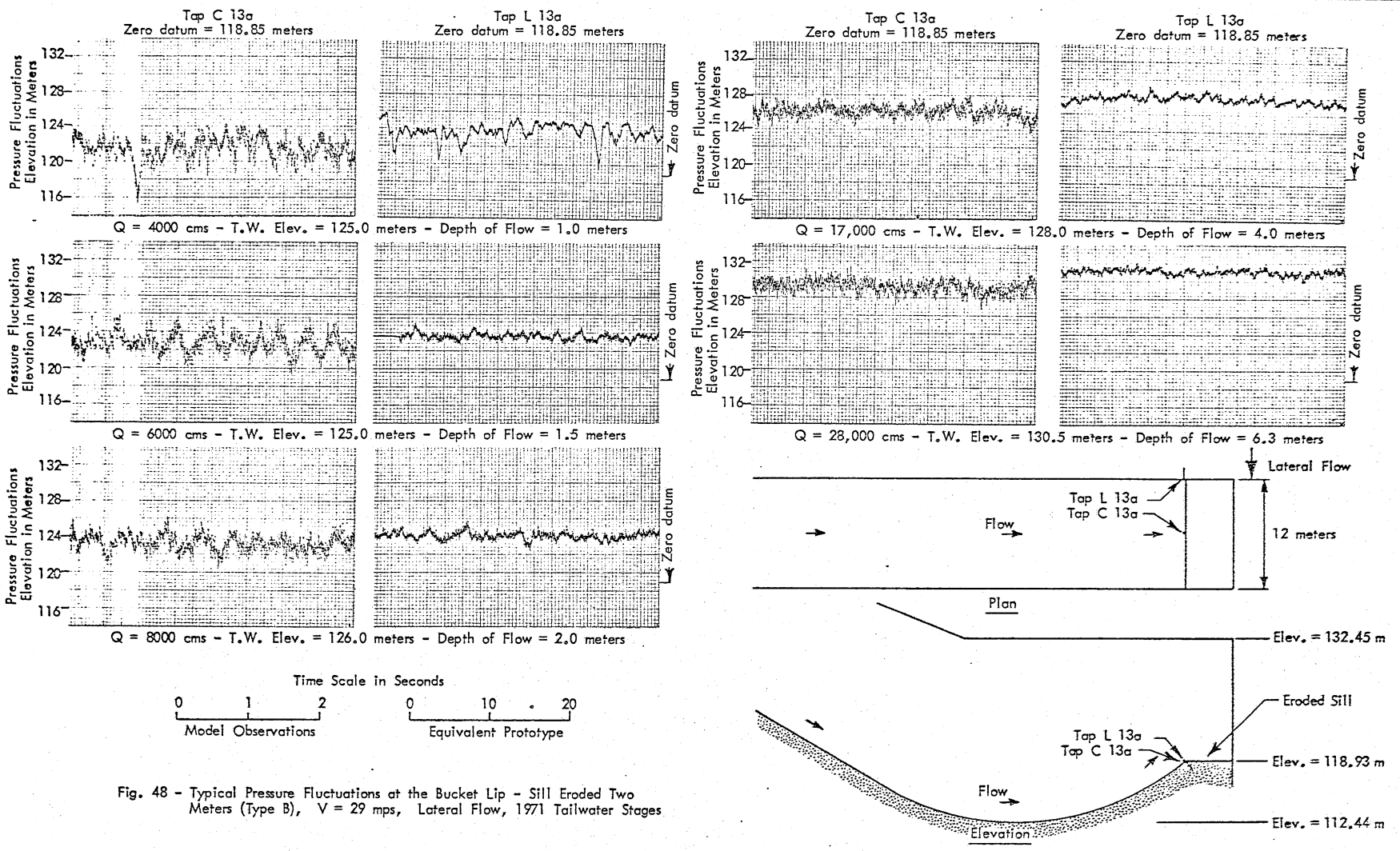

Fig. 48 - Typical Pressure Fluctuations at the Bucket Lip - Sill Eroded Two Meters (Type B), V = 29 mps, Lateral Flow, 1971 Tailwater Stages

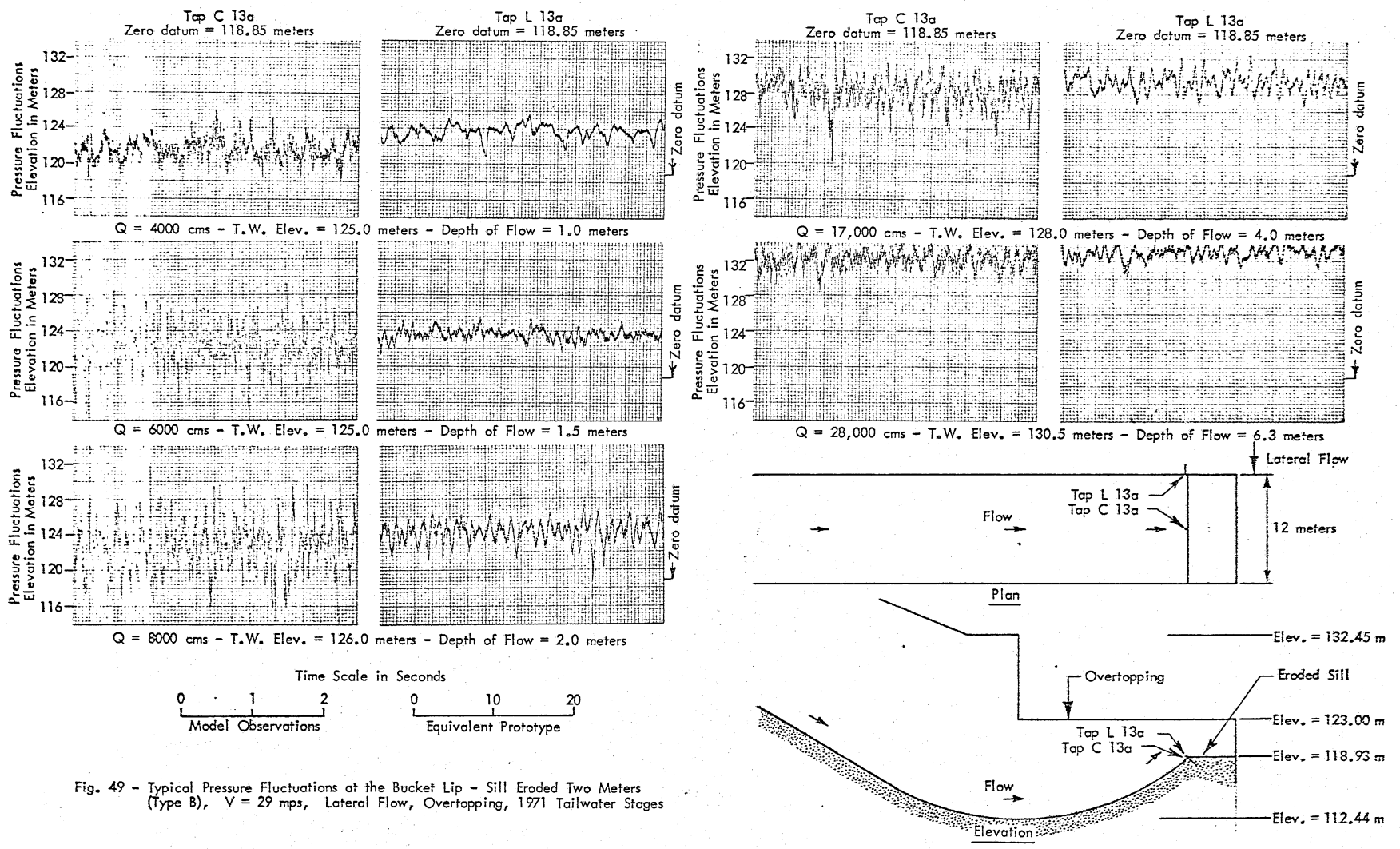

Fig. 49 - Typical Pressure Fluctuations at the Bucket Lip - Sill Eroded Two Meters (Type B), V = 29 mps, Lateral Flow, Overtopping, 1971 Tailwater Stages

Fig. 49

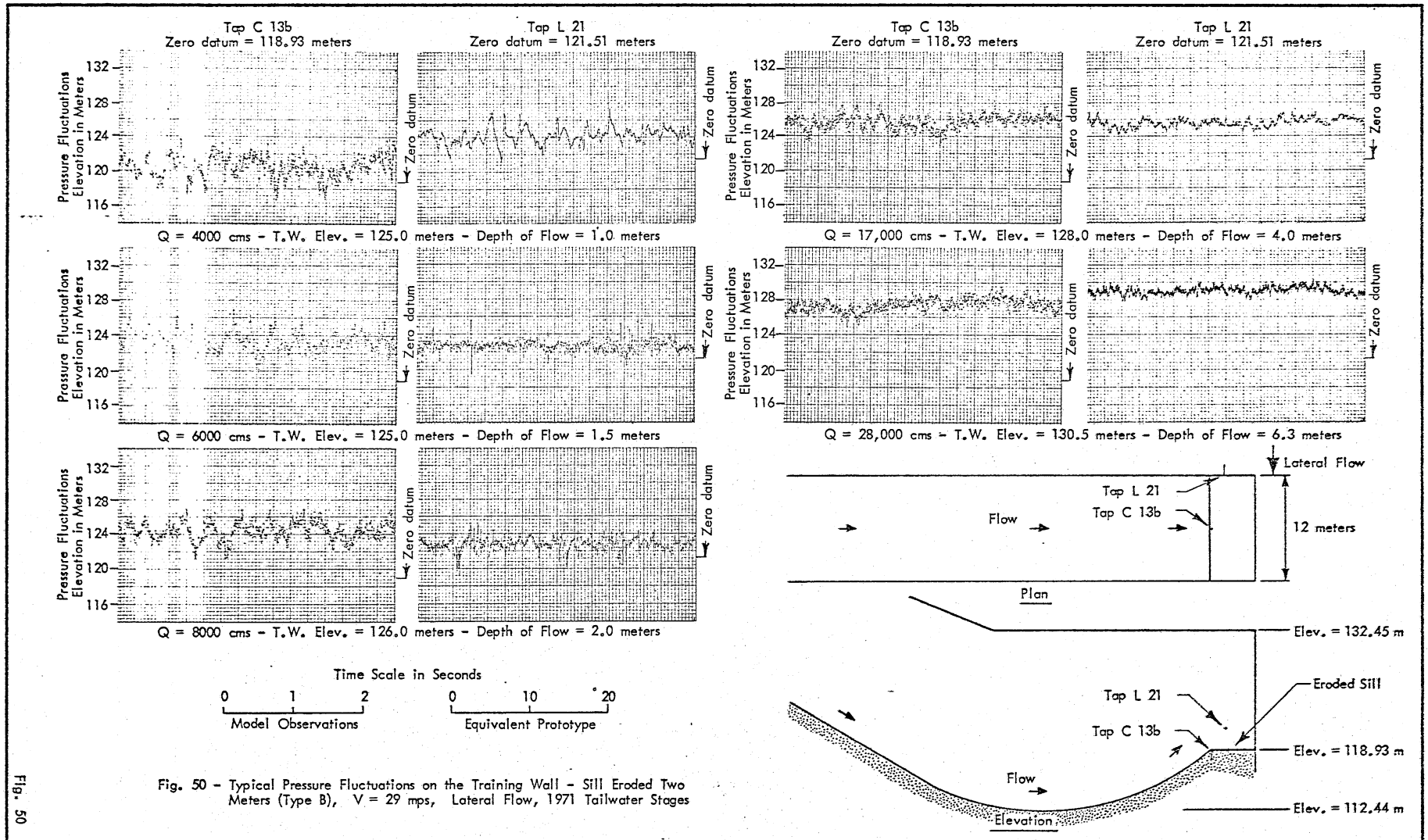

Fig. 50 - Typical Pressure Fluctuations on the Training Wall - Sill Eroded Two Meters (Type B), V = 29 mps, Lateral Flow, 1971 Tailwater Stages

Fig. 50

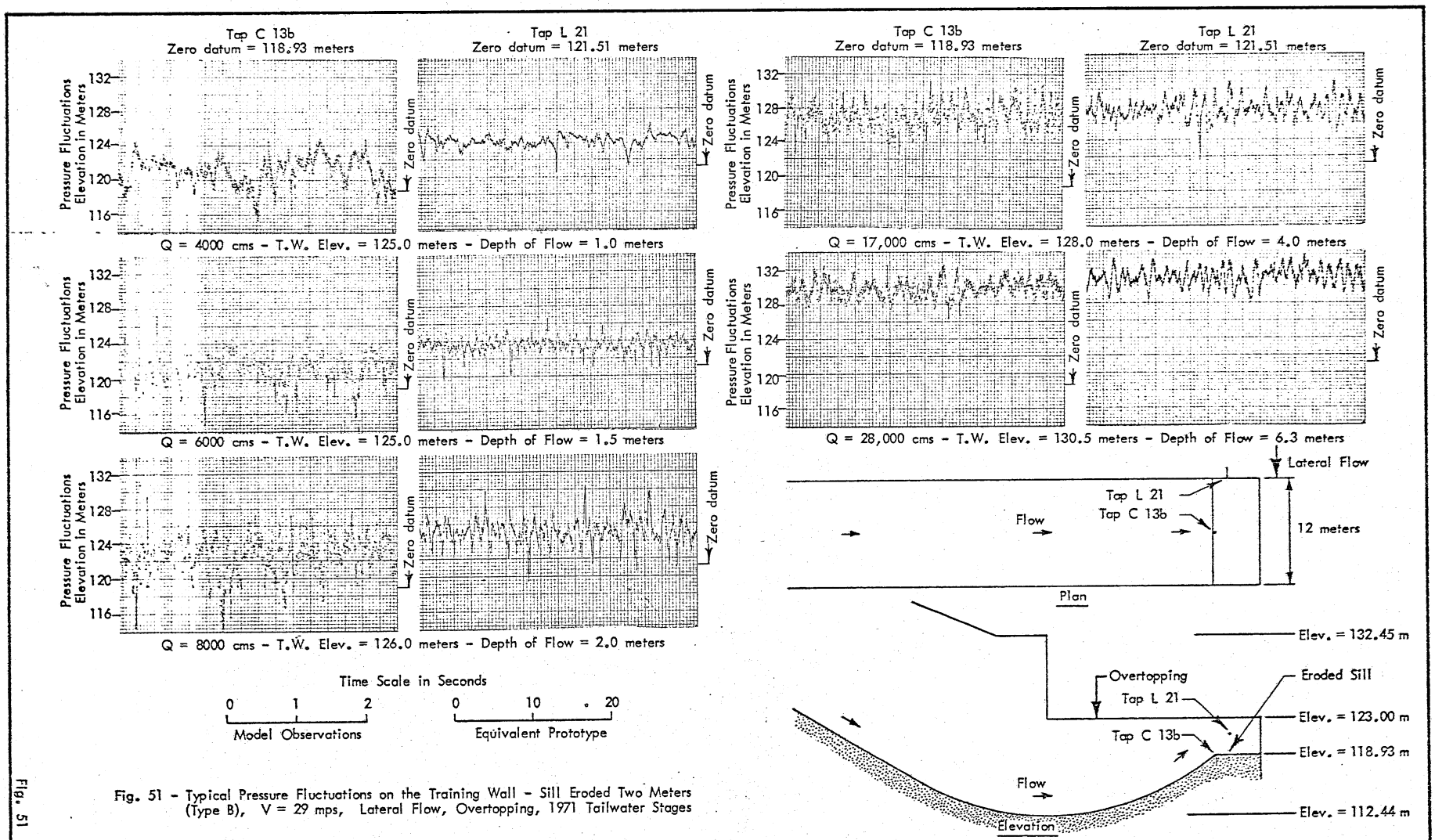

Fig. 51 - Typical Pressure Fluctuations on the Training Wall - Sill Eroded Two Meters (Type B), V = 29 mps, Lateral Flow, Overtopping, 1971 Tailwater Stages

Fig. 51

FIGURE 52

Tabular Summary of Pressure Fluctuation Data

Original Sill (Type A),

V = 29 mps, No Lateral Flow,

Various Tailwater Stages, Taps C18a and L18

			Tap C18a				Tap L18		
Discharge	Tail-water meters	Depth-d meters	Aver. Press. meters	Min. Press. meters	Max. Fluc. meters	ΔP	Aver. Press. meters	Min. Press. meters	Max. Press. meters
4,000	124	1.0	1.3	0.3	2.0	1.0	1.4	-0.6	3.6
4,000	125	1.0	1.7	0.2	2.2	1.5	1.8	-0.3	3.2
4,000	126	1.0	2.6	1.1	2.2	1.5	2.5	0.0	4.2
4,000	127	1.0	3.4	2.1	2.4	1.3	3.3	0.2	5.4
6,000	124	1.5	1.0	-0.6	2.4	1.6	2.5	0.4	3.6
6,000	125	1.5	1.8	0.3	2.3	1.5	3.0	0.8	3.1
6,000	126	1.5	3.7	2.1	2.5	1.6	3.5	0.9	3.9
6,000	127	1.5	3.3	1.6	2.0	1.7	3.9	0.6	6.0
6,000	128	1.5	4.4	2.4	2.5	2.0*	3.0	-1.0	4.8
6,000	129	1.5	4.9	3.4	2.4	1.5	4.1	0.3	6.5
8,000	124	2.0	0.4	-1.6	2.6	2.0	1.5	-1.2	4.2
8,000	125	2.0	2.3	1.2	1.5	1.1	2.8	0.5	4.0
8,000	126	2.0	2.8	1.3	1.9	1.5	3.9	1.6	4.2
8,000	127	2.0	3.8	2.5	1.7	1.3	4.2	2.2	2.8
10,000	124	2.5	1.3	-0.4	1.9	1.7	2.2	0.4	3.1
10,000	125	2.5	1.9	0.4	1.7	1.5	2.7	0.5	4.0
10,000	126	2.5	2.9	1.6	2.2	1.3	3.7	1.7	3.9
10,000	127	2.5	3.5	2.1	2.2	1.4	4.2	2.0	2.6
12,000	124	3.0	1.2	-0.6	1.6	1.8	2.5	0.2	2.3
12,000	125	3.0	1.9	0.7	1.5	1.2	2.8	0.6	3.3
12,000	126	3.0	3.2	1.9	1.0	1.3	4.2	2.3	2.1
12,000	127	3.0	4.1	3.0	1.3	1.1	4.8	2.6	3.0
17,000	124	4.0	1.4	-0.2	1.3	1.6	2.8	0.9	2.5
17,000	125	4.0	2.2	1.0	1.7	1.2	3.7	1.6	2.9
17,000	126	4.0	3.2	2.0	1.6	1.2	4.8	3.0	2.7
17,000	127	4.0	4.3	3.1	1.4	1.2	5.6	3.4	2.6
17,000	128	4.0	5.1	3.9	1.3	1.2	6.4	4.0	2.5
28,000	124	6.3	2.3	0.3	1.9	2.0	4.3	1.9	2.4
28,000	125	6.3	3.1	1.9	1.5	1.2	5.0	2.9	2.1
28,000	126	6.3	3.8	2.7	1.2	1.1	5.6	4.0	2.8
28,000	130.5	6.3	8.3	6.5	1.6	1.8	9.5	7.6	2.7

*Cp = 0.047

FIGURE 53

Tabular Summary of Pressure Fluctuation Data

Original Sill (Type A),

V = 29 mps, Lateral Flow

Various Tailwater Stages, Taps C18a and L18

			Tap C18a				Tap L18			
Discharge	Tail-water Meters	Depth-d Meters	Aver. Press. Meters	Min. Press. Meters	Max. Fluc. Meters	ΔP	Aver. Press. Meters	Min. Press. Meters	Max. Fluc. Meters	ΔP
4,000	124	1.0	2.0	0.8	1.9	1.2	0.0	-2.4	4.0	2.4
4,000	125	1.0	2.5	0.9	3.0	1.6	-0.1	-2.6	4.0	2.5
4,000	126	1.0	2.9	1.3	2.9	1.6	0.2	-2.2	3.5	2.2
4,000	127	1.0	3.9	1.6	3.4	2.3	1.4	-1.9	6.5	3.3
6,000	124	1.5	1.9	0.0	2.5	1.9	1.2	-2.6	5.6	3.8
6,000	125	1.5	2.8	0.9	1.6	1.9	0.9	-2.6	4.2	3.5
6,000	126	1.5	4.1	2.0	3.1	2.1	1.7	-2.3	4.2	4.0
6,000	127	1.5	3.8	1.9	2.2	1.9	2.0	-1.6	4.8	3.6
6,000	128	1.5	4.2	2.6	2.3	1.6	2.7	-0.9	6.6	3.6
6,000	129	1.5	5.3	3.7	2.2	1.6	3.4	-0.9	5.6	4.3
8,000	124	2.0	1.4	-0.9	2.0	2.3	0.6	-3.5	6.7	4.1
8,000	125	2.0	2.9	0.9	2.3	2.0	0.8	-3.2	4.2	4.0
8,000	126	2.0	3.7	1.7	2.3	2.0	1.7	-2.3	3.4	4.0
8,000	127	2.0	4.2	2.7	2.2	1.5	2.2	-1.2	3.8	3.4
10,000	124	2.5	1.9	-0.1	2.3	2.0	1.1	-2.5	4.4	3.6
10,000	125	2.5	2.8	0.2	2.2	2.6*	0.7	-2.8	2.8	3.5
10,000	126	2.5	3.2	1.6	1.8	1.6	1.7	-1.5	3.0	3.2
10,000	127	2.5	4.2	2.5	2.2	1.7	2.3	-0.6	3.0	2.9
12,000	124	3.0	1.8	-0.4	1.8	2.2	1.0	-3.8	4.4	4.8
12,000	125	3.0	2.5	0.7	2.4	1.8	0.8	-2.3	2.6	3.1
12,000	126	3.0	3.7	2.4	1.7	1.3	2.3	-1.3	3.6	3.6
12,000	127	3.0	4.5	3.1	1.5	1.4	3.1	0.6	2.9	2.5
17,000	124	4.0	2.0	-0.6	2.0	2.6	1.7	-2.9	5.2	4.6
17,000	125	4.0	2.8	0.8	1.5	2.0	2.0	-1.2	3.2	3.2
17,000	126	4.0	3.7	2.6	1.2	1.1	3.0	0.1	2.2	2.9
17,000	127	4.0	4.6	3.3	1.4	1.3	4.2	0.6	2.6	3.6
17,000	128	4.0	5.6	4.2	1.6	1.4	5.1	2.4	2.6	2.7
28,000	124	6.3	2.8	0.6	2.1	2.2	3.0	-2.0	3.7	5.0**
28,000	125	6.3	3.4	1.6	1.2	1.8	3.0	-0.2	2.5	3.2
28,000	126	6.3	4.4	2.8	1.5	1.6	4.1	1.0	2.1	3.0
28,000	130.5	6.3	8.3	6.8	1.5	1.5	8.8	6.4	2.1	2.4

*Cp = 0.061
**Cp = 0.117

FIGURE 54

Tabular Summary of Pressure Fluctuation Data

Original Sill (Type A),

V = 29 mps, Lateral Flow, Overtopping,

Various Tailwater Stages, Taps C18a and L18

			C18a				L18			
Discharge cms	Tail-water Meters	Depth-d Meters	Aver. Press. Meters	Min. Press. Meters	Max. Fluc. Meters	ΔP	Aver. Press. Meters	Min. Press. Meters	Max. Fluc. Meters	ΔP
4,000	124	1.0	1.7	0.1	3.0	1.6	-0.6	-3.7	6.0	3.1
4,000	125	1.0	2.6	-1.9	4.0	4.5	0.8	-3.7	5.4	4.5
4,000	126	1.0	4.2	0.6	3.8	3.6	2.6	-1.8	3.4	4.4
4,000	127	1.0	5.1	2.4	2.0	2.7	3.7	-0.9	2.5	4.6
6,000	124	1.5	2.8	0.5	2.0	2.3	0.7	-3.7	8.5	4.4
6,000	125	1.5	2.8	-2.3	10.2	5.1	1.0	-5.0	8.9	6.0
6,000	126	1.5	4.6	-2.2	7.4	6.8	3.3	-4.5	12.4	7.8
6,000	127	1.5	6.4	1.3	3.9	5.1	4.8	-2.3	11.6	7.1
6,000	128	1.5	7.1	2.6	4.0	4.5	7.0	-0.1	6.4	7.1
6,000	129	1.5	8.2	3.8	4.3	4.4	6.5	0.9	7.9	5.6
8,000	124	2.0	2.2	0.1	1.8	2.1	0.2	-3.6	4.3	3.8
8,000	125	2.0	2.9	0.5	4.0	2.4	1.2	-2.1	4.5	3.3
8,000	126	2.0	4.6	-5.1	9.3	9.7	3.3	-5.3	7.9	8.6
8,000	127	2.0	5.7	-4.3	14.9	10.0*	5.3	-6.0	12.4	11.3**
10,000	124	2.5	1.9	-0.2	1.8	2.1	0.6	-3.8	5.2	4.4
10,000	125	2.5	3.0	-0.6	4.4	3.6	2.0	-3.3	8.0	5.3
10,000	126	2.5	4.7	-0.1	4.9	4.8	3.6	-4.2	6.7	7.8
10,000	127	2.5	5.8	-1.8	7.6	7.6	4.9	-4.8	5.7	9.7
12,000	124	3.0	2.1	0.2	2.0	1.9	0.9	-3.6	4.3	4.5
12,000	125	3.0	2.9	1.2	1.8	1.7	2.1	-1.2	1.9	3.3
12,000	126	3.0	4.5	-0.3	4.1	4.8	4.2	-2.0	10.0	6.2
12,000	127	3.0	5.7	0.3	6.2	5.4	5.8	-3.6	11.5	9.4
17,000	124	4.0	2.4	0.4	1.8	2.0	1.4	-2.3	3.4	3.7
17,000	125	4.0	3.7	1.7	2.2	2.0	3.2	-0.6	2.6	3.8
17,000	126	4.0	5.0	1.3	3.5	3.7	5.1	-0.6	2.5	5.7
17,000	127	4.0	6.0	2.3	2.3	3.7	6.5	2.0	2.6	4.5
17,000	128	4.0	7.3	3.3	3.6	4.0	7.5	2.0	3.6	5.5
28,000	124	6.3	2.7	1.0	1.6	1.7	2.3	-1.7	3.9	4.0
28,000	125	6.3	4.0	2.1	1.5	1.9	3.4	0.6	2.4	2.8
28,000	126	6.3	5.4	3.7	1.2	1.7	5.5	2.6	2.0	2.9
28,000	130.5	6.3	10.4	6.8	1.7	3.6	10.9	6.9	1.6	4.0

* Cp = 0.234

**Cp = 0.264

FIGURE 55

Tabular Summary of Pressure Fluctuation Data

Original Sill (Type A),

V = 29 mps, Lateral Flow,

Various Tailwater Stages, Tap C18c and C19

			Tap C18c				Tap C19			
Discharge cms	Tail-water Meters	Depth-d Meters	Aver. Press. Meters	Min. Press. Meters	Max. Fluc. Meters	ΔP	Aver. Press. Meters	Min. Press. Meters	Max. Fluc. Meters	ΔP
4,000	124	1.0	4.4	1.8	2.2	2.6	3.6	1.0	2.6	2.6
4,000	125	1.0	5.0	3.2	1.8	1.8	4.4	2.9	2.2	1.5
4,000	126	1.0	5.8	3.8	2.0	2.0	2.3	-2.8	3.1	5.1**
4,000	127	1.0	6.4	4.6	2.2	1.8	3.6	-1.2	1.4	4.8
6,000	124	1.5	4.0	1.1	2.2	2.9	3.4	1.0	3.5	2.4
6,000	125	1.5	4.6	2.6	1.8	2.0	4.2	2.0	2.3	2.2
6,000	126	1.5	5.2	3.0	1.8	2.2	5.0	2.9	2.1	2.1
6,000	127	1.5	6.4	4.6	1.9	1.8	5.8	3.9	2.2	1.9
8,000	124	2.0	4.2	1.6	2.0	2.6	3.8	0.3	4.1	3.5
8,000	125	2.0	4.3	1.2	3.0	3.1*	4.2	2.0	3.2	2.2
8,000	126	2.0	5.2	3.6	1.6	1.6	4.9	2.5	2.6	2.4
8,000	127	2.0	6.4	4.4	1.7	2.0	5.7	3.5	2.1	2.2
17,000	128	4.0	7.0	5.2	2.6	1.8	6.7	4.5	2.6	2.2
28,000	130.5	6.3	9.1	7.2	2.5	1.9	8.3	6.7	2.1	0.6
			Overtopping with Lateral Flow							
4,000	124	1.0	4.5	1.4	2.9	3.1	1.8	-6.9	6.6	8.7
4,000	125	1.0	2.4	-1.6	2.8	4.0	2.5	-3.9	2.5	6.4
4,000	126	1.0	3.5	-0.2	1.4	3.7	3.4	-1.9	2.8	5.3
4,000	127	1.0	5.4	1.7	2.0	3.7	4.5	-3.0	9.0	7.5
6,000	124	1.5	4.0	1.6	2.0	2.4	3.8	-0.3	4.5	4.1
6,000	125	1.5	3.2	-3.2	4.8	6.4	3.0	-7.5	10.5	10.5
6,000	126	1.5	4.9	-2.4	5.0	7.3	4.2	-3.8	6.4	8.0
6,000	127	1.5	6.4	-1.4	3.0	7.8	5.6	-1.2	6.6	6.8
8,000	124	2.0	4.3	1.7	3.1	2.6	3.4	-0.2	4.1	3.6
8,000	125	2.0	4.2	-0.2	2.8	4.4	4.2	0.1	6.2	4.1
8,000	126	2.0	5.2	-3.3	4.1	8.5#	4.8	-3.9	10.8	8.7
8,000	127	2.0	6.5	-1.4	7.1	7.9	5.9	-8.0	11.2	13.9##
17,000	128	4.0	8.0	2.6	3.4	5.4	7.6	2.5	3.6	5.1
28,000	130.5	6.3	10.6	7.3	2.3	3.3	10.3	7.0	3.4	3.3

* Cp = 0.072
** Cp = 0.119
\# Cp = 0.198
Cp = 0.325

FIGURE 56

Tabular Summary of Pressure Fluctuation Data

Original Sill (Type A)

V = 29 mps, Lateral Flow,

Various Tailwater Stages, Taps L17 and L19

			Tap L17			Tap L19			
Discharge cms	Tail-water Meters	Depth-d Meters	Aver. Press. Meters	Min. Press. Meters	Max. Fluc. Meters	Aver. Press. Meters	Min. Press. Meters	Max. Fluc. Meters	ΔP
4,000	124	1.0	2.0	0.6	1.6	-0.1	-3.5	2.4	3.4
4,000	125	1.0	3.8	0.2	1.8	0.3	-2.2	2.2	2.5
4,000	126	1.0	6.1	0.4	1.2	1.3	-3.3	3.2	4.6
4,000	127	1.0	5.1	2.9	1.6	1.3	-14.1	7.1	15.4*
6,000	124	1.5	2.6	1.4	1.6	0.3	-5.5	4.4	5.8
6,000	125	1.5	3.4	1.8	2.1	0.3	-5.1	3.7	5.4
6,000	126	1.5	3.8	2.1	2.2	2.5	-2.0	2.8	4.5
6,000	127	1.5	4.7	2.7	2.3	4.5	1.2	2.6	5.7
8,000	124	2.0	2.4	0.7	1.1	0.3	-3.7	4.0	4.0
8,000	125	2.0	3.5	1.5	1.7	1.1	-3.8	3.5	4.9
8,000	126	2.0	3.8	2.2	1.2	2.4	-1.4	5.7	3.8
8,000	127	2.0	5.2	3.6	1.9	3.7	0.1	3.1	3.6
17,000	128	4.0	7.6	6.1	1.6	4.8	1.4	3.7	3.4
28,000	130.5	6.3	11.2	9.7	1.7	7.2	3.5	2.1	3.7
			Overtopping with Lateral Flow						
4,000	124	1.0	1.6	-0.5	2.1	-0.8	-4.1	2.4	3.3
4,000	125	1.0	3.6	1.2	1.4	-1.1	-14.7	10.0	13.6**
4,000	126	1.0	6.9	3.0	1.4	1.5	-11.3	2.5	12.8
4,000	127	1.0	6.3	4.1	1.4	1.6	-11.1	7.0	12.7
6,000	124	1.5	2.1	0.7	2.5	-1.0	-5.0	3.7	4.0
6,000	125	1.5	3.7	0.8	2.2	-0.6	-12.1	3.2	11.5
6,000	126	1.5	5.2	0.1	4.0	1.5	-7.7	3.0	9.2
6,000	127	1.5	6.3	1.6	2.6	3.0	-5.9	1.8	8.9
8,000	124	2.0	2.3	-0.2	1.9	-0.4	-4.6	3.9	4.2
8,000	125	2.0	4.1	1.6	2.4	0.2	-4.8	5.0	5.0
8,000	126	2.0	5.6	1.0	5.0	2.2	-7.1	5.2	9.3
8,000	127	2.0	7.0	0.1	3.6	3.7	-5.9	5.6	9.6
17,000	128	4.0	9.9	5.5	2.1	6.9	1.3	2.4	5.6
28,000	130.5	6.3	13.4	9.7	---	9.2	5.1	1.8	4.1

* Cp = 0.359
** Cp = 0.318

FIGURE 57

Tabular Summary of Pressure Fluctuation Data

Original Sill (Type A)

V = 29 mps, Lateral Flow

Various Tailwater Stages, Taps L21 and L23

			Tap L21				Tap L23			
Discharge cms	Tail-water Meters	Depth-d Meters	Aver. Press. Meters	Min. Press. Meters	Max. Fluc. Meters	ΔP	Aver. Press. Meters	Min. Press. Meters	Max. Fluc. Meters	ΔP
4,000	124	1.0	-0.5	-1.6	2.4	1.1	-1.9	-3.7	3.7	1.8
4,000	125	1.0	1.5	-2.7	3.4	4.2	0.6	-3.7	6.0	4.3
4,000	126	1.0	-0.3	-2.1	3.6	1.8	-1.4	-6.7	8.7	5.3**
4,000	127	1.0	2.5	-1.9	2.0	4.4*	2.6	-0.9	3.5	3.5
6,000	124	1.5	0.8	-2.2	2.6	3.0	-0.8	-2.9	4.1	2.1
6,000	125	1.5	0.8	-1.6	3.1	2.4	-0.9	-3.9	4.3	3.0
6,000	126	1.5	1.3	-0.9	4.3	2.2	-1.1	-5.0	5.3	3.9
6,000	127	1.5	2.5	0.1	4.1	2.4	-0.3	-4.2	5.2	3.9
8,000	124	2.0	0.8	-1.5	3.6	2.3	-0.7	-3.9	4.8	3.2
8,000	125	2.0	1.2	-2.2	4.5	3.4	-0.8	-3.4	3.7	2.6
8,000	126	2.0	1.7	-0.4	2.8	2.1	-0.3	-3.2	4.3	2.9
8,000	127	2.0	2.9	0.8	2.2	2.1	0.1	-3.1	4.4	3.2
17,000	128	4.0	5.4	3.1	2.7	2.3	1.9	-0.9	3.4	2.8
28,000	130.5	6.3	9.4	6.8	2.3	2.6	6.0	3.3	2.7	2.7
			Overtopping with Lateral Flow							
4,000	124	1.0	-0.8	-3.2	3.9	2.4	-2.1	-4.5	6.0	2.4
4,000	125	1.0	0.1	-2.8	3.8	2.7	0.0	-6.5	3.4	6.5
4,000	126	1.0	1.7	-1.6	2.7	3.3	1.4	-2.9	3.6	4.3
4,000	127	1.0	3.4	-0.5	1.8	3.9	2.0	-2.5	4.7	4.5
6,000	124	1.5	0.1	-2.2	2.8	2.3	-1.3	-3.2	3.8	1.9
6,000	125	1.5	1.4	-3.5	5.7	4.9	-0.1	-5.4	7.9	5.3
6,000	126	1.5	3.0	-3.3	4.3	6.3	1.3	-4.5	4.3	5.8
6,000	127	1.5	4.4	-1.2	3.6	5.6	2.6	-4.9	5.2	7.5
8,000	124	2.0	0.5	-2.0	3.0	2.5	-1.0	-2.9	4.4	1.9
8,000	125	2.0	1.3	-3.9	4.1	5.2	0.1	-3.9	4.8	4.0
8,000	126	2.0	3.5	-2.5	8.0	6.0	1.3	-6.4	8.0	7.7
8,000	127	2.0	4.9	-4.3	6.6	9.2#	2.3	-7.0	7.6	9.3##
17,000	128	4.0	7.7	1.6	4.4	6.1	3.6	-2.3	6.0	5.9
28,000	130.5	6.3	10.8	6.5	---	4.3	6.6	-1.5	5.0	8.1

* Cp = 0.103
**Cp = 0.124
\# Cp = 0.215
\#\#Cp = 0.217

FIGURE 58

Tabular Summary of Pressure Fluctuation Data

Original Sill (Type A)

V = 37 mps, Lateral Flow,

Various Tailwater Stages, Taps C18a and L18

			Tap C18a				Tap L18			
Discharge cms	Tail-water Meters	Depth-d Meters	Aver. Press. Meters	Min. Press. Meters	Max. Fluc. Meters	ΔP	Aver. Press. Meters	Min. Press. Meters	Max. Fluc. Meters	ΔP
2,000	124	0.5	4.5	4.0	0.5	0.5	2.7	2.0	0.6	0.7
2,000	127	0.5	6.8	6.2	0.4	0.6	4.6	3.9	0.5	0.7
4,000	124	1.0	0.9	-0.7	1.8	1.6	-0.6	-3.8	3.0	3.2
4,000	125	1.0	1.9	0.0	1.4	1.9	-0.4	-3.5	6.0	3.1
4,000	126	1.0	4.4	0.1	2.2	4.3	2.2	-3.0	3.8	5.2
4,000	127	1.0	5.7	1.2	2.1	4.5*	3.9	-1.0	1.2	4.9
6,000	124	1.5	1.0	-1.2	2.1	2.2	0.3	-4.1	5.1	4.4
6,000	125	1.5	1.8	-0.5	1.9	2.3	0.5	-3.2	5.0	3.7
6,000	126	1.5	2.4	0.1	2.0	2.3	0.8	-2.8	5.6	3.6
6,000	127	1.5	3.3	1.2	3.4	2.1	2.0	-2.5	4.0	4.5
8,000	124	2.0	0.8	-1.7	3.0	2.5	0.1	-5.4	6.8	5.5**
8,000	125	2.0	1.6	-0.7	2.2	2.3	0.5	-3.5	5.4	4.0
8,000	126	2.0	3.1	0.8	3.3	2.3	1.7	-2.5	5.8	4.2
8,000	127	2.0	3.9	1.8	2.4	2.1	2.3	-1.7	5.6	4.0
17,000	128	4.0	5.0	2.5	2.8	2.5	4.1	-0.8	4.4	4.9
28,000	130.5	6.3	8.0	6.1	1.8	1.9	8.7	4.7	4.5	4.0
			Overtopping with Lateral Flow							
2,000	124	0.5	4.0	3.6	0.4	0.4	1.7	1.2	0.5	0.5
2,000	127	0.5	6.6	5.7	0.5	0.9	4.2	3.5	0.6	0.7
4,000	124	1.0	1.8	-0.9	2.1	2.7	-0.4	-4.1	11.1	3.7
4,000	125	1.0	3.9	-1.0	2.0	4.9	1.4	-3.6	2.1	5.0
4,000	126	1.0	5.2	1.7	1.8	3.5	2.6	-3.3	2.9	5.9
4,000	127	1.0	5.8	2.8	2.1	3.0	3.3	-1.6	3.8	4.9
6,000	124	1.5	0.9	-1.4	2.3	2.3	-0.1	-4.3	6.5	4.2
6,000	125	1.5	4.0	-1.9	6.6	5.9	0.9	-7.4	9.0	8.3
6,000	126	1.5	5.6	-0.1	4.6	5.7	2.7	-7.3	6.7	10.0##
6,000	127	1.5	6.7	0.1	3.0	6.6	4.1	-4.6	4.0	8.7
8,000	124	2.0	0.7	-1.5	2.8	2.2	-0.3	-5.4	8.2	5.1
8,000	125	2.0	3.0	-1.0	7.2	4.0	0.9	-3.0	5.1	3.9
8,000	126	2.0	5.4	0.3	7.0	5.1	3.7	-5.2	15.0	8.9
8,000	127	2.0	6.6	-1.3	5.0	7.9#	4.9	-5.0	4.4	9.9
17,000	128	4.0	6.9	-0.5	7.4	7.4	8.1	-0.6	11.0	8.7
28,000	130.5	6.3	11.3	5.9	---	5.4	10.3	2.7	---	7.6

* Cp = 0.065
** Cp = 0.080
\# Cp = 0.115
Cp = 0.145

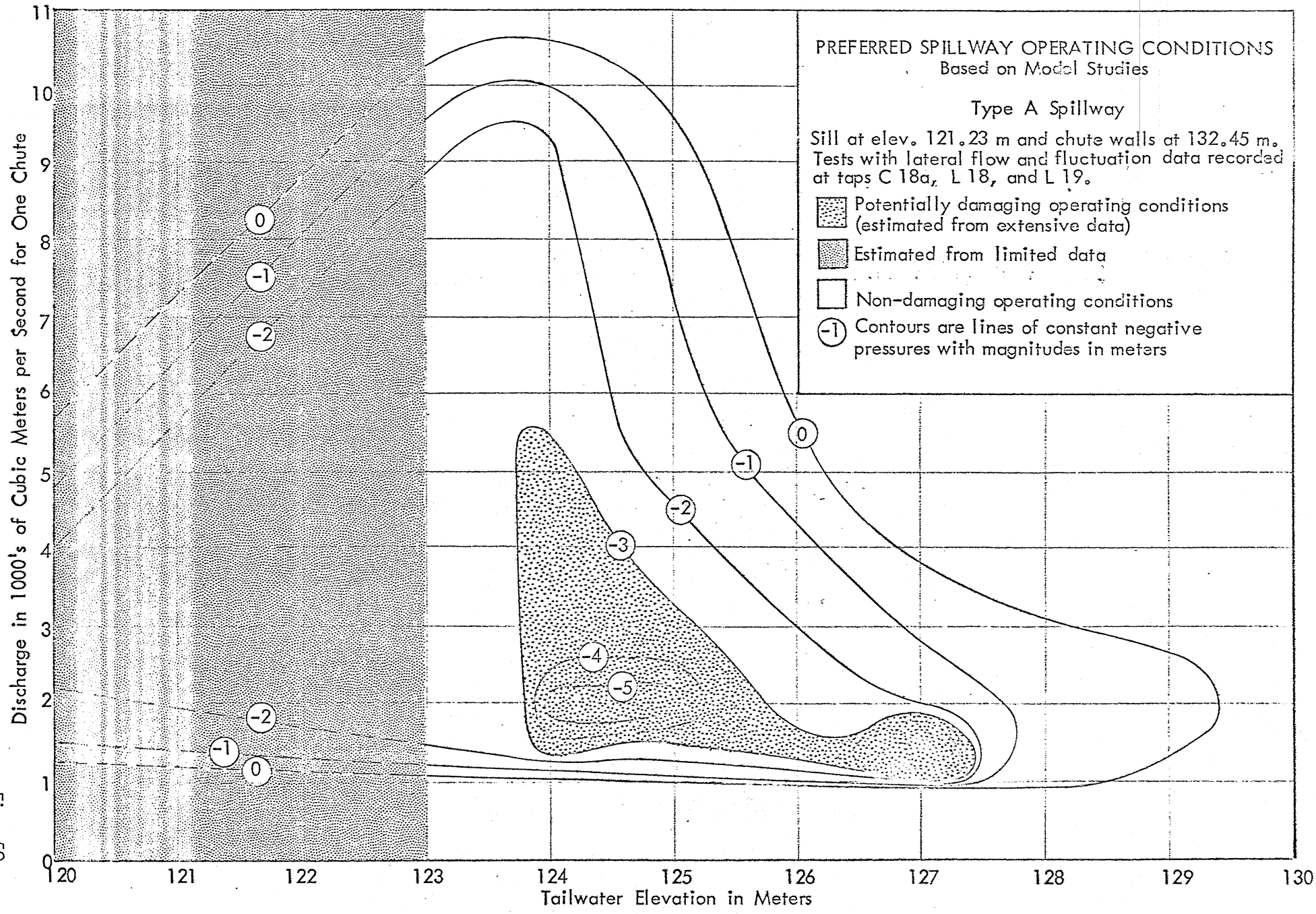
PREFERRED SPILLWAY OPERATING CONDITIONS
Based on Model Studies
Type A Spillway
Sill at elev. 121.23 m and chute walls at 132.45 m.
Tests with lateral flow and fluctuation data recorded at taps C 18a, L 18, and L 19.
Potentially damaging operating conditions (estimated from extensive data)
Estimated from limited data
Non-damaging operating conditions
(-1) Contours are lines of constant negative pressures with magnitudes in meters
Discharge in 1000's of Cubic Meters per Second for One Chute
Tailwater Elevation in Meters
0
1
2
3
4
5
6
7
8
9
10
11
120
121
122
123
124
125
126
127
128
129
130
0
-1
-2
-3
-4
-5

Fig. 59

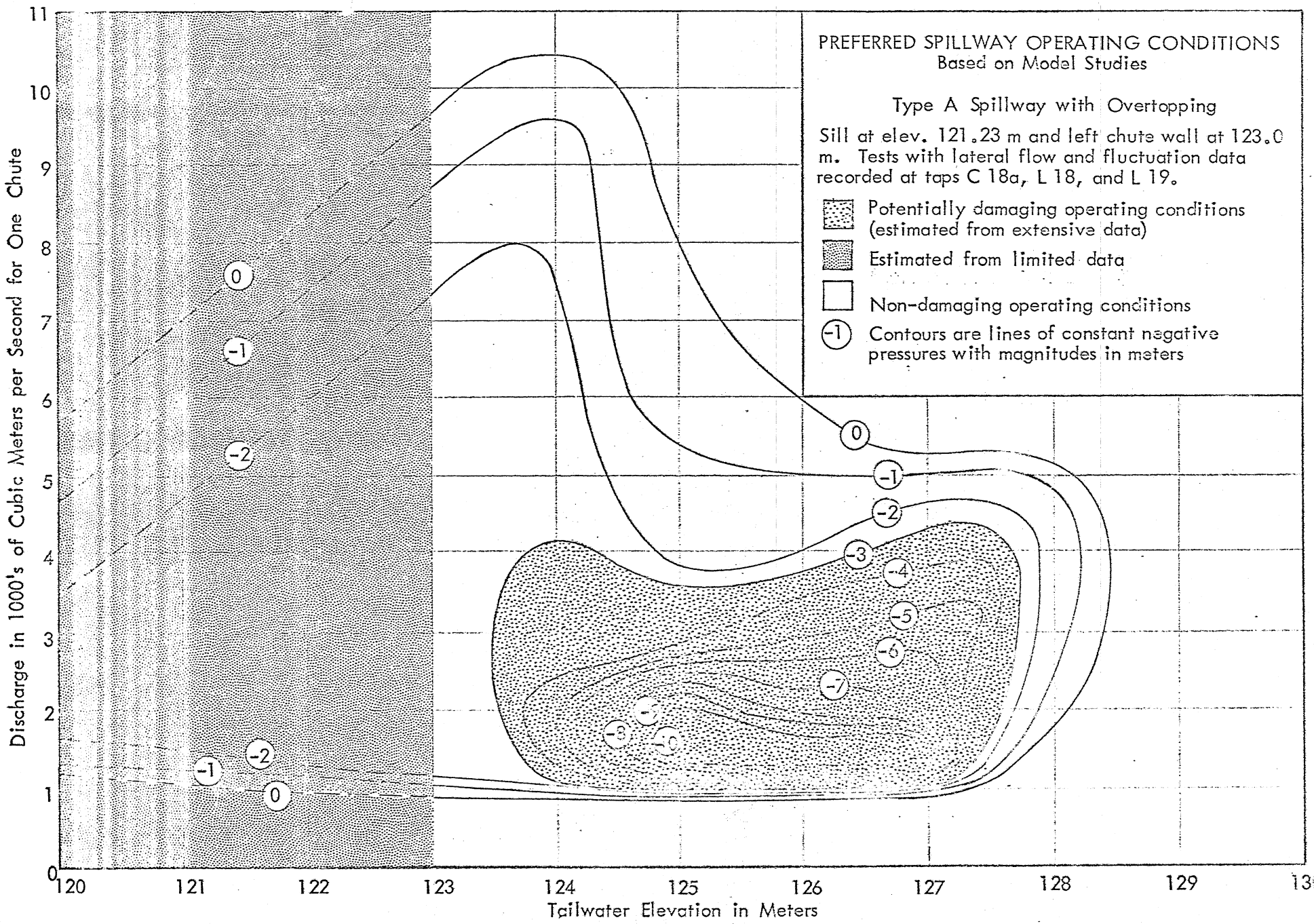
PREFERRED SPILLWAY OPERATING CONDITIONS
Based on Model Studies
Type A Spillway with Overtopping
Sill at elev. 121.23 m and left chute wall at 123.0 m. Tests with lateral flow and fluctuation data recorded at taps C 18a, L 18, and L 19.
Potentially damaging operating conditions (estimated from extensive data)
Estimated from limited data
Non-damaging operating conditions
-1 Contours are lines of constant negative pressures with magnitudes in meters
Discharge in 1000's of Cubic Meters per Second for One Chute
Tailwater Elevation in Meters
0
1
2
3
4
5
6
7
8
9
10
11
120
121
122
123
124
125
126
127
128
129
130

Fig. 60

FIGURE 61

Tabular Summary of Pressure Fluctuation Data
on the Lip of the Sill Extension-Sill Extended (Type C)
V = 29 mps, Lateral Flow
Various Tailwater Stages, Taps C18b and L18b

			C18b				L18b			
Discharge cms	Tail-water Meters	Depth-d Meters	Aver. Press. Meters	Min. Press. Meters	Max. Fluc. Meters	ΔP	Aver. Press. Meters	Min. Press. Meters	Max. Fluc. Meters	ΔP
4,000	124	1.0	3.8	2.4	2.0		1.0	-1.3	3.0	2.3
4,000	125	1.0	5.0	3.4	2.0		2.0	-1.3	4.2	3.3
4,000	126	1.0	4.5	2.2	1.8		2.8	-0.5	2.9	3.3
4,000	127	1.0	5.3	2.9	3.2		4.1	0.9	2.6	3.2
6,000	124	1.5	5.0	3.0	3.3		1.2	-2.9	4.4	4.1
6,000	125	1.5	5.3	3.6	2.4		1.9	-1.7	4.0	3.6
6,000	126	1.5	6.6	4.4	2.4		3.4	-0.1	4.4	3.5
6,000	127	1.5	7.4	5.4	2.1		4.0	1.2	4.3	2.8
8,000	124	2.0	5.4	3.4	3.4		1.0	-2.4	3.2	3.4
8,000	125	2.0	6.0	4.3	3.1		1.4	-3.0	4.2	4.4*
8,000	126	2.0	6.5	4.5	1.8		2.4	-1.3	4.5	3.7
8,000	127	2.0	7.7	5.5	2.6		4.5	2.1	2.6	2.4
17,000	128	4.0	9.3	7.4	2.0		6.3	4.2	2.3	2.1
28,000	130.5	6.3	12.4	10.6	2.2		8.7	6.7	4.0	2.0
			Overtopping with Lateral Flow							
4,000	124	1.0	3.9	2.3	1.9		0.4	-2.9	4.2	3.3
4,000	125	1.0	3.5	1.0	2.2		1.2	-1.8	3.2	3.0
4,000	126	1.0	5.0	1.8	2.9		2.4	-0.6	3.0	3.0
4,000	127	1.0	6.0	2.9	1.9		3.8	1.4	1.8	2.4
6,000	124	1.5	4.9	2.5	3.4		0.8	-2.1	4.2	2.9
6,000	125	1.5	5.0	1.0	6.9		1.5	-3.1	5.3	4.6
6,000	126	1.5	6.3	1.0	5.0		2.7	-6.8	9.4	9.5**
6,000	127	1.5	7.0	2.1	4.4		3.7	-1.3	3.8	5.0
8,000	124	2.0	5.2	3.5	1.5		0.6	-3.0	3.2	3.6
8,000	125	2.0	5.7	2.2	5.2		2.1	-2.1	4.0	4.2
8,000	126	2.0	6.8	-3.4	9.3	10.2#	3.7	-2.2	7.0	5.9
8,000	127	2.0	8.2	1.5	5.2		5.2	-2.4	9.0	7.6
17,000	128	4.0	11.0	6.1	4.3		8.0	3.3	3.7	4.7
28,000	130.5	6.3	13.0	10.8	--		9.8	6.9	2.9	2.9

* Cp = 0.103
** Cp = 0.222
\# Cp = 0.333

FIGURE 62

Tabular Summary of Pressure Fluctuation Data
on the Lip of the Sill Extension-Sill Extended (Type C)
V = 37 mps, Lateral Flow
Various Tailwater Stages, Taps C18b and L18b

			Tap C18b				Tap L18b			
Discharge cms	Tail-water Meters	Depth-d Meters	Aver. Press. Meters	Min. Press. Meters	Max. Fluc. Meters	ΔP	Aver. Press. Meters	Min. Press. Meters	Max. Fluc. Meters	ΔP
2,000	124	0.5	1.9	1.6	0.3	0.3	2.0	1.3	0.5	0.7
2,000	127	0.5	4.3	3.9	0.4	0.4	4.4	3.5	0.9	0.9
4,000	124	1.0	2.7	1.1	1.9	1.6	0.7	-1.5	3.6	2.2
4,000	125	1.0	3.0	0.9	3.4	2.1	1.4	-1.8	5.1	3.2
4,000	126	1.0	2.7	0.4	1.4	2.3	2.8	-0.3	2.4	3.1
4,000	127	1.0	4.1	2.3	1.6	1.8	3.8	0.6	1.8	3.2
6,000	124	1.5	3.5	1.9	1.7	1.6	1.5	-1.0	3.8	2.5
6,000	125	1.5	4.3	1.8	2.5	2.5	2.5	-0.8	3.0	3.3
6,000	126	1.5	4.9	3.1	2.7	1.8	3.3	0.9	3.0	2.4
6,000	127	1.5	5.5	3.6	2.8	1.9	4.6	2.2	2.4	2.4
8,000	124	2.0	4.5	2.3	2.2	2.2	2.1	-2.0	3.6	4.1
8,000	125	2.0	5.2	2.9	1.8	2.3	3.1	-0.9	4.3	4.0
8,000	126	2.0	5.9	3.8	2.6	2.1	3.4	0.9	3.8	2.5
8,000	127	2.0	6.3	3.6	2.5	2.7*	5.2	2.3	3.4	2.9
17,000	128	4.0	8.7	6.3	2.4	2.4	7.4	4.4	3.0	3.0
28,000	130.5	6.3	12.1	9.5	--	2.6	9.5	4.9	2.1	4.6**
			Overtopping with Lateral Flow							
2,000	124	0.5	1.3	0.9	0.3	0.4	0.7	0.1	0.4	0.6
2,000	127	0.5	4.4	4.0	0.5	0.4	4.1	3.6	0.7	0.5
4,000	124	1.0	2.8	0.8	2.0	2.0	0.7	-1.0	4.5	1.7
4,000	125	1.0	2.1	-0.9	1.6	3.0	-0.2	-2.2	1.8	2.0
4,000	126	1.0	3.1	0.8	1.6	2.3	2.1	-0.1	1.2	2.2
4,000	127	1.0	4.4	2.5	1.6	1.9	1.5	1.6	2.3	0.1
6,000	124	1.5	3.3	1.4	2.7	1.9	1.3	-1.1	3.5	2.4
6,000	125	1.5	3.8	-1.8	8.1	5.6	2.8	-1.6	3.2	4.4
6,000	126	1.5	4.9	-0.1	5.8	5.0	3.5	-3.5	6.2	7.0
6,000	127	1.5	5.9	0.7	3.2	5.2	4.5	-2.8	7.0	7.3##
8,000	124	2.0	4.3	2.1	2.4	2.2	2.1	-1.1	3.8	3.2
8,000	125	2.0	4.7	-0.5	3.9	5.2	3.7	0.3	4.4	3.4
8,000	126	2.0	5.6	-0.5	5.9	6.1	4.6	-0.5	6.0	5.1
8,000	127	2.0	6.7	0.7	5.2	6.0	5.6	0.9	6.9	4.7
17,000	128	4.0	10.2	2.4	9.1	7.8#	8.9	3.5	3.4	5.4
28,000	130.5	6.3	--	10.3	--	--	12.2	6.8	--	5.4

* σ_p = 0.059
** σ_p = 0.06
# σ_p = 0.113
σ_p = 0.106

FIGURE 63

Tabular Summary of Pressure Fluctuation Data
At the Bucket Lip-Sill Eroded Two Meters (Type B),
V = 29 mps, Lateral Flow,
Various Tailwater Stages, Taps C13a and L13a

			Tap C13a			Tap L13a		
Discharge cms	Tail-water Meters	Depth-d Meters	Aver. Press. Meters	Min. Press. Meters	Max. Fluc. Meters	Aver. Press. Meters	Min. Press. Meters	Max. Fluc. Meters
4,000	124	1.0	2.1	-1.0	3.2	3.6	2.4	1.2
4,000	125	1.0	2.6	-3.6	6.4	4.5	0.5	1.2
4,000	126	1.0	3.9	-0.1	4.7	6.2	2.4	1.6
4,000	127	1.0	4.8	1.2	3.1	6.9	4.5	0.8
6,000	124	1.5	2.7	-1.0	4.3	4.1	2.5	1.6
6,000	125	1.5	4.1	0.5	4.1	4.7	3.5	1.2
6,000	126	1.5	5.1	1.6	3.4	5.6	4.1	1.1
6,000	127	1.5	5.4	2.5	4.4	6.7	5.3	1.4
6,000	128	1.5	8.7	6.0	2.8	8.1	6.8	1.0
6,000	129	1.5	7.5	0.6	4.4	9.4	8.5	1.2
8,000	124	2.0	2.7	-1.2	3.8	2.7	1.7	1.1
8,000	125	2.0	3.2	-0.2	4.2	4.2	3.1	1.0
8,000	126	2.0	4.8	1.5	4.2	5.5	3.6	1.2
8,000	127	2.0	5.5	2.2	4.2	7.1	5.5	1.1
10,000	124	2.5	1.9	-1.9	3.0	3.4	1.3	1.6
10,000	125	2.5	2.5	-0.3	2.9	4.4	2.7	1.9
10,000	126	2.5	4.0	1.5	2.9	5.3	3.4	1.9
10,000	127	2.5	5.4	3.2	3.3	6.7	4.8	1.8
12,000	124	3.0	2.6	-0.2	3.1	3.8	2.3	1.9
12,000	125	3.0	3.3	0.4	3.0	5.0	3.3	1.9
12,000	126	3.0	3.7	1.4	2.6	5.6	4.1	1.7
12,000	127	3.0	5.1	2.1	2.3	6.9	4.8	2.0
17,000	124	4.0	2.9	0.5	2.7	4.1	2.4	2.0
17,000	125	4.0	3.3	0.7	2.4	5.2	3.1	1.2
17,000	126	4.0	4.2	1.6	2.0	6.0	4.2	1.9
17,000	127	4.0	5.4	3.6	2.1	7.4	5.4	1.8
17,000	128	4.0	6.4	3.4	1.9	8.7	6.7	1.6
28,000	124	6.3	3.0	0.7	3.5	4.9	3.2	1.8
28,000	125	6.3	3.7	1.1	2.6	5.8	3.9	1.1
28,000	126	6.3	4.7	1.9	2.3	6.8	4.9	1.2
28,000	130.5	6.3	9.4	7.0	2.0	12.0	10.8	1.2

FIGURE 64

Tabular Summary of Pressure Fluctuation Data
At the Bucket Lip-Sill Eroded Two Meters (Type B),
V = 29 mps, Lateral Flow, Overtopping,
Various Tailwater Stages, Taps C13a and L13a

			Tap C13a			Tap L13a		
Discharge cms	Tail-water Meters	Depth-d Meters	Aver. Press. Meters	Min. Press. Meters	Max. Fluc. Meters	Aver. Press. Meters	Min. Press. Meters	Max. Fluc. Meters
4,000	124	1.0	1.8	-1.3	3.5	2.7	0.7	2.3
4,000	125	1.0	2.7	-3.9	7.0	5.0	1.9	1.5
4,000	126	1.0	3.9	-0.7	5.0	6.0	2.6	0.7
4,000	127	1.0	4.8	1.0	4.5	7.1	3.6	1.0
6,000	124	1.5	2.7	-0.9	5.4	3.8	2.3	1.6
6,000	125	1.5	2.9	-6.0	17.5	4.7	1.8	2.0
6,000	126	1.5	3.5	-5.7	12.9	5.6	-1.9	2.6
6,000	127	1.5	4.8	-5.5	11.3	7.2	1.9	1.4
6,000	128	1.5	4.6	-0.8	6.5	8.8	7.7	1.1
6,000	129	1.5	8.6	2.9	3.8	10.1	9.0	0.7
8,000	124	2.0	2.3	-1.5	4.8	2.8	1.1	3.1
8,000	125	2.0	3.5	-2.3	10.5	4.1	2.1	1.4
8,000	126	2.0	3.0	-7.0	16.2	5.3	-0.1	2.4
8,000	127	2.0	5.6	-6.3	9.5	7.3	2.2	3.0
10,000	124	2.5	3.2	0.3	2.7	3.0	1.4	2.0
10,000	125	2.5	4.1	0.4	5.0	5.3	3.2	2.1
10,000	126	2.5	4.8	-2.2	5.3	6.0	1.2	2.1
10,000	127	2.5	4.9	-2.4	6.2	6.9	2.0	2.4
12,000	124	3.0	2.5	-0.4	2.3	3.6	2.2	1.8
12,000	125	3.0	3.9	1.0	2.8	4.8	3.3	1.2
12,000	126	3.0	5.2	-0.5	4.2	6.6	3.2	2.8
12,000	127	3.0	6.2	0.2	5.0	8.0	3.7	2.2
17,000	124	4.0	2.6	-0.4	3.0	3.6	2.0	1.4
17,000	125	4.0	4.0	1.2	2.5	5.5	3.8	1.4
17,000	126	4.0	6.2	1.3	2.8	7.4	3.5	2.1
17,000	127	4.0	6.9	2.5	3.5	8.8	4.7	1.0
17,000	128	4.0	9.3	1.2	2.6	10.1	5.4	2.9
28,000	124	6.3	3.1	0.6	3.6	4.7	2.7	1.2
28,000	125	6.3	4.8	2.1	2.0	6.2	4.4	1.2
28,000	126	6.3	6.0	3.5	1.9	7.9	6.2	1.5
28,000	130.5	6.3	12.1	8.8	2.7	13.9	11.0	1.7

FIGURE 65

Tabular Summary of Pressure Fluctuation Data
at the Bucket Lip-Sill Eroded Two Meters (Type B)
V = 29 mps, Lateral Flow
Various Tailwater Stages, Tap C13b

Discharge cms	Tail-water Meters	Depth-d Meters	Tap C13b Aver. Press. Meters	Tap C13b Min. Press. Meters	Tap C13b Max. Fluc. Meters
4,000	124	1.0	3.9	0.4	2.2
4,000	125	1.0	2.1	-4.5	1.4
4,000	126	1.0	2.9	-1.3	3.5
4,000	127	1.0	4.4	-1.5	2.7
6,000	124	1.5	3.5	-0.5	2.6
6,000	125	1.5	4.7	0.9	2.2
6,000	126	1.5	5.1	2.1	2.5
6,000	127	1.5	6.3	3.5	3.2
8,000	124	2.0	3.5	-2.1	1.0
8,000	125	2.0	4.7	-0.1	3.2
8,000	126	2.0	5.5	2.2	1.0
8,000	127	2.0	6.4	3.6	1.7
17,000	128	4.0	6.6	4.1	2.2
28,000	130.5	6.3	8.7	5.9	1.9
		Overtopping with Lateral Flow			
4,000	124	1.0	1.1	-4.5	4.3
4,000	125	1.0	2.7	-3.6	2.0
4,000	126	1.0	3.6	-3.4	4.5
4,000	127	1.0	4.1	-2.1	2.8
6,000	124	1.5	2.7	-1.4	1.8
6,000	125	1.5	2.3	-5.0	6.3
6,000	126	1.5	3.5	-5.8	7.1
6,000	127	1.5	4.7	-4.6	4.0
8,000	124	2.0	0.9	-3.0	2.6
8,000	125	2.0	2.5	-3.2	2.8
8,000	126	2.0	3.6	-6.1	3.6
8,000	127	2.0	5.1	-3.8	6.0
17,000	128	4.0	8.3	2.9	2.8
28,000	130.5	6.3	11.1	7.4	2.4

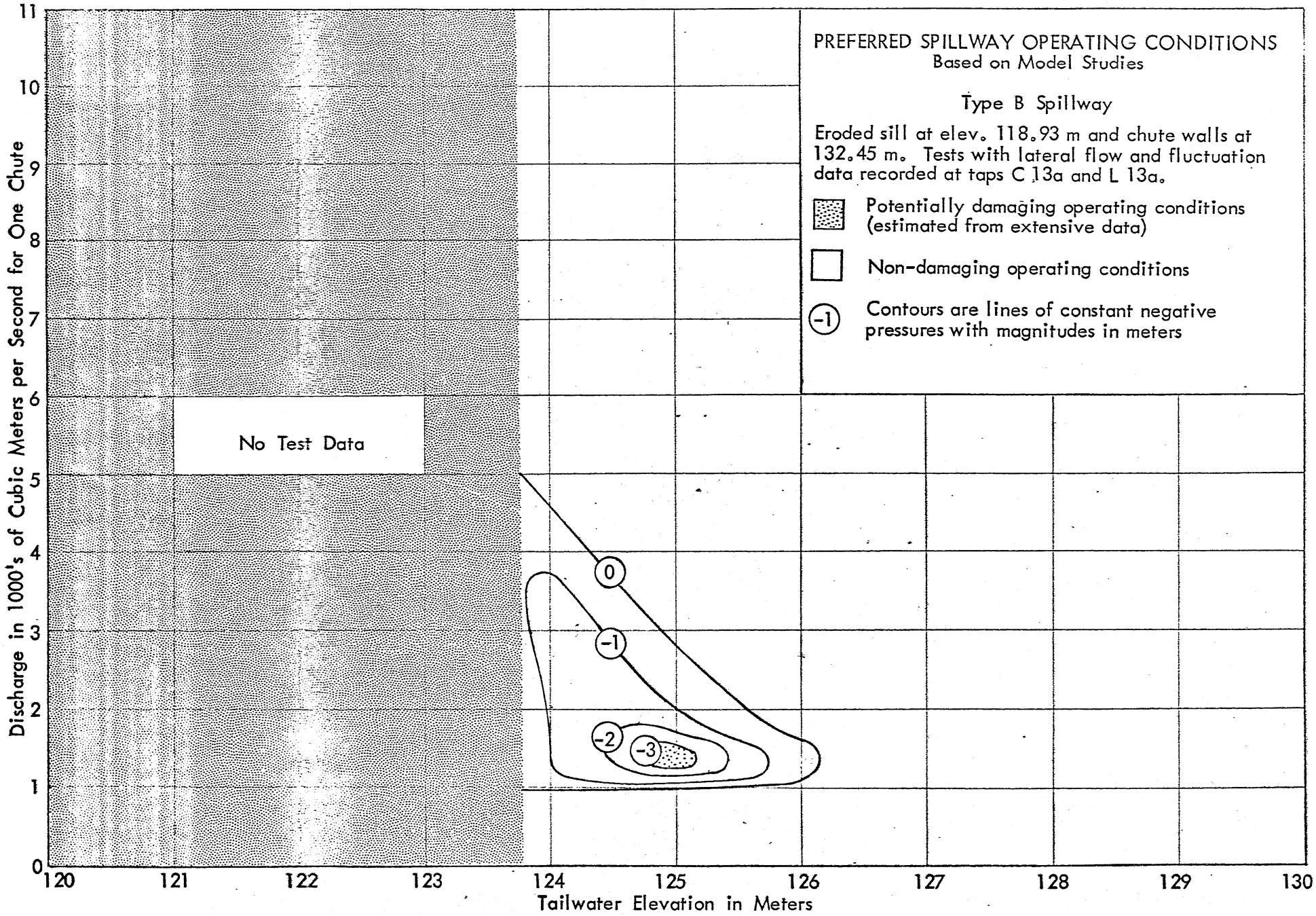
PREFERRED SPILLWAY OPERATING CONDITIONS
Based on Model Studies
Type B Spillway
Eroded sill at elev. 118.93 m and chute walls at 132.45 m. Tests with lateral flow and fluctuation data recorded at taps C 13a and L 13a.
Potentially damaging operating conditions (estimated from extensive data)
Non-damaging operating conditions
-1
Contours are lines of constant negative pressures with magnitudes in meters
No Test Data
0
-1
-2
-3
Discharge in 1000's of Cubic Meters per Second for One Chute
Tailwater Elevation in Meters
0
1
2
3
4
5
6
7
8
9
10
11
120
121
122
123
124
125
126
127
128
129
130

Fig. 66

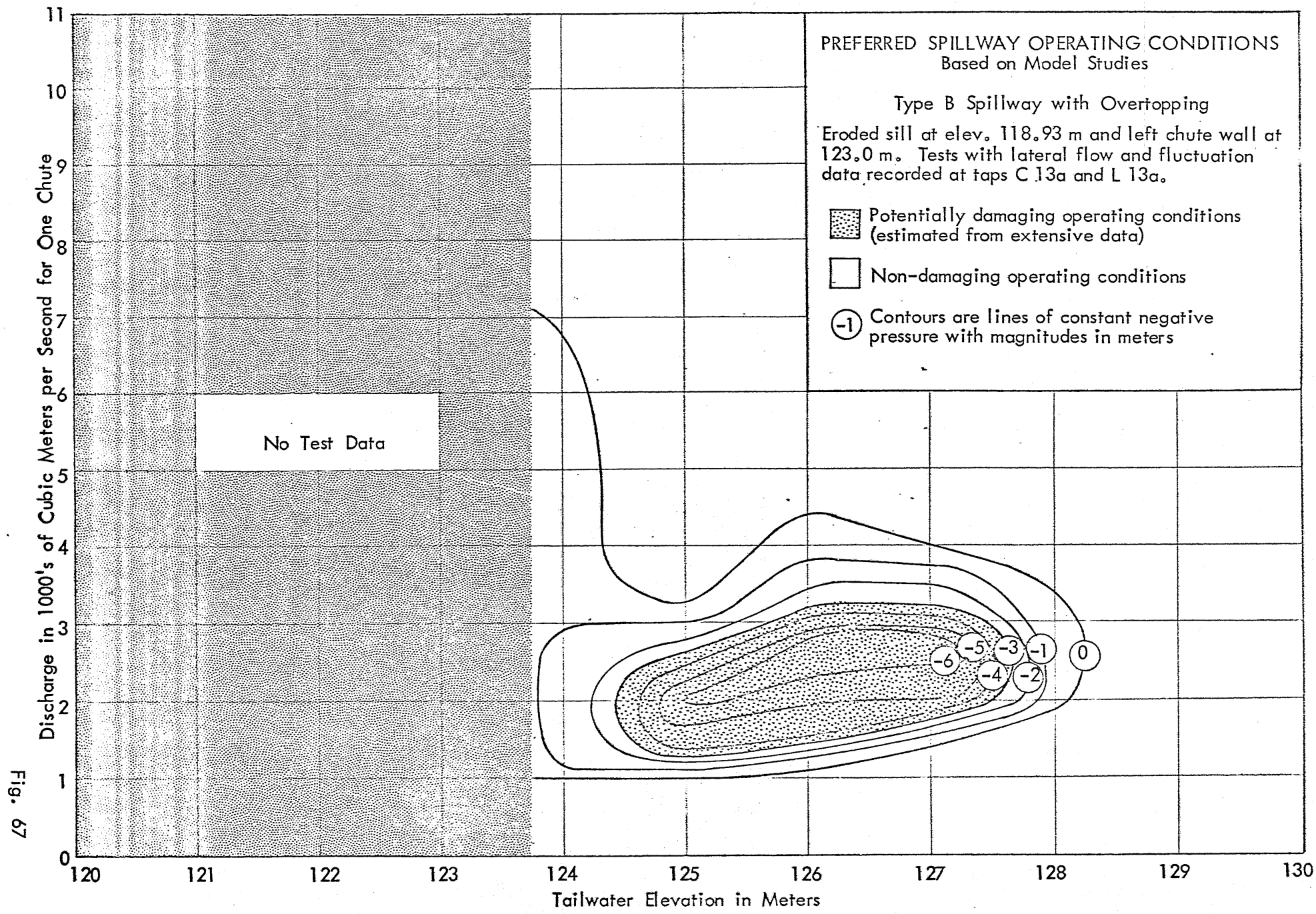
PREFERRED SPILLWAY OPERATING CONDITIONS
Based on Model Studies
Type B Spillway with Overtopping
Eroded sill at elev. 118.93 m and left chute wall at 123.0 m. Tests with lateral flow and fluctuation data recorded at taps C 13a and L 13a.
Potentially damaging operating conditions (estimated from extensive data)
Non-damaging operating conditions
(-1) Contours are lines of constant negative pressure with magnitudes in meters
No Test Data
-6
-5
-4
-3
-2
-1
0
Discharge in 1000's of Cubic Meters per Second for One Chute
Tailwater Elevation in Meters
0
1
2
3
4
5
6
7
8
9
10
11
120
121
122
123
124
125
126
127
128
129
130

Fig. 67

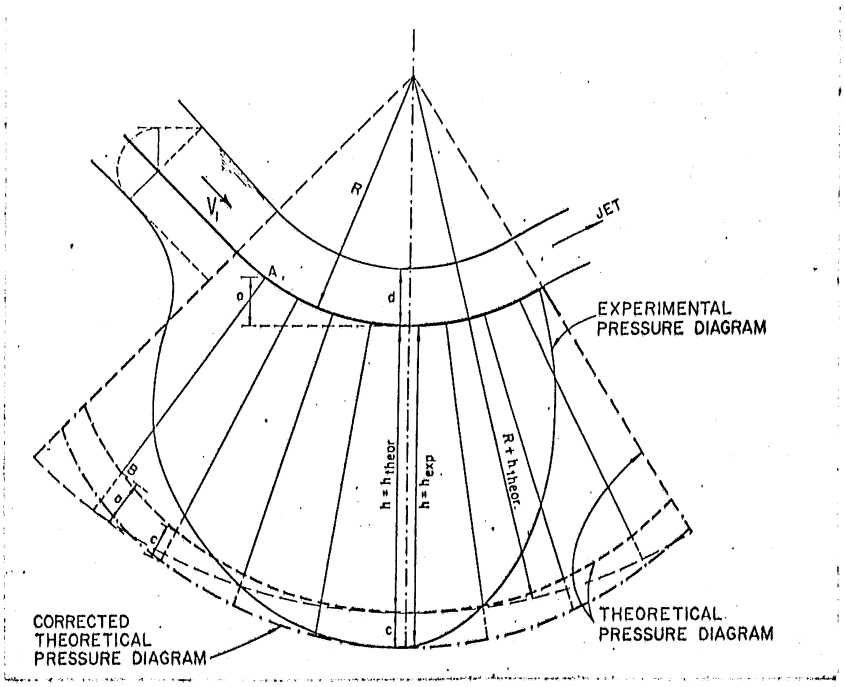

Fig. 68 - Theoretical and Experimental Pressure Diagrams (from Ref. [2])

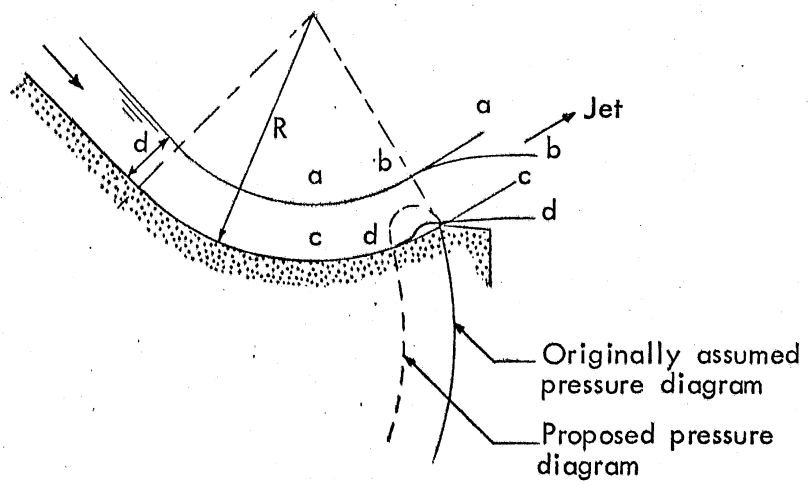

Fig. 69 - Suggested Streamline Adjustments at the Bucket Lip (Pressure diagram and streamline dd greatly exaggerated)

Appendix A

THEORY OF PRESSURE ON THE SPILLWAY CHUTE AND BUCKET

In theory, the pressure head on a straight portion of a spillway chute having a slope θ should be approximated by the product of the depth and the cosine of θ. The data of Fig. 18 show that this value was essentially achieved in the St. Anthony Falls experiments.

The maximum pressure head acting on the floor of a circular spillway bucket can also be approximated by assuming that the flow in the bucket is an irrotational vortex. The resulting equation, as developed by Balloffet [2], is

$$h = d + \frac{V_1^2}{2g}\left[1 - \left(\frac{R - d}{R}\right)^2\right]$$

The variables of the equation are as shown in Fig. 68.

A theoretical correction, c, applied to the above equation increases the agreement of the equation with experimental data shown in the figure. It is noteworthy, however, that the agreement occurs only at the bottom of the bucket and that upstream of this point the experimental curve falls steeply and inflects to join the pressure gradient of the chute. Downstream of the bucket bottom the curve also falls steeply to approach zero where the jet discharges to the atmosphere at the bucket lip.

As is shown in Fig. 68, the theoretical low chute pressure abruptly jumps to the theoretical high bucket pressure at the upstream tangent point of the bucket curve. The experimental curve shows that the theoretical pressure singularity cannot exist in nature and the real boundary flow lines adjust themselves to a form somewhat different from that of the rigid boundary. This is accomplished physically by a natural separation of the flow from the solid boundary. A similar singularity exists at the lip of the bucket, where the vortex pressure falls abruptly to zero. It is apparent from Fig. 68 that the experimental curve also provides a pressure adjustment in the downstream region. The details of this adjustment in the immediate vicinity of the lip appear to have been ignored both in theory [3] and in the numerous model studies cited in Refs. [2] and [3] in which bucket pressures have been measured. The assumption seems to have been made universally that the pressure falls to zero at the lip. It was, therefore,

rather surprising to find that the free discharge measurements made in the current tests (see Fig. 22) showed definite negative values upstream of the bucket lip. However, contemplation of the possible readjustments of flow lines at the lip suggests that this is simply a response of the freely discharging jet to the influence of the force of gravity. It is not difficult to accept the idea that the streamlines of the water surface must adjust from a-a as shown in Fig. 69 to some form such as b-b. It is conjectured that it is equally reasonable to reject the idea that the bottom streamline must rigorously follow the boundary to the lip, as with c-c, before beginning to curve under the influence of gravity. In light of the previously discussed adjustment that took place at the chute tangent point, it is suggest that flow at the lip does in fact separate upstream of the bucket lip in accord with a streamline of the form d-d. This streamline would require the pressure diagram which is designated as "proposed" in Fig. 69. The proposed diagram is consistent with the limited data obtained at St. Anthony Falls and shown in Fig. 22. The indicated low pressures which were measured as manometric or static values are enhanced negatively when impinging eddies in the flow rebound from the boundary, yielding additive transient negative pulses. The magnitudes of the pressure heads of such added dynamic pulses are given by the ΔP values of Figs. 52 through 58 with their strengths ranging from ≈ 1 to ≈ 10 m, depending on the violence of the impinging eddies. As described in the body of the report, very strong eddies commonly resulted with overtopping flow, but equally strong eddies resulted from certain non-overtopping flows with bucket rollers uniquely positioned above the lip.

It is believed that the combination of a low static pressure and strong eddy pulses caused the cavity-forming negative pressure which resulted in the observed erosion damage at Guri.

Lenau and Cassidy [3] imply that as the Froude number is decreased, the influence of gravity on the form of the streamlines increases. They state that for a flip bucket this influence is roughly approximated by the ratio of H, the total head on the bucket, to R, the radius of the bucket. For the Guri bucket $H = 215 - 112.44 = 102.56$ m and $R = 30$ m, yielding $H/R = 3.4$. The data of Refs. [2] and [3] indicate that the H/R values of the flip buckets studied by others were generally considerably greater than the value employed at Guri. This suggests that the

damage at Guri may be traceable to the fact that a somewhat larger R was employed at Guri than in other designs. However, insufficient detail is given for the other studies to indicate what an acceptable limit of R would have been. The studies at St. Anthony Falls, as discussed herein, are believed to be the most detailed that have been made and the first to disclose the possibility of negative pressures upstream of the lip.

Appendix B

THE MECHANISM OF CAVITATION DAMAGE

The term "cavitation," when applied to a flowing hydraulic system, refers to the formation and subsequent collapse of pockets or cavities within the flowing water. The cavities are largely filled with water vapor and are caused by the vaporization of water upon entering a local region in which the pressure falls below the inherent vapor pressure-temperature limits of the liquid. The vapor will condense to the liquid state and the cavity will collapse or disappear when the local pressure rises above the vapor pressure. The vapor pressure of water in terms of absolute pressure is about one-quarter meter of water head at 20°C and varies with temperature. As a negative or relative value with respect to atmospheric pressure it will approximate -10 m of water head and will vary depending on the atmospheric pressure.

For a smooth spillway such as existed at Guri, local dynamic or flow pressures as low as -10 m of water head can result in a flow from a combination of the following dynamic effects:

1. Negative pressure effects can be contributed by the flow passing over a convex portion of the boundary or a convex separation zone that serves as a pseudo-boundary. Appendix A and Fig. 69 describe how gravitational effects on the discharging jet at Guri might cause such a separation zone on the bucket lip. The resulting curved flow generates an essentially static pressure depression on the boundary that depends on the flow velocity, the flow depth, and the radius of curvature. The data of Fig. 22 for a chute velocity of 29 mps demonstrate that manometer measurements of mean pressure on such a boundary may be as low as -2 m even when several meters of water depth exist above the boundary pressure tap. Similar measurements at a chute velocity of 37 mps produced a value as low as -4 m relative to atmospheric.

2. Negative pressure effects may be contributed by a large eddy striking or impinging on a boundary and then rebounding. During the impingement phase the local dynamic pressure abruptly rises above the normal static pressure in the area, and during the

rebound it dips transiently to a low value. It is probable that the transient pressures measured on the Guri model were predominantly from this source. The values found were quite commonly between -1 m and -3 m in the tests and under some rare conditions reached -10 m.

3. Internal to the large eddy described above is a complex structure of lesser eddies or vortices inherent in the general turbulence of the flow. Each of these vortices spins rapidly about some center. The pressure at this center can be far less than the pressure surrounding the vortex. The value of the pressure at the vortex center depends on the intensity and scale of the vortex and can readily contribute several meters of pressure depression. It is doubtful that this depression is sensed by the pressure measuring transducer. It is probably due to this depression that experience indicates that measured values of only -3 to -4 m may actually produce damaging cavitation.

Since all three of the foregoing pressure depressions can exist concurrently in a given area, their pressure values are additive and under adverse conditions can readily total the -10 m required to cause vaporization of the water. In view of the fact that the damage at Guri occurred only at the bucket lip, it appears that items 2 and 3 above combined could produce damaging negative pressures only when supplemented by low values from item 1. It should be noted that all three of these pressure sources are dynamic in nature and will increase approximately with the square of the velocity.

It should be pointed out that once a significant cavity has formed in water, the vapor pressure therein cannot be appreciably reduced by lowering the surrounding pressure. Any attempt to do so will serve only to increase the rate of vaporization and the size of the cavity.

The collapse of the cavity as it moves into a region of higher pressure actively involves only a small mass of water immediately surrounding the cavity. However, the entire collapsing small mass is focused toward a point at the center of the cavity, and the walls of the cavity may collapse with a velocity reaching a hundred or more mps near the terminal point. Consequently, at the collapse focal point all mass particles are very rapidly decelerated to rest and the accompanying waterhammer-type pressure

rise reaches a very high value, possibly of the order of 3500 kilograms per sq cm (50,000 psi). If the collapse takes place directly on or immediately adjacent to a solid boundary, the pressure intensity produced by small-scale cavitation may be sufficient to fracture and erode the surface through small-scale pitting. Cumulatively this pitting can erode very large volumes.

Experience indicates that most materials in most systems will not show evidence of damage when velocities are less than about 15 mps (50 fps). However, above this lower threshold velocity the rate of erosive loss increases as some exponential value of the velocity. Various experimenters have found this to be about V^6. Consequently, many designers attempt to hold flow velocities below about 30 mps (100 fps) on readily erodible materials. Where this cannot be done, more resistant boundary materials are commonly used to reduce the rate of damage. The velocity conditions at Guri approximate this common limit, and the damage encountered is in general consistent with the experience of others in which the increasingly high heads on modern hydraulic structures produce more frequent problems with cavitation erosion.

The effect of a collapsing cavity on a boundary surface varies both with the intensity of the collapse and with the damage-resistant character of the material. Materials vary greatly in their resistance characteristics. The variation depends on the inherent characteristics of the material and on the water environment to which it is exposed. Increasing resistance is generally accompanied by increasing cost, and selection for a given application is an economic compromise.

It is difficult to rigorously evaluate the resistance characteristics of various practical construction materials that might be employed in a reconstruction of the Guri spillway lip. However, based on a number of investigations, the resistance of some usable materials can be rated approximately as follows in terms of relative comparable erosion:

Material	Relative Life
Conventional portland cement concrete prepared using good aggregates and good practices	1
Concrete with selected kinds and amounts of aggregates bonded with epoxy plastic polymers	10 to 100
Carbon steel	10 ±
Stainless steel	100 to 150

The basic portland cement concrete varies widely depending on aggregate strength, aggregate shape, aggregate sizing, cement, water-cement ratio, and mixing and placing procedures.

The epoxy concretes also differ according to aggregate properties and aggregate bonding with the epoxy. Epoxy has been used in some cases without aggregate, and with some types of epoxy resins may demonstrate excellent cavitation resistance due to the inherent elastic properties. Epoxy resins are organic in nature, and their characteristics are not yet well understood on a long life basis. Laboratory experiments using epoxy resins or elastomeric polymers for coatings or overlays have shown them to have remarkable resistance, but in the field, failure due to loss of adhesion or bond with the substrate is quite common. On the basis of present experience, the use of epoxy resins or other plastics cannot be safely recommended for long life.

The use of carbon steel for armoring against cavitation erosion is relatively low in cost and might prove to be practical in the restoration of damage at Guri. However, cavitation erosion is not strictly a process of mechanical damage, but also involves accelerated electro-chemical processes. Where water is chemically aggressive, cavitation erosion on steel may proceed at a quite rapid rate. In view of the fact that the water at Guri is reported to be aggressive, armoring with mild steel should be considered very cautiously.

Stainless steel may vary considerably in erosive life depending on the kinds (nickel, chromium) and amounts of alloys used and on the fabrication procedure (cast, rolled, weld overlays, annealing, etc.). The life also depends on the aggressive character of the water. Present experience indicates that stainless steel of a suitable type is probably the most practical armor material for the severe cavitation condition that exists at the Guri bucket lip. Stainless steel has an important advantage in that if it evidences pitting after extended exposure, the eroded portions can be restored using field welding and grinding techniques that have been well established in hydraulic turbine maintenance practice.

Appendix C

THE MOTION PICTURE RECORD

As a permanent photographic record of the project a motion picture has been produced. This is a 16 mm color, sound film 650 ft in length with a 17-minute running time.

The film very briefly describes the site and the nature of the damage problem at Guri and then shows the model facilities which were used to study the problem at the St. Anthony Falls Hydraulic Laboratory. The bulk of the film deals with model flows for a variety of significant flow conditions in which various discharge and tailwater values are combined to show action on various bucket sill configurations.

Slow-motion pictures are especially useful in showing the flow character of two particular conditions:

1. The roller which forms in the bucket for certain combinations of tailwater and discharge; and
2. The powerful turbulence that is formed by the wall-overtopping stream falling into the bucket.

An understanding of these two turbulence mechanisms is important because their eddies pulse on the lip of the bucket to cause the negative pressure peaks which in turn support vapor cavitation and cavitation damage on the lip.